主論文

PULSE FLUOROMETRIC STUDY ON ACTO-HEAVY MEROMYOSIN

パルス蛍光法によるアクト-ヘビィ-メロミオシンの研究

神山勉

PULSE FLUOROMETRIC STUDY ON ACTO-HEAVY MEROMYOSIN

By

TSUTOMU KOUYAMA

DEPARTMENT OF PHYSICS
FACULTY OF SCIENCE
NAGOYA UNIVERSITY

(MARCH 1980)

CONTENTS

Abbreviations:

ADP	Adenosine-5'-diphosphate
AMPPNP	Adenyl imisodiphosphate
ANM	N-(1-Anilinonaphthyl-4)maleimide
ATP	Adenosine-5'-triphosphate
CT	α-Chymotrypsin
DTT	1,4-Dithiothreitol
EDTA	Ethylenediamine tetraacetic acid
EGTA	Ethylene glycol-bis(β-aminoethyl ether)N,N'-tetraacetic acid
FWHM	Full Width of Half Maximum
NADH	Dihydronicotinamide adenine dinucleotide
NEM	N-Ethylmaleimide
MCA	Multi-Channel Analyser
PIAA	N-(1-Pyrenyl)iodoacetamide
P_i	Inorganic phosphate
PM	N-(1-Pyrenyl)maleimide
PMIA	N-(1-Pyrenyl)methyl-iodoacetate
S1-A1,S1-A2	Myosin Subfragment-1 with Alkali-1 Light Chain and with Alkali-2 Light Chain, respectively
SDS	Sodium Dodecyl Sulfate
SH	Sulfhydryl (group)
TR	Trypsin

I INTRODUCTION

Active movement in the living cell is being maintained in the flow of free energy in a way just like a water mill being worked in the flow of water. The useful energy absorbed from the sun light is converted to and stored as the chemical energy and then consumed for activation of the various reactions which are essential for maintenance of the "life". Before the "life" being understood well, the question should be answered as to how the photon or chemical energy may be used to do useful work in a biological system. As to muscle contraction, the problem is how the energy released on the hydrolysis of ATP may be converted to the mechanical energy for the contraction. This problem may be also interesting in the field of physics. That is, it would be not easy to devise molecular machines such as muscle, in which the chemical free energy (scalor quantity) is converted directly to the force for the directional movement (vector quantity) with high efficiency. The main difficulty may be raised from the fact that the molecules under consideration are always in the violently fluctuating environment because of the smallness. Within the framework of conventional thermodynamics, it does not seem probable that a satisfactory explanation is given as to how the directional force is generated under isotropical thermal agitations.

Although the mechanism of muscle contraction has been made clear up to near a molecular level, a large number of

mechanisms must be elucidated before the above problem will be discussed without any speculations; for example, tertiary structuresof the indivisual proteins (e.g., actin and myosin) participating in the force generation have not been determined yet. Furthermore, there has been little information about transient conformations of the each protein during the muscle contraction or during the hydrolysis of ATP by acto-myosin. As a matter of fact, few techniques have been developed which can monitor these transient conformations. This is because of lacking of the probe which is suitable to sense the conformational change of actin or myosin. It is very desired to find such a probe, since identification of these transient conformations may be a key of the understanding of essentials of muscle contraction.

Fluorometry has been recently developed as an important tool in the fields of biochemistry and biophysics. Fluorometry may be the method which is hard to handle, because the relation is not always simple between the observable quantity and actually occuring phenomena. However, once its characteristics (the principle or the limitation) is well understood, it may become a very valuable tool because of the sensitivity for microenvironment. Various kinds of fluorescent probes have been produced in these several years, and the fluorometric studies using extrinsic probes have been actively made. This method is very suitable for the study about the specific sites in proteins or membranes. In future work, this method will

be indispensable for elucidation of the transient conformations of the individual proteins during the muscle contraction. On the other hand, recent developments in the techniques of electronics permit to measure the time-resolved fluorescence (pulse-fluorometry). By the use of the pulse-fluorometer, the obscurity that was inherent to the fluorometry can be removed; and, at the same time, the application of the fluorometry to various biological systems has been made possible.

The present thesis is concerning with the following two purposes. One is to study the basic problems in the fluorometry that have not been made clear but may be important in application of the method to labile system of proteins. The other and main purpose is to find by the fluorometry what kind of conformational changes in actin molecule may occur associated with the polymerization of actin and with the binding of myosin heads to F-actin.

In chapter II of this thesis, the author would like to make a historical survey of the studies on the interaction of actin with myosin. Chapter III will be devoted to brief reviews about fluorescence kinetics and about fluorescence anisotropy decay. In chapter IV, methods and materials used in this study are explained. Physicochemical properties of the conjugates of actin with fluorescent reagents will be also described. In chapter V, the study on basic problems in pulse-fluorometry will be presented; that is, the problems in determination of fluorescence anisotropy

decay and in analysis of experimental fluorescence decay curves will be discussed. Chapter VI and VII are the main parts of this dissertation. In chapter VI, the fluorescence behaviours of labelled actin observed on the G-F transformation will be presented. In chapter VII, conformational changes of actin filament induced by the binding of heavy meromyosin or subfragment-1 are examined by using the fluorometry.

II HISTORICAL SURVEY OF THE STUDIES ON THE INTERACTION BETWEEN ACTIN AND MYOSIN

II-1 Introduction

The fine structure of muscle is believed to be related to the mechanism of muscle contraction. Fig. II-1 is a diagrammatic presentation of structure of striated muscle. Contractile system of striated muscle is composed of thick filaments (black bars) and of thin filaments (white bars). In the cases of most vertebrate striated muscle, the length of thick filament is about 1.6 μm and that of thin filament is about 1.0 μm. The thick and thin filaments are usually 10 to 20 nm laterally appart. Observations under optical and electron microscopes suggested that, when muscle contracts, the arrays of filaments slide past each other without change in their lengths [1,2]. Most of efforts in the study of muscle contraction have been devoted for elucidation of the active molecular process which translates one type of filament past the neibouring of the other type.

In skeletal muscle, there are two principal structural proteins. One of them is myosin (60 % of the total structural protein of muscle) and actin (20 %). Thick filament is an assembly of several hundreds molecules of myosin. Individual myosin molecule has a head and tail structure and its tail points towards the center of filament as shown in Fig. II-2. Actin is a major protein among the components of thin filament and forms double-stranded helical structure

(Fig. II-3). Tropomyosin and troponin attach to actin filaments and regulate the interaction of actin with myosin depending on the concentration of calcium [3]. In actin filament, all the actin protomers are oriented in the same direction giving polarity to the filament. The actin filament extends, centering the Z membrane, to both sides and the polarity of actin filament is reversed on the two sides of Z-membranes (Fig. II-4). In the region where thick and thin filaments overlap, actin and myosin always have the same sense of polarity with each other [4]. In the model proposed by A. Huxley [5], it is supposed that the projection from the thick filament goes through repetitive cycle of attachment to and detachment from actin filament; during the period of attachment the individual projection pulls actin filaments and develops the sliding force. In the arrangement as shown in Fig. II-4, the force produced by individual cross-bridges in the overlap region will be additive. Accepting this mechanism, the question is how the chemical energy supplied by hydrolysis of ATP is transformed to mechanical work during the cycle of attachment and detachment of the projection. From this point of view, it is important to study the molecular mechanism of the interaction of actin with myosin in the absence and presence of ATP in detail.

II-2 Actin

In 1942, Straub [6] succeeded in isolating actin from

muscle. Actin is extracted into water from the dried powder of muscle treated with acetone after removal of myosin. Actin assumes a monomeric form (G-actin) in a salt-free solvent, and a long fibrous polymer (F-actin) in the presence of physiological concentration of salt (Fig. II-5).

II-2-1 Structure of G-actin

Actin is made up of a single polypeptide chain, and both one molecule of nucleotide (ATP or ADT) and divalent cation (Mg^{++} or Ca^{++}) are binding per molecule. Elzinga et al. (1973) [71] have determined the complete amino-acid sequence of actin of rabbit skeletal muscle. The polypeptide chain consists of 374 residues and has a calculated molecular weight of 41,785 daltons (or 42,300 including divalent cation and nucleotide). There are five free sulfhydryl groups, at the positions 10, 217, 256, 284 and 373. Sulfhydryl group of the residue 373 reacts fast with NEM [8]. Faust et al. (1974) [9] have shown that ATP binding site of actin is located near Cys-217. Jacobson and Rosenbusch (1976) [10] recently found that actin has a protease-resistant core extending from residue 68 (or 69) to the carboxyl-terminal end of the protein; this core binds ATP but not calcium ions and it fails to polymerize to the filamentous form of actin ~~and~~ or to stimulate myosin ATPase activity.

II-2-2 Structure of F-actin

In 1963, Hanson and Lowy [11] have shown that F-actin

in a double-helical polymer of about 8 nm in diameter, whose helical pitch is about every 36 nm, the strands being chains of approximately spherical subunits which repeat at about 5.5 nm intervals along each chain. That is, 13 monomers are contained in the two strands per half-pitch. The two strands wind around a common axis about 180° out of phase and the sense of the helix is right-handed. H.E. Huxley [4] (1963) found that when decorated with myosin or heavy meromyosin the actin filament exhibits a characteristic "arrowhead" structure and all arrowheads point in the same direction along the whole length in any given filament. Actin monomer is not a symmetric sphere but has head-and-tail directionality in itself. Wakabayashi et al. (1975) [12] analysed electron micrographs of the actin-tropomyosin complex by three-dimensional reconstruction and found that the general shape of the actin monomer looks globular and "chicken-shaped".

II-2-3 G-F transformation of actin

G-actin molecules are polymerized into F-actin by addition of neutral salts up to 0.1 M [6,13]. During the polymerization of actin, ATP bound to G-actin is dephosphorylated into ADP and inorganic phosphate [14]:

$$\text{G-actin-ATP} \longrightarrow \text{F-actin-ADP} + P_i$$

The nucleotide bound to G-actin are rapidly exchanged with free nucleotide in the solvent, whereas the ADP bound to F-actin is not easily exchanged [15]. In aqueous solution, G-actin without ATP loses polymerizability rapidly.

Although the splitting of ATP bound to G-actin accompanies polymerization, it is not absolute requisite for polymerization; that is, G-actin-ADP [16] and nucleotide-free G-actin [17] retain the capacity to polymerize under certain conditions. The binding of ATP to G-actin promotes the polymerization by making the structure of G-actin favourable for polymerization but the splitting of ATP is not coupled to polymerization; that is, G-actin-AMPPNP (a chemical analog of ATP which is not hydrolysed on polymerization of actin) can polymerize with a rate similar to G-actin-ATP [18].

F-actin polymerized *in vitro* is extremely long whose length attains several microns and thus the amount of F-actin can be determined from the flow-birefringence or viscosity [19]. Oosawa et al. (1959) [20] studied the equilibrium properties of actin solution and found that no F-actin is formed at extremely low actin concentration even in the presence of neutral salt. Above a critical value of the actin concentration, F-actin is formed whose amount is equal to the difference between the total actin concentration and the critical actin concentration. The concentration of G-actin coexisting with F-actin is kept constant above the critical actin concentration independently of the amount of F-actin formed [21]. It has been shown from the kinetic analysis of the initial phase of actin polymerization that the cooperation of three or four monomers is required for the initiation of polymerization [22]. The G-F transformation of actin is essentially to be regarded as a kind of condensation phenomenon such as the well-known

gas-liquid transition [23]. Oosawa and Kasai (1962) [24] proposed the scheme of polymerization of actin, by which the thermodynamic behaviours of actin during the G-F transformation can be understood well. According to their model, the rate limiting step in the polymerization of actin is the formation of nuclei of the helical polymer in which two kinds of bonds are formed between actin monomers.

The critical actin concentration depends strongly on ionic strength; and it also depends on the species of salt ions, pH, temperature, and so on. The concentration of KCl which is optimal for the polymerization is 0.1 to 0.12 M.

II-2-4 Changes in the tertiary structure of actin molecule during the polymerization

Higashi and Oosawa (1965) [25] found that the polymeization of G-actin-ADP into F-actin-ADP is accompanied by a change in ultraviolet absorption, which apparently originates partly from the translocation of tryptophan and tyrosine residues from the outside to the inside of protein and also partly from increase in the content of α-helix and/or β-structure. Polymerization is also accompanied by the changes in the intrinsic fluorescence [26] and in the circular dichroic spectra [27]. Recently, Rich and Estes [28] found in a study of limited proteolysis of G-actin and F-actin that the addition of 0.1 M KCl induces a rapid change in the conformation of G-ATP-actin to F-ATP-actin monomers prior to the formation of nuclei of the helical polymer.

II-3 Myosin

In 1941, Banga and Szent-Györgyi [29] found that "myosin" which had been discovered by Kühne [30] in 19-th century was a complex of actin and myosin. Myosin is extracted with Guba-Straub solution [31] (0.3 M KCl, 0.15 M phosphate buffer, pH 6.5) from minced muscle. Myosin exists in an monomeric state at high ionic strength (0.6 M KCl); while, it aggregates at low ionic strength (below 0.1 M KCl). H.E. Huxley (1963) [4] showed by the negative-staining technique of electron microscopic observation that aggregates of purified myosin are similar in appearance and dimensions to the naturally occuring thick filaments; the aggregates have large numbers of irregular-looking projections on their surface except a central zone of 0.15 to 0.2 μm in length. This appearance is explained by considering that the myosin molecule has a projection at one end and that the myosin molecules in either half of the filament are arrayed with opposite polarities (Fig. II-2).

II-3-1 Structure of myosin molecule

The molecular weight of myosin is about 470,000 daltons [32]. A myosin molecule consists of two large polypeptide "heavy" chains with molecular weights of 200,000 daltons and four small polypeptide "light" chains with molecular weights of 16,000 to 24,000 daltons. It was shown by S. Lowey et al. [33] that the myosin molecule consists of two globular "heads", each about 7 nm in diameter, attached

to a double-stranded-helical rod about 140 nm long. The rod-like portion is responsible for the formation of thick filament under the physiological ionic condition; while, each globular head, which corresponds to projection of thick filament, contains an actin binding site and an active site for ATP hydrolysis. Moore et al. (1969) [34] analysed electron micrographs of F-actin decorated with subfragment-1 (the "head" subunit) by the three-dimensional reconstruction technique and estimated that the subfragment-1 is approximately 15 nm long and 3 to 4.5 nm wide.

II-3-2 Myosin subfragments

The heavy chain contains regions which are susceptible to mild proteolytic cleavage (Fig. II-6). When myosin is digested with trypsin [35,36] or with chymotrypsin [37], cleavage occurs in a region about 90 nm from the tip of the tail, yielding light meromyosin (MW = 140,000) and heavy meromyosin (MW = 340,000). When digested with papain [33], cleavage occurs in a region close to the globular head, yielding subfragment-1 (MW = 115,000) and myosin rod (MW = 230,000). Light meromyosin and myosin rod, whose helical contents are 90-100 % [38], are insoluble at low ionic strength; while, heavy meromyosin and subfragment-1 show no tendency to aggregate. The important properties of myosin, i.e., ATPase activity and combination with actin, are retained in heavy meromyosin and subfragment-1 [39].

The first study of divalent cation effects on the proteolytic digestion of myosin was made by Balint et al.

[40], who showed that inclusion of EDTA in a tryptic digestion resulted in production of subfragment-1 and subfragment-2 as well as heavy meromyosin. Weeds and Pope [41] have recently shown that chymotryptic digestion of polymeric myosin (in 0.12 M NaCl) in the absence of divalent cations produces subfragment-1, whereas the digestion in the presence of divalent cations produces heavy meromyosin; the two regions of myosin which are susceptible to proteolytic cleavage are discriminated by the presence or absence of divalent cations (a few millimolar), and protection of the subfragment-1 site requires the presence of DTNB light chains with intact calcium binding site.

II-3-3 ATPase activity of myosin

It has been demonstrated in several laboratories that the maximum number of ATP binding is 2 moles per mole of myosin and heavy meromyosin. However, it is controversial whether the two binding sites are identical or not; that is, different amplitudes of the transient-phase of P_i production (the phosphate initial burst) [42] during ATP hydrolysis have been reported in literature. Corresponding to these discrepancies, the different schemes of ATP hydrolysis by myosin have been proposed [43-47].

II-4 Interaction between Actin and Myosin

Interaction between F-actin and myosin in the presence of ATP is one of the fundamental process of muscle contraction.

Under physiological salt conditions, namely, 0.1 ∿ 0.15 M KCl and 1 ∿ 2 mM $MgCl_2$ at neutral pH, myosin strongly binds to F-actin and this complex forms precipitates. Szent-Györgyi (1951) [48] found that addition of ATP to F-actin-myosin complex leads to a superprecipitation, *via* clearing phase [49] in which the majority of myosin molecules dissociate from F-actin. This process has been considered to relate to the mechanism of muscle contraction and a great number of studies have been made to elucidate the molecular process of superprecipitation.

II-4-1 Acto-myosin complex

Moore et al. [34] showed by use of three dimensional reconstruction technique of electron micrograph that one subfragment-1 molecule can attach to each of G-actin unit in F-actin. It is now widely accepted that the stoichiometric binding ratio of subfragment-1 to F-actin is one mole of subfragment-1 per mole of actin monomer. Since one myosin or heavy meromyosin has two active sites of binding to F-actin, a question as to the functional significance of duplicate sites in myosin may be raised. Co-operative interaction between subunits of myosin has been actively pursued. The problem about the stoichiometric binding ratio of heavy meromyosin to F-actin has not been understood completely yet. There have been reports that heavy meromyosin can bind only one mole of F-actin monomer [4,50-52] while, there have been also reports that the saturation of actin-heavy meromyosin binding occurs with one mole

of heavy meromyosin per mole of actin dimer [53-55]. It has been recently reported by Highsmith that the binding affinity of heavy meromyosin to F-actin decreases as the molar ratio of heavy meromyosin to actin increases [56].

T.L. Hill [57] considered the statistical problem about the binding of heavy meromyosin to F-actin in the case that two manners of binding of heavy meromyosin are allowed; i.e., single-headed and two-headed bindings (Fig. II-7). He obtained the following relation between the concentration of free heavy meromyosin, c, and the degree of the saturation of the binding of myosin heads to F-actin, θ:

$$\theta = \frac{K_1 c\left\{1 + K_1 c + \sqrt{(1 + K_1 c)^2 + 4K_2 c}\right\} + 2K_2 c}{\left\{1 + K_1 c + \sqrt{(1+K_1 c)^2 + 4K_2 c}\right\}\sqrt{(1+K_1 c)^2 + 4K_2 c}}$$

where K_1 and K_2 are conventional binding equilibrium constants (units M^{-1}) (one head and two heads, respectively). If $K_2 >> K_1$, two-headed binding will predominate when c is small, but single-headed binding will eventually take over as $c \to \infty$. This kind of binding problem has not been taken into account in the earlier analyses of the binding affinity of heavy meromyosin to F-actin.

II-4-2 ATP hydrolysis by actomyosin

The fundamental study of the steady-state kinetics of ATPase activity by acto-heavy meromyosin was made by Eisenberg and Moos [58,59], who showed that two competing reactions are involved; the dissociation of acto-heavy

meromyosin by ATP and the activation of myosin ATPase by actin. More detailed studies of ATP hydrolysis by acto-heavy meromyosin have been made by many workers. Lymn and Taylor [60] have proposed the reaction scheme which involves the following steps: 1) the binding of ATP to acto-heavy meromyosin and subsequent very rapid dissociation of actomyosin, 2) the splitting of ATP on the free myosin, 3) recombination of actin with the myosin-ADP-P_i complex and 4) the displacement of products. It is assumed in this scheme that actin promotes the release of ADP and P_i from myosin. On the other hand, Tonomura and his co-workers [46,53] proposed another scheme in which there are two independent routes in ATP hydrolysis by actomyosin; and it is assumed that the two sites in myosin are not identical and only one site operates during the actomyosin ATP hydrolysis. Up to date, many extended schemes have been proposed [61-63], but no convincing evidence that decides which scheme is correct has not been obtained yet.

II-4-3 Conformational changes in actin filament on the binding of myosin heads

The earlier X-ray studies on muscle at rest and during contraction showed that F-actin does not undergo any large or detectable structural changes [64,65]. Because of lack of the convincing evidence for the conformational change of actin, importance of conformational change in F-actin has been scarcely taken into consideration by researchers

as to the molecular process of muscle contraction.

On the other hand, Offer et al. (1972) [66] showed that the ability of G-actin to activate the ATPase of subfragment-1 is considerably less than the activation obtained with F-actin under identical conditions. They considered three possibilities which would explain the relative impotence of G-actin compared with F-actin; 1) the tertiary structure differs from that of F-actin subunits; 2) the site on F-actin interacting with subfragment-1 may not be confined to a single subunit; 3) conformational changes occur in the subunits of F-actin during the interaction with subfragment-1.

Since Szent-Györgyi and Prior found a rapid exchange of the ADP bound to F-actin during superprecipitation of acto-myosin [67], many workers have been interested in the problem as to what kind of conformational change occurs in actin filaments under influence of myosin [67-69]. Although the observation of the rapid exchange of the bound ADP is recently questioned [70,71], information on specific conformational changes of the proteins during actin-myosin interaction will be indispensable for elucidation of the molecular mechanism of force generation of muscle contraction.

Heavy meromyosin and subfragment-1 are soluble even at low ionic strength and, therefore, has advantage in the spectroscopic studies of the interaction with actin. The first study on conformational changes in actin filaments induced by binding of heavy meromyosin was made by Tawada

(1968) [51]. He observed that the degree of flow birefringence of F-actin solution decreases on addition of heavy meromyosin; the decrease of birefringence is optimal at the molar ratio of heavy meromyosin to actin equal to about 1 : 6; with further increase in heavy meromyosin, the birefringence recovers to the value of F-actin alone. Similar biphasic responses with increasing binding of heavy meromyosin (and/or subfragment-1) have been reported by several workers [72-75]. There have been, however, controversies among their interpretations. Fujime and Ishiwata [72] considered that F-actin becomes most flexible when the molar ratio of heavy meromyosin to F-actin is 1 : 6; whereas, Abe and Maruyama [73] considered that the heavy meromyosin-F-actin complex forms a fragile network in solution. Furthermore, there have been also reports which made doubt on the biphasic change itself [76-79]. Up to date, a unique understanding about the conformational changes of actin filaments on the binding of myosin heads has not been obtained yet. In such a stage, it is desirable to perform a systematic study of conformational changes of actin during interaction of F-actin with myosin heads as well as during G-F transformation of actin.

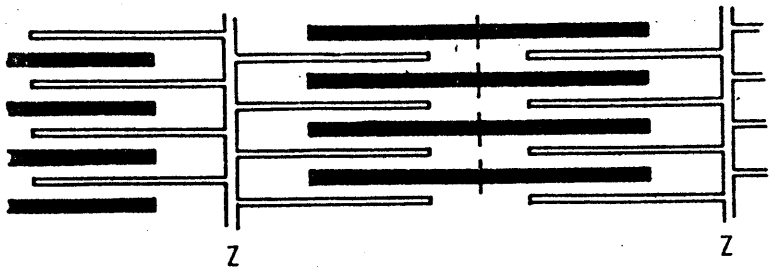

Fig. II-1 A diagrammatic presentation of the structure of striated muscle. Contractile system of striated muscle is formed both with thick filaments(black bars) and thin filaments (horizontal white bars); vertical white bars correspond to Z membanes.

Fig II-2 The structure of thick filament.

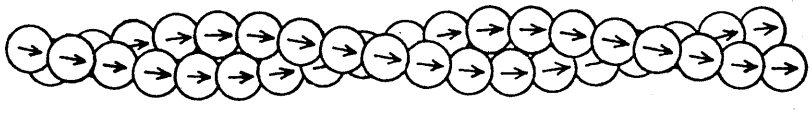

Fig. II-3 The structure of actin filament.

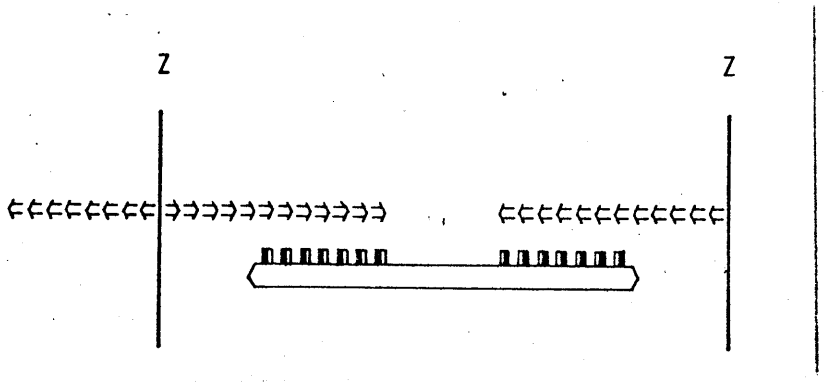

Fig. II-4. Structural polarity in striated muscle

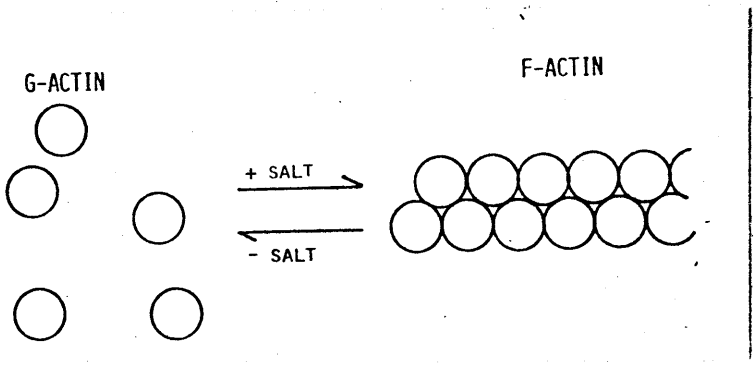

Fig. II-5. G-F transformation of actin

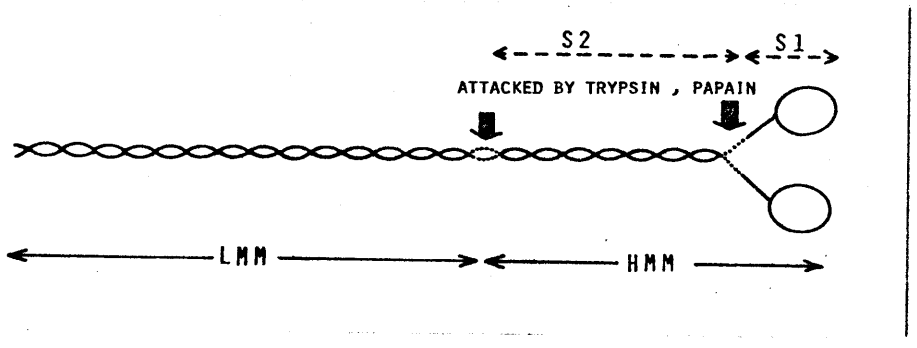

Fig. II-6. Structure of the myosin molecule. HMM; heavy meromyosin. LMM; light meromyosin. S1; subfragment-1. S2; subfragment-2.

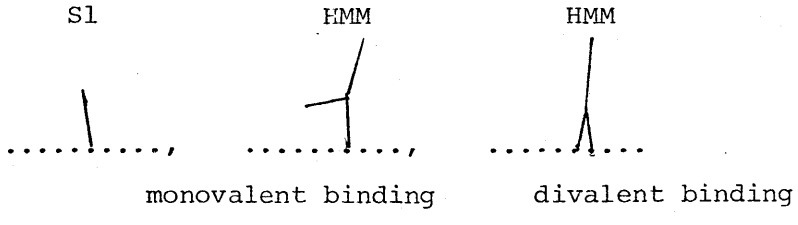

Fig. II-7. Monovalent and divalent bindings of myosin heads to F-actin.

Fig. II-8. Historical survey of studies on muscle proteins

1864	"Myosin"	W.Kühne [30]
1930	Structure of "Myosin"	A.von Muralt & J.T.Edsall [80]
1935	"Myosin" thread	H.H.Weber [81]
1939	ATPase activity of "Myosin"	W.A.Engelhardt et al. [82]
1941	Myosin and superprecipitation	A.Szent-Györgyi & I.Banga [29]
1942	Actin and its G-F transformation	F.B.Straub [13]
1946	Tropomyosin	K.Bailey [83]
	Actomyosin-ATP system	A.Szent-Györgyi [84]
1950	Specific binding of ATP to Actin	F.B.Straub & G.Feuer [14]
1953	Heavy meromyosin	E.Mihalyi et al. [85]
	Subunits of Myosin (Light chain)	T.C.Tsao [86]
1954	Initial burst in Myosin ATPase	A.Weber & W.Hasselbach [42]
	Hydrolysis of ATP by Myosin	D.E.Koshland et al. [87]
	Sliding filament model	A.Huxley & Niedergerke [2]/ H.Huxley & J.Hanson [1,88]
1957	Moving cross-bridge model	A.Huxley [5]
1959	Thermodynamics of Actin polymerization	F.Oosawa et al. [20,24]
1962	Myosin subfragment-1	H.Mueller & S.V.Perry [89]
	Efficiency of energy conversion	D.F.Cain & R.E.Davies [90]
1963	Double-helical structure of thin filament	J.Hanson & J.Lowy [11]
	"Arrowhead" structure of F-actin*Myosin	H.E.Huxley [4]
1965	Troponin	S.Ebashi & A.Kodama [91]
	Heat production in muscle contraction	A.V.Hill [92]
1967	Fine structure of thick filament	H.Huxley & W.Brown [65]
1969	Two heads of a myosin molecule	S.Lowey et al. [33]
1968-71	Three components of Troponin	D.J.Hartshone et al. [93]/ S.Ebashi et al. [94]/ M.C.Schaub & S.V.Perry [95]
1970	Fine structure of F-actin*S1	P.B.Moore et al. [34]
1970-72	Reaction intermediate of Myosin	Y.Tonomura et al. [46]/ E.W.Taylor et al. [43,44]
1972	Amino acid sequence of Tropomyosin	J.Sodek et al. [96]
1973	Amino acid sequence of Actin	M.Elzinger et al. [7]
1974	Amino acid sequence of Troponin-C	J.H.Collins et al. [97,98]

III FLUOROMETRY

III-1 Introduction

The first report about fluorescence was published by Herschel in 1845 [99]. He found that, when the aqueous solution of quinine sulfonate was exposed to the sunlight, it emitts a pale and non-polarized light. The important study which succeeded to this discovery was made by Stokes [100], who noted an important relation between the wavelength of absorption and that of fluorescence emitted; i.e., the so-called Stokes law. Based on this observation, he firstly introduced the idea that the two processes of absorption and emission exist in the interaction of materials with photons. Fluorescence emission from an excited molecule is usually competed by the radiationless processes such as intersystem crossing, quenching and excitation-energy transfer. These processes are strongly dependent on the property of the microenvironment around the excited molecule. Therefore, valuable information about the microenvironment can be obtained from the measurement of fluorescence spectra, lifetimes and quantum yields.

In 1920, Weigert [101] discovered that, when a viscous solution containing fluorescent molecules is illuminated with polarized lights, it emits a partially polarized fluorescence. Perrin [102] showed that the rotational diffusion constant of a fluorescent molecule can be determined by measuring fluorescence polarization. The first application

of the fluorescence depolarization method to a biological system was made by G. Weber (1952)[103]. Recently developed pulse-fluorometry permits direct measurements of time-dependent fluorescence polarization [104-106].

In this chapter, brief descriptions about fluorescence kinetics (Section III-2) and about fluorescence anisotropy decay (Section III-3) will be presented.

III-2 Fluorescence Kinetics

III-2-1 General principle

When a molecule is excited by visible or ultraviolet lights, the electronic state of the molecule goes to an upper singlet energy state S_n. Then it rapidly comes down the lowest excited state S_1 by losing the excess energy into the surrounding medium. This radiationless process usually occurs within 10^{-10} sec. From the excited equilibrium state, the molecule may go to any of the rotational and vibrational levels of the ground electronic state S_0 by a radiative process (fluorescence) or by radiationless processes. One of the radiation processes is the so-called internal conversion in which the excited molecule goes to the upper vibrational levels of the ground state and finally to the equilibrium state by interacting with other molecules (Fig. III-1). The rate constant of the radiative process varies from 10^{-9} to 10^{-6} sec, which is characterized by the chromophore. In addition, the excited molecule can

go to a triplet state by intersystem crossing, and then it may be deactivated through a still slower process (phosphorescence, internal conversion). The rate of the deactivation of the lowest excited state may be given by the following equation:

$$\frac{d[C^*]}{dt} = -(k_F + k_C + k_{isc})\,[C^*] \qquad \text{(III-1)}$$

Here $[C^*]$ means the concentration of the excited molecule at a given time t, k_F is the radiative rate constant corresponding to fluorescence emission, k_C is the rate constant of internal conversion and k_{isc} is the rate constant of intersystem crossing. The experimental fluoresence lifetime is given by the relation:

$$\tau = (k_F + k_C + k_{isc})^{-1} \qquad \text{(III-2)}$$

The fluorescence quantum yield η is the ratio of the number of photons emitted to the number of photons absorbed;

$$\eta = k_F / (k_F + k_C + k_{isc}) = \tau/\tau_0 \qquad \text{(III-3)}$$

Here $\tau_0 = k_F^{-1}$ is the natural fluorescence lifetime.

III-2-2 Relationship between absorption intensity and natural fluorescence lifetime

The fundamental relationship between the transition probabilities for induced absorption and emission and that for spontaneous emission has been drived by Einstein [107]: The spontaneous emission probability is directly proportional to the corresponding absorption probability and to the

third power of the frequency of the transition. Einstein's equations are applicable only to atomic system, whose transitions are sharp. Stricker and Berg [108] have drived the formula which is applicable to the molecules with broad absorption bands. The natural lifetime is given by the following relation:

$$1/\tau_0 = 2.88 \times 10^{-9}\ n^2\ \langle \nu_F^{-3} \rangle_{av}^{-1} \int \varepsilon(\nu)\ d(\ln\nu) \quad \text{(III-4)}$$

where n is the refractive index of the solvent; ε the molar extinction coefficient of the solute; ν the wave number; the integral is over the whole of the electronic absorption band corresponding to the transition $S_0 \rightarrow S_1$; $\langle \nu_F^{-3} \rangle_{av}$ is the mean value of ν_F^{-3} in the fluorescence spectrum $F(\nu)$,

$$\langle \nu_F^{-3} \rangle_{av} = \int F(\nu)\ \nu^{-3}\ d\nu\ /\ \int F(\nu)\ d\nu \quad \text{(III-5)}$$

Equation (III-4) is valid for the molecule whose lowest singlet electronic absorption band is fairly strong. If there is a strong overlapping of the bands corresponding to the electronic transitions $S_0 \rightarrow S_1$ and $S_0 \rightarrow S_2$, an apparent discrepancy will appear between the natural lifetime estimated using Eqn (III-3) and that estimated using Eqn (III-4). Hidden transitions may be revealed by this means.

III-2-3 The effect of molecular interaction upon the fluorescence decay

We consider here a case that the fluorescent molecule has two ways to interact with its surrounding. Corresponding

to these ways, there are two kinds of the configurations by which the correlation between the fluorescent molecule and the other molecules are given. We designate the corresponding configurations by A_1 and A_2. When the fluorescent molecule is in the excited state, the configurations may be designated by A^*_1 and A^*_2. Then the scheme which is necessary for the interpretation of fluorescence decay can be expressed as follows:

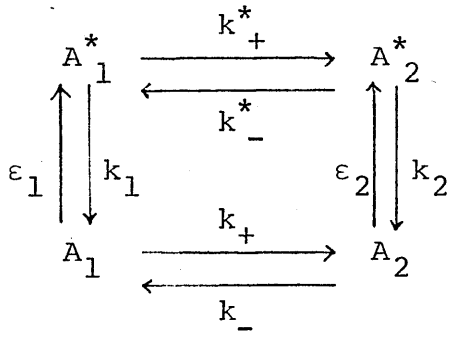

(III-6)

where $\varepsilon_{1,2}$ are the rates of photon absorption and are proportional to the molar extinction coefficients of the fluorescent molecule; $k_{1,2}$ are the sums of the rate constants of decativation by radiative and non-radiative processes and the inverses of $k_{1,2}$ are the fluorescence lifetimes $\tau_{1,2}$ which would be observed if the exchange reaction did not occur in the excited state; $k_{+,-}$ and $\overset{*}{k}_{+,-}$ are the rates of exchange reactions in the ground state and those in the excited state, respectively.

The following reactions can be described by the above scheme [109].

i) Quenching of fluorescence [110]: A fluorescent molecule F becomes non-fluorescent product when it interacts with a quencher Q;

$$\overset{*}{A}_1 \;:\; \overset{*}{F} + Q$$

$$\overset{*}{A}_2 \;:\; \overset{*}{F}Q \qquad \text{(III-7)}$$

The rate constant $\overset{*}{k}_+$ must be replaced with the product of the concentration of Q and the association rate constant of quencher to the excited molecule: $\overset{*}{\kappa}[Q]$. The rate of deactivation of $\overset{*}{A}_2$ (or $\overset{*}{F}Q$) may be extremely rapid due to the presence of the strong radiationless transition.

ii) Acid-base reaction [111-114]: The fluorescence emission from aromatic acids or bases may be affected by the reactions of protonation and deprotonation in the excited state;

$$\overset{*}{A}_1 \;:\; \overset{*}{F}H\cdot H_2O \qquad (\text{or } \overset{*}{F}\cdot H_2O)$$

$$\overset{*}{A}_2 \;:\; \overset{*}{F}^- + H_3O^+ \qquad (\text{or } \overset{*}{F}H^+ + OH^-) \qquad \text{(III-8)}$$

iii) Complex formation (Exciplexes and excimers) [115-117]: An excited molecule may form a fluorescent complex with another non-excited molecule.

$$\overset{*}{A}_1 \;:\; \overset{*}{F} + B \qquad (\text{or } \overset{*}{F} + F)$$

$$\overset{*}{A}_2 \;:\; \overset{*}{F}\cdot B \qquad (\text{or } \overset{*}{F}\cdot F) \qquad \text{(III-9)}$$

There have been many reports that fluorescence decays from the chromophores which are intrinsically or extrinsically introduced into protein can be described by the scheme of Eqn (III-6); that is, there are intra- (or inter-)molecular interactions which are comformation dependent [118,119].

The rate equations for the configurations $\overset{*}{A}_1$ and $\overset{*}{A}_2$

are given by, respectively:

$$\frac{d[\overset{*}{A}_1]}{dt} = \varepsilon_1[A_1] - (k_1 + \overset{*}{k}_+)[\overset{*}{A}_1] + \overset{*}{k}_-[\overset{*}{A}_2]$$

$$\frac{d[\overset{*}{A}_2]}{dt} = \varepsilon_2[A_2] - (k_2 + \overset{*}{k}_-)[\overset{*}{A}_2] + \overset{*}{k}_+[\overset{*}{A}_1] \qquad \text{(III-10)}$$

where $[A_{1,2}]$ and $[\overset{*}{A}_{1,2}]$ are the concentrations of $A_{1,2}$ in the grand states and in the excited states, respectively. The solution for steady-excitation is obtained by setting the left-hand sides equal to zero:

$$[\overset{*}{A}_1] = \{(k_2+\overset{*}{k}_-)\varepsilon_1[A_1] + \overset{*}{k}_-\varepsilon_2[A_2]\}/\{(k_2+\overset{*}{k}_-)(k_1+\overset{*}{k}_+) - \overset{*}{k}_+\overset{*}{k}_-\}$$

$$[\overset{*}{A}_2] = \{(k_1+\overset{*}{k}_+)\varepsilon_2[A_2] + \overset{*}{k}_+\varepsilon_1[A_1]\}/\{(k_1+\overset{*}{k}_+)(k_2+\overset{*}{k}_-) - \overset{*}{k}_+\overset{*}{k}_-\} \qquad \text{(III-11)}$$

The fluorescence quantum yield η is given by

$$\eta = \{k_{f1}[\overset{*}{A}_1] + k_{f2}[\overset{*}{A}_2]\}/\{\varepsilon_1[A_1] + \varepsilon_2[A_2]\} \qquad \text{(III-12)}$$

where $k_{f1,f2}$ are the rates of deactivation by radiation process. From Eqn (III-11);

$$\eta = \frac{\varepsilon_1[A_1]\{k_{f1}(k_2+\overset{*}{k}_-) + k_{f2}\overset{*}{k}_+\} + \varepsilon_2[A_2]\{k_{f2}(k_1+\overset{*}{k}_-) + k_{f1}\overset{*}{k}_-\}}{\{(k_2+\overset{*}{k}_-)(k_1+\overset{*}{k}_+) - \overset{*}{k}_+\overset{*}{k}_-\}\{\varepsilon_1[A_1] + \varepsilon_2[A_2]\}} \qquad \text{(III-13)}$$

For quenching of fluorescence, this becomes:

$$\eta = \eta_a\,(1 + \tau_a\overset{*}{\kappa}[Q])^{-1}\,(1 + \varepsilon_2\kappa[Q]/\varepsilon_1 k_-)^{-1} \qquad \text{(III-14)}$$

Here η_a and τ_a are the fluorescence quantum yield and lifetime obtained in the absence of the quencher, respectively; and, $\kappa[Q] = k_+$.

The fluorescence decay after pulse-excitation is obtained by setting ε_1 and ε_2 in Eqn (III-11) equal to zero at $t > 0$. The solutions are:

$$[\overset{*}{A}_1] = \alpha_{11}\exp(-\lambda_1 t) + \alpha_{12}\exp(-\lambda_2 t)$$
$$[\overset{*}{A}_2] = \alpha_{21}\exp(-\lambda_1 t) + \alpha_{22}\exp(-\lambda_2 t) \qquad \text{(III-15)}$$

where

$$\lambda_{1,2} = \frac{1}{2}\{(\overset{*}{k}_1 + \overset{*}{k}_2 + \overset{*}{k}_+ + \overset{*}{k}_-) \pm \sqrt{(\overset{*}{k}_1 - \overset{*}{k}_2 + \overset{*}{k}_+ - \overset{*}{k}_-)^2 + 4\overset{*}{k}_+\overset{*}{k}_-}\} \qquad \text{(III-16)}$$

The coefficients α_{ij} in Eqn (III-15) are the functions of the rate constants $k_{1,2}$, $k_{+,-}$ and $\overset{*}{k}_{+,-}$ [110]. The values of these rate constants, if determined experimentally, will bring about valuable knowledge on the dynamic property of protein conformation.

III-3 Decay of Fluorescence Anisotropy

III-3-1 Experimental definition of fluorescence anisotropy

Let x, y, and z be a space-fixed coordinate system. Let the fluorescent sample be placed at the origin (Fig. III-2). Let the exciting lights travel along the x direction, polarized along the z axis. The fluorescence, polarized along the z axis (I''), and along the x axis ($I^{\perp}$), will be observed along the y axis. Then the fluorescence (polarization) anisotropy is given by the following expression [120]:

$$r = (I'' - I^{\perp})/(I'' + 2\,I^{\perp}) \qquad \text{(III-17)}$$

For an isotropic medium in which the fluorescent chromophore distributes in the all direction with equal probability, the fluorescence anisotropy is a function of the orientational correlation between the absorption oscillator at the time of absorption and the emission oscillator at the time of emission. On the other hand, the quantity $I'' + 2I^{\perp}$ $(= S)$, which is called the total fluorescence intensity, is independent of the orientational distribution of the emission oscillator [121].

III-3-2 Fluorescence anisotropy in the absence of rotaion

Let us consider the case that no appreciable rotation of the chromophore occurs during the lifetime of the excited state, as in the case of a highly viscous medium. For an isotropic medium, the probability of excitation is proportional to $\cos^2\theta$, where θ is the angle between Oz and the direction OA of the absorption oscillator. Thus the orientation distribution of the excited molecule is expressed as follows:

$$f(\theta,\psi) = (3/4\pi)\cos^2\theta \; ; \quad \int f(\theta,\psi)\, d\Omega(\theta,\psi) = 1 \qquad \text{(III-18)}$$

where ψ is the azimuth angle of the direction OA. If the orientation OE of the emission oscillator is parallel to the direction OA, the principal components of polarized fluorescence is:

$$I'' = \varepsilon \int \cos^2\theta \; f(\theta,\psi)\, d\Omega(\theta,\psi)$$
$$I^{\perp} = \varepsilon \int \sin^2\theta \cos^2\psi \; f(\theta,\psi)\, d\Omega(\theta,\psi) \qquad \text{(III-19)}$$

where ε is a constant. From Eqn (III-18),

$$I'' = \varepsilon/5, \quad I^{\perp} = \varepsilon/15 \qquad \text{(III-20)}$$

Therefore the fluorescence anisotropy reduces to a simple quantity:

$$r = 2/5 \qquad \text{(III-21)}$$

Let us consider the case that the absorption oscillator and the emission oscillator are not the same, but subtend an angle of β with respect to each other. In this case, the probability to find an emission oscillator at the orientation (θ,ψ) is [104]:

$$f(\theta,\psi) = (3/4\pi)(\cos^2\theta\cos^2\beta + \frac{1}{2}\sin^2\theta\sin^2\beta) \qquad \text{(III-22)}$$

By putting this in Eqn (III-19), one will obtain the principal components of polarized fluorescence:

$$I'' = \frac{\varepsilon}{3} + \frac{2\varepsilon}{5}\cos^2\beta \quad , \quad I^{\perp} = \frac{2\varepsilon}{5} - \frac{\varepsilon}{5}\cos^2\beta \qquad \text{(III-23)}$$

Thus the fluorescence anisotropy is:

$$r = \frac{2}{5}\left(\frac{3}{2}\cos^2\beta - \frac{1}{2}\right) \qquad \text{(III-24)}$$

This quantity is called the fundamental anisotropy r_0. As $0 \leq \beta \leq \pi/2$,

$$-\frac{1}{5} \leq r_0 \leq \frac{2}{5} \qquad \text{(III-25)}$$

In general, β or r_0 is a function of the exciting wavelength. The so-called polarization spectrum of dyes is the set of values of r_0 obtained on varing continuously the exciting wavelength. The polarization spectrum can be interpreted on the picture that there are several absorption oscillators

making variable angles with the emission oscillator.

III-3-3 Depolarization by isotropic rotation

Let us consider the case that the fluorescent molecule undergoes an infinitesimal rotation with angular displacement $\Delta\alpha_1$ immediately after excitation of the molecule. Let $(I'')_0$ and $(I^{\perp})_0$ be the principal components of polarized fluorescence which would be observed if such a rotation is absent; and, let $(I'')_1$ and $(I^{\perp})_1$ be those observed in the presence of the rotation. Taking account of isotropic property of the rotation, one will obtain the following relations:

$$(I'')_1 = (I'')_0 \cos^2\Delta\alpha_1 + (I^{\perp})_0 \sin^2\Delta\alpha_1 \qquad \text{(III-26)}$$

$$(I^{\perp})_1 = (I^{\perp})_0 \cos^2\Delta\alpha_1 + (1/2)\{(I'')_0+(I^{\perp})_0\}\sin^2\Delta\alpha_1$$

Thus, the fluorescence anisotropy after the rotation is:

$$r_1 = \{(I'')_1 - (I^{\perp})_1\}/\{(I'')_1 + 2(I^{\perp})_1\}$$

$$= \frac{(I'')_0 - (I^{\perp})_0}{(I'')_0 + 2(I^{\perp})_0}\left(\frac{3}{2}\cos^2\Delta\alpha_1 - \frac{1}{2}\right)$$

$$= r_0\left(\frac{3}{2}\cos^2\Delta\alpha_1 - \frac{1}{2}\right) \qquad \text{(III-27)}$$

If infinitesimal rotations are repeated, the fluorescence anisotropy will be given by the following expression:

$$r_n = r_0 \prod_{i=1}^{n}\left(\frac{3}{2}\cos^2\Delta\alpha_i - \frac{1}{2}\right) \qquad \text{(III-28)}$$

III-3-4 Rotational Brownian motion of spherical macromolecules

Let us consider a small solid sphere of volume V immerged

freely in a liquid of viscosity η and of temperature T. Because of the thermal agitation, this sphere turns all the time in perfectly irregular way. The average of the square of the angle $\Delta\alpha$ by which the sphere turns in time Δt, around some axis, e.g. x-axis, is given as follows (Einstein equation) [122]:

$$\overline{(\Delta\alpha_x)^2} = (kT/3V\eta)\,\Delta t \qquad \text{(III-29)}$$

where k is Boltzmann constant. Due to rotational Brownian motion, the direction of emission oscillator of the chromophore which is attached confirmly to the sphere will make an angle $\Delta\theta$ with its initial orientation:

$$\overline{\Delta\theta^2}\ (= 2\,\overline{\Delta\alpha^2}) = \frac{2}{3}\frac{kT}{V\eta}\,\Delta t \qquad \text{(III-30)}$$

From Eqn (III-27), it is clear that the fluorescence anisotropy at time Δt after excitation of fluorescent probe can be expressed as follows:

$$r(\Delta t) = r_0\,(1 - \frac{3}{2}\,\overline{\Delta\theta^2}) = r_0\,(1 - \frac{kT}{V\eta}\,\Delta t) \qquad \text{(III-31)}$$

At time $t = n\cdot\Delta t$ after excitation, it becomes:

$$r(t) = r_0\,(1 - \frac{kT}{V\eta}\,\Delta t)^n = r_0\,(1 - \frac{kT}{V\eta}\,\Delta t)^{t/\Delta t} \qquad \text{(III-32)}$$

In limitation $\Delta t \longrightarrow 0$, the following expression is obtained:

$$r(t) = r_0\,\exp(-\frac{kT}{V\eta}\,t) = r_0\,\exp(-t/\Theta) \qquad \text{(III-33)}$$

where Θ is the rotational correlation time.

The macromolecule in solution has a few layers of

hydration around its surface. Some layers of hydration are considered to be bound confirmly to the surface and thus to rotate together with the macromolecule. The kinetic volume V which may be obtained from the anisotropy decay measurement must be considered as the sum of the volume of a dried macromolecule and the volume of the surrounding layers of hydration [123]

$$V = M\ (v + h)/N_a \qquad \text{(III-34)}$$

where N_a is the Avogadro number, M is the molecular weight of the macromolecule and v is the dry volume of 1 g of the macromolecule. h represents the contribution from the hydration; values between 0.4 v and 0.6 v are used for most proteins.

III-3-5 Rotational Brownian motion of ellipsoidal molecules

The general formula of fluorescence depolarization for an ellipsoid molecule was established by Perrin [124,125]. Many workers have considered the more restricted case in order to obtain the formula by which the shapes of biological macromolecules can be estimated [104]. For an ellipsoid, the fluorescence anisotropy decay is in general a sum of five exponentials: For a symmetric ellipsoid, the number of exponentials is reduced to three [126]:

$$r(t) = A_1 \exp(-t/\theta_1) + A_2 \exp(-t/\theta_2) + A_3 \exp(-t/\theta_3) \qquad \text{(V-35)}$$

The three correlation times $\theta_{1,2,3}$ may be written as follows:

$$\theta_1 = (6D^{\perp})^{-1},\quad \theta_2 = (5D^{\perp} + D'')^{-1},\quad \theta_3 = (2D^{\perp} + 4D'')^{-1} \qquad \text{(V-36)}$$

where D" and $D^{\perp}$ are the principal rotational-diffusion

coefficients which are functions of the axial ratio of the ellipsoid [104]. The coefficients A_1, A_2, A_3 appearing in Eqn (III-35) depend on the orientations of the absorption and emission oscillators with respect to the principal axes of the ellipsoid. They may be expressed using the angles shown in Fig. (III-3) as follows [127]:

$$A_1 = \frac{1}{10}(3\cos^2\delta_1 - 1)(3\cos^2\delta_2 - 1)$$

$$A_2 = \frac{3}{10}\sin 2\delta_1 \sin 2\delta_2 \cos\phi \qquad \text{(III-37)}$$

$$A_3 = \frac{3}{10}\sin^2\delta_1 \sin^2\delta_2 \cos 2\phi$$

If the fluorescent probe is attached to the macromolecule with random orientation, A_1, A_2, A_3 have to be averaged:

$$A_1 = A_2 = 2A_3 = \frac{2}{5} r_0 \qquad \text{(III-38)}$$

III-3-6 Intramolecular motion

Many proteins have their own form with hydrogen bonds and hydrophobic forces. The molecular backbone as whole may be rigid, but some side chains may have rotational freedom about various C-C bonds. The probe may be permitted to move in the protein. This intramolecular motion as well as the rotational motion of the protein itself will contribute to the fluorescence depolarization.

When the probe is allowed to rotate around the axis which is fixed in the spherical protein, the anisotropy decay is given by the following formula [128,129]:

$$r(t) = \exp(-t/\theta_p) \{ A_1 + A_2 \exp(-2t/3\theta_I) + A_3 \exp(-t/6\theta_I) \} \quad \text{(III-39)}$$

where θ_p is the rotational correlation time of the protein and θ_I is the correlation time of the intramolecular motion.

III-3-7 The presence of heterogeneity in the excited state

In the above discussions, we have assumed implicitly that the fluorescent probe has a single fluorescence lifetime. There occasionally exists heterogeneity in the excited state of the probe. This may result from the existence of more than one conformation around the labelling site of the protein. In such a case, the total fluorescence decay $s(t)$ $(= I_{\parallel}(t) + 2\, I_{\perp}(t))$ may be not described with a single-exponential decay but with a sum of exponential decays:

$$s(t) = \sum_{k=1}^{p} \alpha_k \exp(-t/\tau_k) \quad \text{(III-40)}$$

Here τ_k is the decay time of the excited state corresponding to the k-th local conformation and the amplitude α_k may be proportional to the fraction of the k-th conformation. On the other hand, the anisotropy decay corresponding to the k-th conformation may be different from those corresponding to the other conformations. Now we shall restrict our discussion to the case that fluorescent probes bind

confirmly to a symmetric-ellipsoidal macromolecule with several manners of binding; e.g., there are several binding sites in the macromolecule, or there are several orientations of the probe with respect to the macromolecule in spite of the single binding site. Then the k-th anisotropy decay $r_k(t)$ may be expressed by the following expression:

$$r_k(t) = \sum_{i=1}^{3} A_{ki} \exp(-t/\theta_i) \qquad \text{(III-41)}$$

where θ_i are the correlation times as given in Eqn (III-36). Let $d_k(t)$ be the product of $r_k(t)$ and $s_k(t) = \alpha_k \exp(-t/\tau_k)$. Then the difference fluorescence decay $d(t)$ ($= I''(t) - I^{\perp}(t)$) is given by the following sum [130]

$$d(t) = \sum_{k=1}^{p} d_k(t) = \sum_{k=1}^{p} r_k(t) \cdot s_k(t)$$

$$= \sum_{k=1}^{p} \sum_{i=1}^{3} A_{ki} \alpha_k \exp\{-(1/\tau_k + 1/\theta_i)t\} \qquad \text{(III-42)}$$

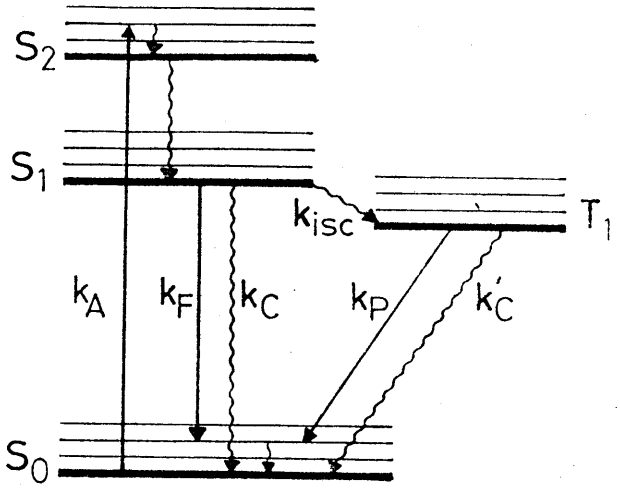

Fig. III-1. Jablonski diagram

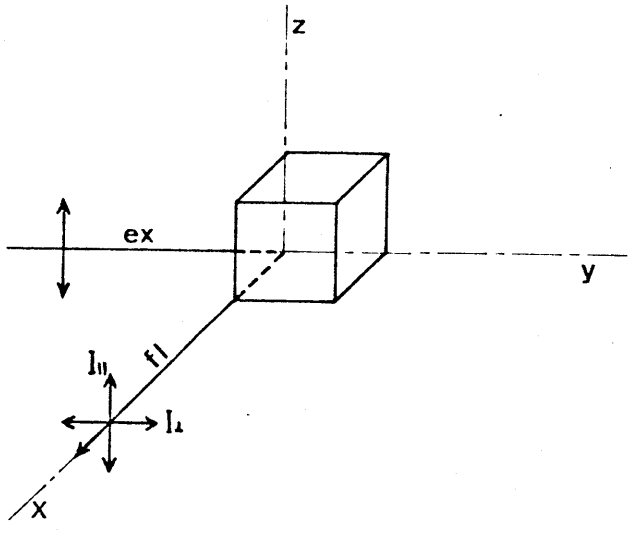

Fig. III-2. Experimental definition of the polarized components of the fluorescence.

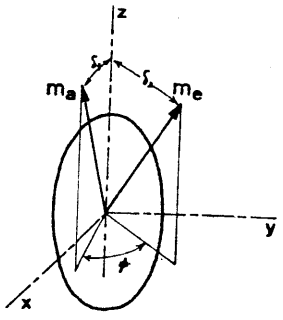

Fig. III-3. Directions of absorption oscillator OA and of emission oscillator OE with reference to the axis of an ellipsoidal molecule.

IV METHODS AND MATERIALS

IV-1 Methods

IV-1-1 Steady-excitation fluorometry

Steady excitation fluorometry was made with Hitachi MPF-2A spectrofluorometer. The sample cuvette used was of the dimension of $1 \times 1 \times 4$ cm^3 or $0.3 \times 0.3 \times 3$ cm^3. Variation in the incident photon flux as a function of wavelength was corrected using rhodamine B in ethylene glycol as a quantum counter [131]. Emission spectra were corrected with the fluorescence of β-naphthol in acetate buffer [132]. Quantum yields were determined with quinine sulfonate in 0.1 N H_2SO_4 as a standard of quantum yeild 0.5 0 [133]. Fluorescence polarization anisotropy r was determined as follows [134];

$$r = \frac{I'' - G I^{\perp}}{I'' + 2 G I^{\perp}} \qquad \text{(IV-1)}$$

where I'' and $I^{\perp}$ were the fluorescence intensities of vertically and horizontally polarized components obtained after the sample solution being excited with vertically polarized light; G was a correction factor which compensates for a degree of polarization added by the mirrors and grating in the emission monochrometer.

IV-1-2 Pulse-excitation fluorometry

Determination of transient fluorescence was performed with a single-photoelectron counting apparatus consisting

of ORTEC light pulser 9354, RCA 8850 photomultiplier, electronic NIM modules of the ORTEC 9200 system and Cambera 8100 multi-channel analyser. The block diagram of the system is shown in Fig. IV-1. The power supplied voltage of the light pulser was 7-10 kV, at which 10,000 to 20,000 flashes were produced per second. Electric spark in air (1 atm) was used for excitation (Fig. IV-2). The N_2 emission at 337 nm was isolated with a Koshin 337 interference filter ($\Delta\lambda$ = 8 nm) or a combination of Nikon U-35 glass filter and $NiSO_4$ solution filter; the N_2 emission at 358 nm was isolated with MTO-357 interference filter. The photomultiplier was operated at 2.4 kV. Fluorescence emission from the sample cuvette (1 × 1 × 4 cm^3) was viewed through Spex monochrometer "MINIMATE" and/or a series of Fuji-Film SC cut-off filters. Temperature in the cuvette was controlled within $\pm$ 0.5 °C,

One of signals furnished from the Timing Pickoff unit of the light pulser was used for identification of the exact time at which the light pulse was generated. The other one was used to monitor the pulse-height of the output signal. The time at which fluorescence induced ejection of a photoelectron was identified by the signal from the anode of the phototube. The strobe circuit, which composed of the preamplifier and single-channel analyser, analysed the signal from the 12-th dynode of the phototube. Only when the energy was within the range of amplitude corresponding to single-photoelectron events, this circuit allowed the time-to-amplitude converter to furnish the timing information

to the MCA memory. The time axis for the multichannel analyser was calibrated using ORTEC 425 delay line. Linearity between the time after excitation and the channel number of the MCA memory was checked with the fluorescence decays of quinine sulfonate in 0.1 N N_2SO_4 and of N-(1-pyrenyl) methyliodoacetate in ethyleneglycol (Fig. IV-3).

In measurement of fluorescence anisotropy decay, the polarizer holder in the excitation side was rotated back and forth in a plane transverse to the light path; and, the fluorescence emission polarized vertically was observed. In this system, complication in definition of fluorescence anisotropy due to difference of transmitance between two principal components of polarized lights in the monochrometer could be avoided. The principal components I" and $I^{\perp}$ of polarized fluorescence were observed alternatively at intervals of one minute and stored in separate quarters of the MCA memory respectively. The polarizer used was prepared by streching poly-vinylalcohol film permeated with iodine in one direction [135]. The polarizer thus obtained transmitted 42-52 % at 315-500 nm when the axis of the polarizer was set in parallel to the direction of polarization of incident beam and less than 0.2 % at 280-500 nm in perpendicular.

Fluorescence emission spectra corresponding to any time window during the decay (time-resolved spectra)[136] were obtained as follows: The signals from the time-to-amplitude converter were sent to the discriminaters which selected a time window during the decay; the signals after

the discrimination were collected in MCA which was set in the mode of multichannel scalling; a grating in the monochrometer was automatically rotated so that the channel number in MCA corresponded to the emission wavelength linearly.

IV-1-3 Miscellaneous techniques

Absorption spectra were measured with Zeiss PMQ-II spectro-photometer. The sample cuvette used was of a dimension of $1 \times 1 \times 4$ cm^3 or $0.5 \times 1 \times 4$ cm^3.

The ATPase activities of heavy meromyosin and myosin subfragment-1 in the absence and in the presence of F-actin were measured at 25 °C. After the reaction was stopped by addition of trichloroacetic acid, the liberated inorganic phosphate was assayed according to the method of Martin and Doty [137].

SDS polyacrylamide gel electrophoresis was performed according to the method of Weber and Osborn [138]. The gel of 7.5 % acrylamide was polymerized in the buffer containing 0.1 M Na-phosphate (pH 7.0). Samples were incubated with 1 % SDS and 1 % 2-mercaptoethanol for 3-5 min in boiling water. Running buffer contained 0.1 % SDS and 0.1 M Na-phosphate (pH 7.0). The gel was stained with coomasie brilliant blue. Densitometric measurement of SDS-gel electrophoresis patterns was performed with Gilfold 6050.

Viscosity of actin solution was measured with an Oswald-type viscometer.

IV-2 Preparation Method of Muscle Proteins

IV-2-1 Introduction

All the muscle proteins were extracted from rabbit back and leg striated muscle, in which red muscle was removed. Distilled and ion-exchanged water was used in the preparation of dried muscle and myosin; doubly distilled water was used in the preparation of actin. Purity of the proteins obtained was checked by use of SDS gel electrophoresis.

IV-2-2 Actin

Rabbit dried muscle was prepared by the method of Straub [6] with the following modification; tropomyosin and troponin were removed before the acetone treatment of the myosin-extracted minced muscle [139].

In the preparation of the conjugates of actin with PM and ANM, the following procedure was used for purification of actin. G-actin was extracted with 120 ml of doubly distilled water from 6 g of the acetone powder at 0 °C. After clarification, the extract was made up to 30 mM KCl so that actin polymerized: The partial polymerization served to remove tropomyosin-like contaminatant [140]. F-actin thus obtained was sedimented by centrifugation at 5×10^4 rpm for 60 min. F-actin pellet was homogenized and depolymerized to G-actin in 0.2 mM ATP solution containing 0.1 mM $MgCl_2$, 0.05 mM EGTA and 2 mM Imidazole-HCl (pH 7.0) [141].

In the preparation of the conjugates of actin with PMIA and PIAA, another procedure was used for purification of actin. The extract of G-actin was made up to 0.1 M KCl so that actin polymerized. After one hour, the concentration of KCl was increased up to 0.5 M KCl; this process served to remove tropomyosin-like contaminatant [142]. Polymerized actin was sedimented by centrifugation at 4.5×10^4 rpm for 60 min. F-actin pellet obtained was washed with 0.1 M KCl solution and then dissolved in 0.2 mM ATP solution containing 0.1 mM $CaCl_2$, 1 mM bicarbonate and 1 mM sodium azide. For further purification of actin, the cycle of polymerization (0.1 M KCl) and depolymerization at low ionic strength was performed.

The protein concentration of actin was determined by biuret reaction. The molecular weight of actin was taken to be 4.23×10^4 [7].

IV-2-3 Myosin

Myosin was prepared by the method of A. Szent-Györgyi [48] with slight modifications[143]. Myosin was extracted with 0.3 M KCl, 0.15 M phosphate buffer (pH 6.3) from minced muscle at 0 °C for 15 min. After clarification, the extract solution was diluted 15 fold with cold water. Aggregated myosin was collected by decantation and by centrifugation at 5000 rpm for 15 min, and washed with 30 mM KCl (pH 6.5) and then suspended in 0.3 M KCl (pH 6.7). This solution was centrifuged at 10,000 rpm for 60 min and the supernatant obtained was diluted 10 fold with cold water. Aggregated

myosin was again collected and resuspended in 0.5 M KCl or 0.5 M NaCl (pH 7.0). Finally the myosin solution was clarified by centrifugation at 50,000 rpm for 60 min. Purified myosin was preserved in a 50 % glycerine solution at -20 °C. The concentration was determined from ultraviolet absorbance, using an extinction coefficient $E^{1\%}_{280\ nm}$ = 5.6 cm^{-1} [144].

IV-2-4 Heavy meromyosin

Two kinds of heavy meromyosin were prepared. The one was obtained by tryptic digestion of myosin; heavy meromyosin(TR). The other one was obtained by chymotryptic digestion; heavy meromyosin(CT).

(i) Heavy meromyosin(TR)

Heavy meromyosin(TR) was prepared according to the method of Lowey and Cohen [32]. Digestion of purified myosin with trypsin (Sigma Chemical Co) was carried out at 20 °C for 5 min in the presence of 0.5 M KCl, 1 mM EDTA (or 1 mM $MgCl_2$), 10 mM phosphate buffer (pH 7.0). The weight ratio of trypsin to myosin was 1/500 to 1/200. The reaction was stopped by addition of trypsin inhibitor (Sigma Chemical Co.); The weight ratio of trypsin inhibitor to trypsin was 1.3 to 3.0. Then the solution was dialysed against 30 mM KCl, 1 mM $MgCl_2$ and 3 mM phosphate buffer (pH 6.4). Heavy meromyosin(TR) was separated from insoluble materials by centrifugation at 50,000 rpm for 60 min and then purified by ammonium-sulfate fractionation

between 45 % and 55 % saturation. The concentration of heavy meromyosin(TR) was determined by biuret reaction.

(ii) Heavy meromyosin(CT)

Heavy meromyosin(CR) was prepared according to Weeds and Pope [41]. Digestion of myosin with α-chymotrypsin (Sigma Chemical Co.) was carried out at 20 °C for 10 min in the presence of 0.1 M (or 0.01 M) NaCl, 1 mM $MgCl_2$ and 10 mM phosphate buffer (pH 7.0). The concentrations of myosin and α-chymotrypsin were 10 mg/ml and 0.05 mg/ml, respectively. The reaction was stopped by addition of phenylmethanesulphonyl fluoride at the final concentration of 1 mM. Heavy meromyosin(CT) obtained was purified by the same procedure as in the purification of heavy meromyosin(TR). The concentration of heavy meromyosin(CT) was determined from ultraviolet absorbance, using an extinction coefficient $E^{1\%}_{280\ nm} = 6.45\ cm^{-1}$ [145].

The molecular weight of heavy meromyosin (both TR and CT) was taken to be 3.4×10^5 [33].

IV-2-5 Subfragment-1

Subfragment-1 was obtained by digestion of myosin with α-chymotrypsin according to Weeds and Taylor [146]. Digestion was carried out at 20 °C for 10 min in the presence of 0.1 M NaCl, 1 mM EDTA and 10 mM phosphate buffer (pH 7.0). The concentrations of myosin and α-chymotrypsin were 10 mg/ml and 0.05 mg/ml, respectively. The reaction was stopped by addition of phenylmethanesulphonyl

fluoride. The crude subfragment-1 was purified by ammonium-sulfate fractionation between 55 % and 67 % saturation. The concentration was determined from ultraviolet absorbance, using an extinction coefficient $E^{1\%}_{280\ nm} = 7.5\ cm^{-1}$. The molecular weight of subfragment-1 was taken to be 1.15×10^5 [145].

In some cases, purified subfragment-1 was fractionated into the one with alkali-1 light chain and the one with alkali-2 light chain (namely S1-A1 and S1-A2, respectively) by gel chromatography on DEAE-cellulose(Brown) [146].

IV-3 Preparation of Labelled Actin

IV-3-1 PM-labelled actin

N-(1-pyrenyl)maleimide was prepared from 1-aminopyrene purchased from Tokyo Chemical Industry Co. as described by Weltman et al. [147]. The purity of the product was checked by chromatography on silica gel sheets. When the product was developed with a solvent consisting of acetone, chroloholm and acetic acids (5/95/1 by volume), a single spot was observed [148]. PM(1 mM)dissolved in acetone was mixed with G-actin in the presence of 0.2 mM ATP, 0.1 mM $MgCl_2$, 0.05 mM EGTA and 2 mM Imidazole-HCl (pH 7.0). The concentration of G-actin in the mixture was 0.5 mg/ml and the molar ratio of the dye to actin was about 1:1. The mixture was left standing for 30 to 60 min at 0 °C and then centrifuged at 5×10^4 rpm for 30 min.

The supernatant was made up to 60 mM KCl and the resulting labelled F-actin was sedimented by centrifugation at 5×10^4 rpm for 60 min. The pellet of PM-labelled F-actin was depolymerized to G-actin by lowering the ionic strength. Finally, dusts were removed by centrifugation at 5×10^4 rpm. Purification of PM-labelled actin was done below 5 °C. PM-labelled actin was used within one week after the labelling. The degree of the labelling was 60-70 %; the molar absorptivity of PM adduct with actin was determined to be 3.4×10^4 $M^{-1}cm^{-1}$ at 344 nm according to the method of Betcher-Lange and Lehrer [149].

The ability of PM-labelled F-actin to activate the Mg^{++}-ATPase of heavy meromyosin was tested (Fig. IV-10). The double reciplocal plots [59] of the rate of Mg^{++}-ATPase of acto-heavy meromyosin and the concentration of the added actin show that the apparent activation of Mg^{++}-ATPase of heavy meromyosin by PM-labelled F-actin was lower than the activation by the unlabelled F-actin. The value of K_d was 5×10^{-6} M and V_{max} was 7μmoles/(mg·min) for unlabelled F-actin; on the other hand, K_d was 7×10^{-6} M and V_{max} was 5μmoles/(mg·min) for PM-labelled F-actin.

Relationship between actin concentration and specific viscosity was measured in the presence of 0.1 M KCl, 1 mM $MgCl_2$, 0.2 mM ATP and 10 mM phosphate buffer (pH 7.0). The increases in specific viscosity of PM-labelled actin and unlabelled actin were parallel (Fig. IV-11). The critical concentration of unlabelled actin was about 0.005 mg/ml and that of PM-labelled actin was about 0.010 mg/ml

under the solvent condition. No difference in the rate of polymerization between PM-labelled actin and unlabelled actin (0.5 mg/ml) was detected from the observation of the time course of viscosity increase after addition of 0.1 M KCl (Fig. IV-12). Therefore, we concluded that the labelling did not essentially affect polymerization of actin, though there was a slight difference in the critical concentration.

IV-3-2 ANM-labelled actin

N-(1-anilinonaphthyl-4)maleimide (ANM) [150] was purchased from TEIKA and used without further purification. ANM-labelled actin was prepared by the same procedure as that described in the preparation of PM-labelled actin.

IV-3-3 PMIA-labelled actin

N-(1-pyrenyl)methyliodoacetate [PMIA] was purchased from Molecular Probes (U.S.A.) and used without further purification. When the dye was developed on silica gel sheets with a solvent containing n-hexane and acetic acid (99/1 by volume), a single spot was observed.

PMIA (10 mM) disolved in acetone was mixed with F(Ca)-actin in the presence of 0.1 M KCl, 1 mM $MgCl_2$, 0.1 mM $CaCl_2$, 0.2 mM ATP, 1 mM bicarbonate (pH 7.6) and 1 mM sodium azide. The concentration of actin was 1 mg/ml and the molar ratio of dye to protein was about 1:1. The conjugation reaction was continued in the dark at 20 °C for 12 h and then Whatmann CF-11-cellulose was added at the final concentration

of 1 % (wt/wt). After removal of the cellulose, PMIA-labelled F-actin was sedimented and resuspended in a solvent containing 0.2 mM ATP, 0.1 mM $CaCl_2$, 1 mM bicarbonate and 1 mM sodium azide. Purification of PMIA-labelled actin was made by repetition of the cycle of polymerization and depolymerization.

The degree of the labelling was found to be 60-90 %; the molar absorptivity of PMIA adduct with G-actin was determined to be 2.9×10^4 M^{-1} cm^{-1} at 347 nm [149].

The relationship between the concentration of actin and specific viscosity was investigated in the presence of 0.1 M KCl, 1 mM $MgCl_2$, 0.1 mM $CaCl_2$, 0.2 mM ATP, 10 mM phosphate buffer (pH 7.0) and 1 mM sodium azide. The increases in specific viscosity of PMIA-labelled actin and unlabelled actin were parallel (Fig. IV-13). The critical concentrations of both PMIA-labelled actin and unlabelled actin were about 0.005 mg/ml.

IV-3-4 PIAA-labelled actin

N-(1-pyrenyl)iodoacetamide [PIAA] was purchased from Molecular Probes (U.S.A.) and used without further purification. Purity of the dye was checked by chromatography on a silica gel sheet; the dye was firstly conjugated with 2-mercaptoethanol, which was then developed with a solvent consisting of chloroform, hexane and acetic acid (90/10/1 by volume). There was a main spot which exhibited strong fluorescence in dioxane and a faint spot which scarecely exhibited fluorescence.

PIAA (3 mM) dissolved in a mixture of 33 % acetone and 67 % dioxane was mixed with F(Ca)-actin in the presence of 0.1 M KCl, 1 mM $MgCl_2$, 0.1 mM $CaCl_2$, 0.2 mM ATP, 10 mM phosphate buffer (pH 7.0) and 1 mM sodium azide. The concentration of actin in the mixture was 1 mg/ml and the molar ratio of dye to protein was 1:1. The conjugation was continued in the dark at 20 °C for 20 h and then Whatmann CF-11-cellulose was added at the final concentration of 1 % (wt/wt). After removal of the cellulose adsorbing unreacted dye, PIAA-labelled F-actin was sedimented by centrifugation at 4.5×10^4 rpm for 70 min and resuspended in a solvent containing 0.2 mM ATP, 0.1 mM $CaCl_2$, 2 mM Imidazole-HCl (pH 7.0), 1 mM mercaptoethanol and 1 mM sodium azide [G-buffer]. Denatured actin was removed during two cycles of polymerization and depolymerization. Further purification of PIAA-labelled G-actin was made by gel chromatography on Sephacryl superfine (Phermacia) [151].

The degree of the labelling was found to be 60-95 %; the molar absorptivity of PIAA adduct with G-actin was 2.2×10^4 M^{-1} cm^{-1} at 343 nm which was determined according to the method of Betcher-Lange and Lehrer [149].

Before doing spectroscopic study, effect of the labelling on the polymerization of actin was investigated. The relationship between the concentration of actin and specific viscosity in the solution containing 0.1 M KCl, 1 mM $MgCl_2$, 0.1 mM $CaCl_2$, 0.2 mM ATP, 10 mM phosphate buffer (pH 7.0) 1 mM 2-mercaptoethanol and 1 mM sodium azide [F-buffer] at 20 °C is shown in Fig. IV-14. It

can be seen that the critical concentration of the labelled actin was about 0.005 mg/ml. This value is the same as the one obtained for unlabelled actin. In order to estimate the content of denatured actin, we measured the protein concentration in the supernatant after centrifugation (at 4×10^4 rpm for 90 min) of PIAA-labelled F-actin (0.2 mg/ml) in F-buffer: The protein concentration was estimated from the fluorescence intensity of the tryptophan residues. Then about 2 % of the total actin was found to lose the polymerizability after the conjugation.

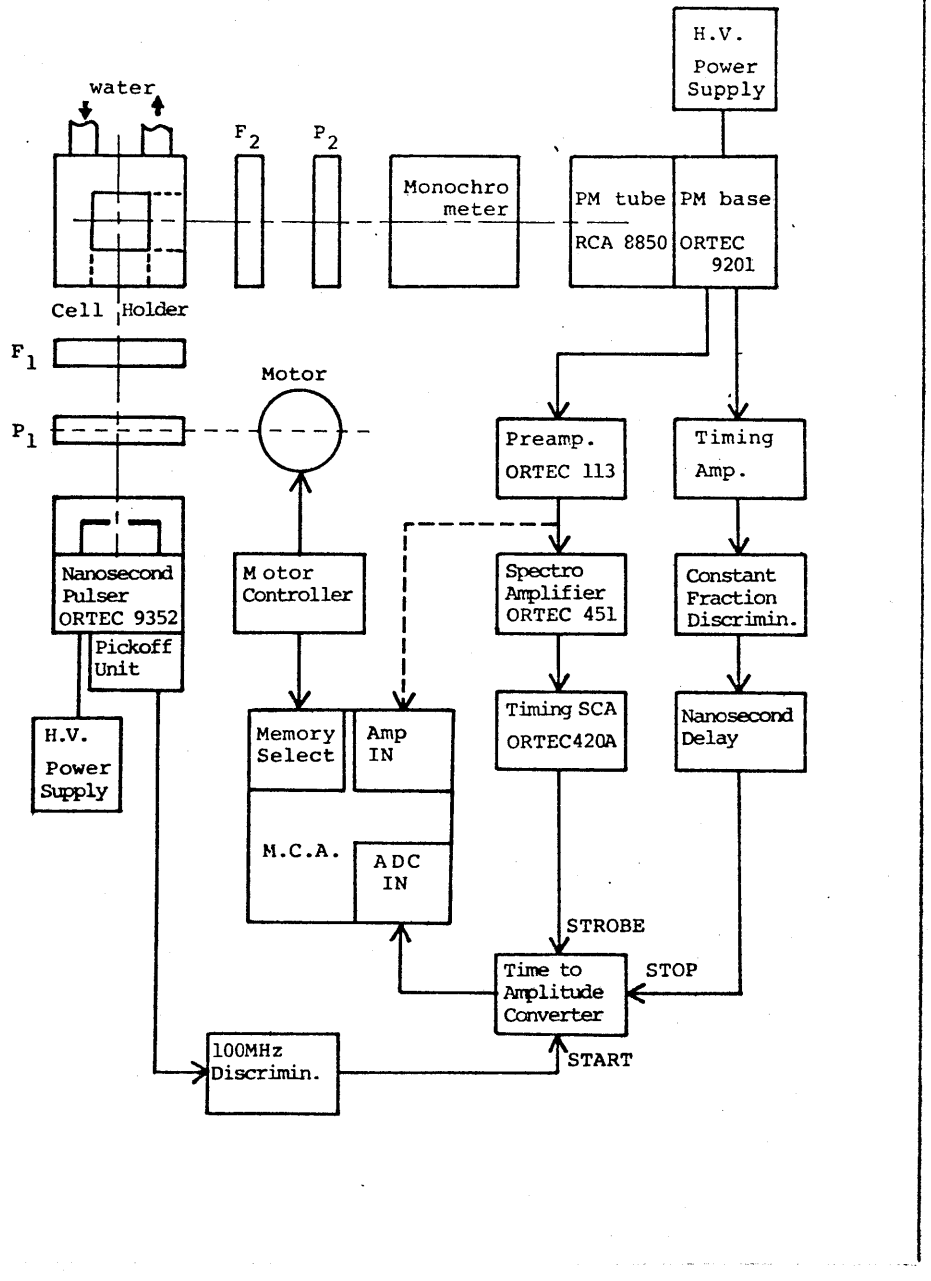

Fig. IV-1. Block diagram of the experimental system of pulse-fluorometry. F_1, F_2: optical filter, P_1, P_2: polarizer, ——-—— - represents the optical path.

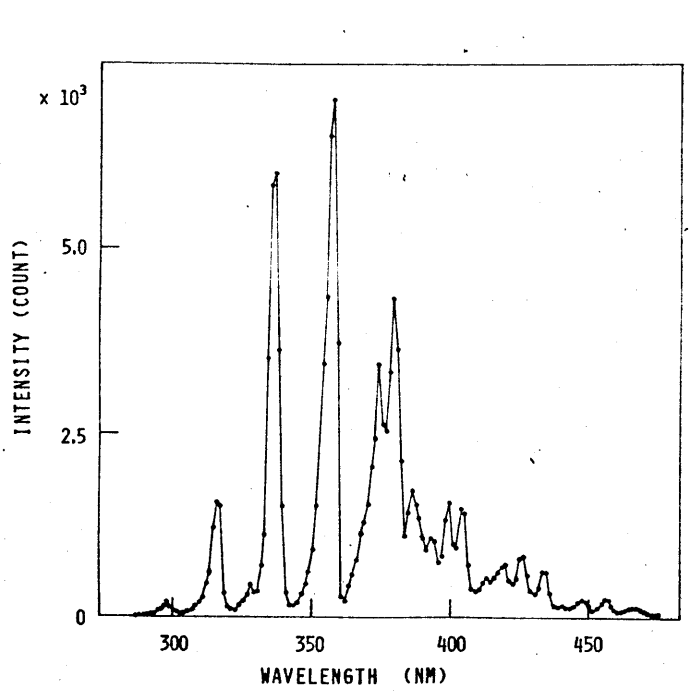

Fig. IV-2. Emission spectrum of an airflash. The emission intensity was not corrected and was measured with RCA 8850 photomultiplier via Spex monochrometer "MINIMATE". The wavelength resolution was 0.2 nm.

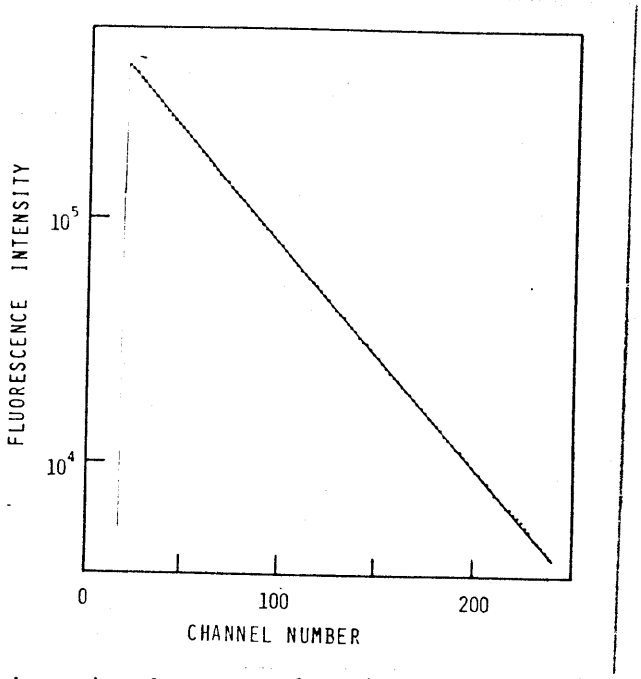

Fig. IV-3. Linearity between the time after excitation and the channel number of the MCA memory. The fluorescence decay of the conjugate of N-(1-pyrenyl)methyliodoacetate with 2-mercaptoethanol was measured in ethyleneglycol at 15°C. Excitation was at 337 nm and emission above 370 nm was collected altogether. One channel corresponds to 4.0 nsec.

Fig. IV-4

Preparation Method of Muscle Proteins

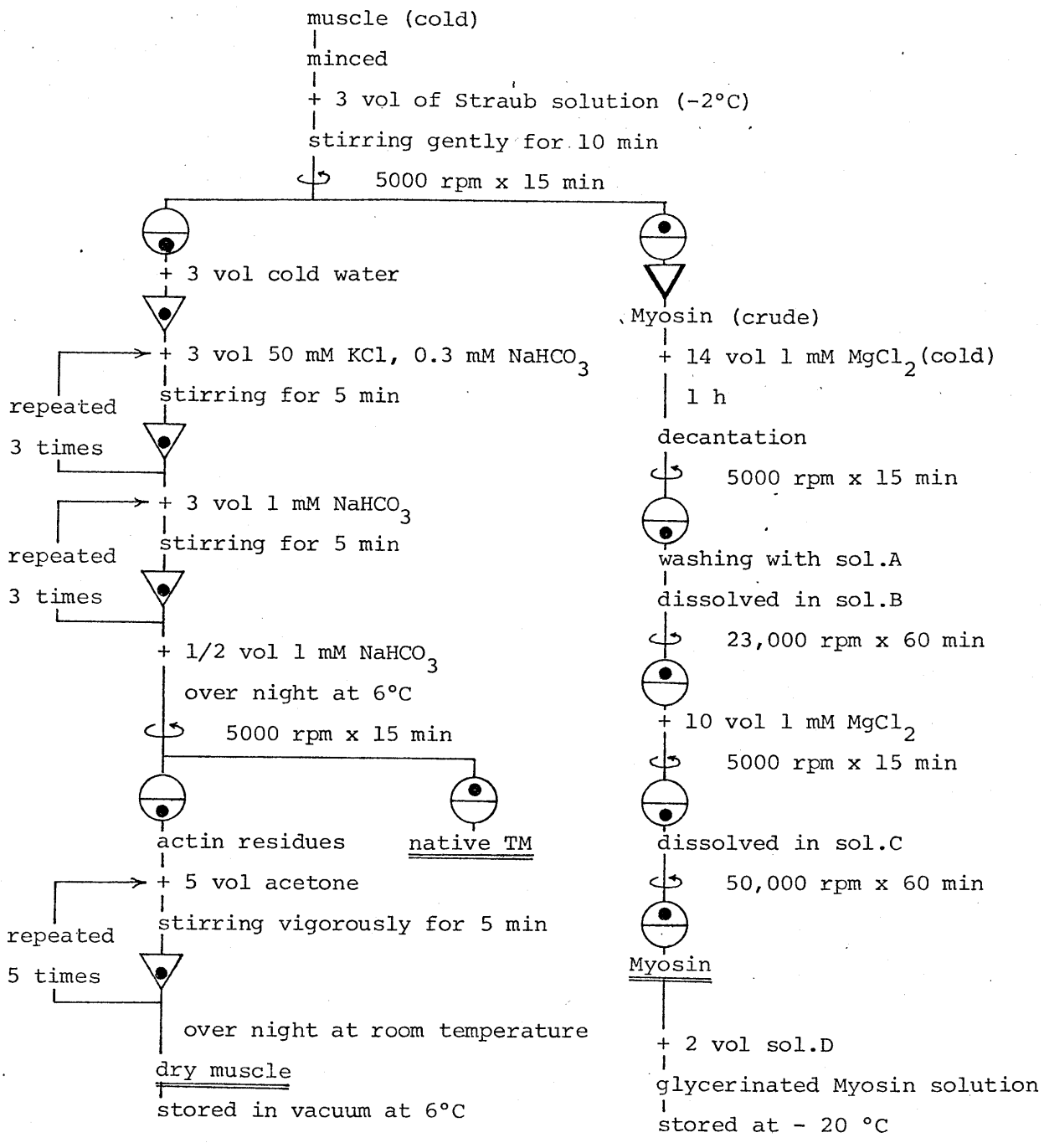

Struab solution ; 0.3 M KCl, 0.15 M $K\text{-}PO_4$, pH 6.3

sol.A ; 30 mM KCl, 1 mM $MgCl_2$, 5 mM $K\text{-}PO_4$, pH 6.5

sol.B ; 0.3 M KCl, 1 mM $MgCl_2$, 10 mM $K\text{-}PO_4$, pH 6.7

sol.C ; 0.5 M NaCl, 1 mM $MgCl_2$, 10 mM $Na\text{-}PO_4$, pH 7.0

sol.D ; 79 ml glycerine, 17 ml 3 M NaCl, 2 ml 0.5 M $Na\text{-}PO_4$ (pH 7.0), 1 ml 0.1 M $MgCl_2$, 1 ml 10 mM EGTA / 100 ml

Fig. IV-5

Preparation of G-actin

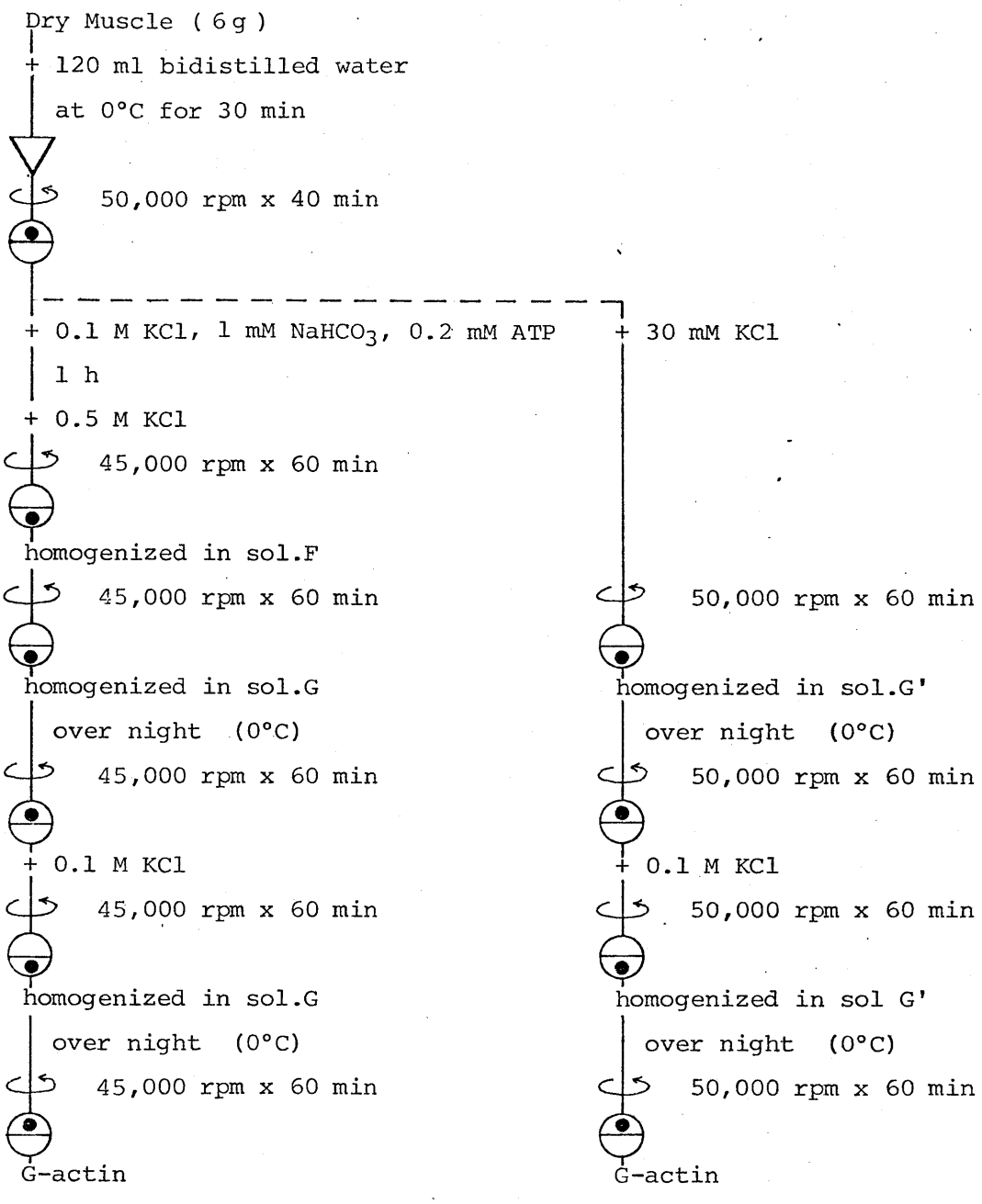

sol.F ; 0.1 M KCl, 0.1 mM $CaCl_2$, 0.2 mM ATP, 1 mM $NaHCO_3$, 1 mM NaN_3

sol.G ; 0.1 mM $CaCl_2$, 0.2 mM ATP, 1 mM $NaHCO_3$, 1 mM NaN_3

sol.G' ; 0.1 mM $MgCl_2$, 0.2 mM ATP, 0.05 mM EGTA, 2 mM Imidazole-HCl (pH 7.0)

Fig. IV-6

Preparation Method of Heavy Meromyosin and Myosin Subfragment-1 using α-chymotrypsin

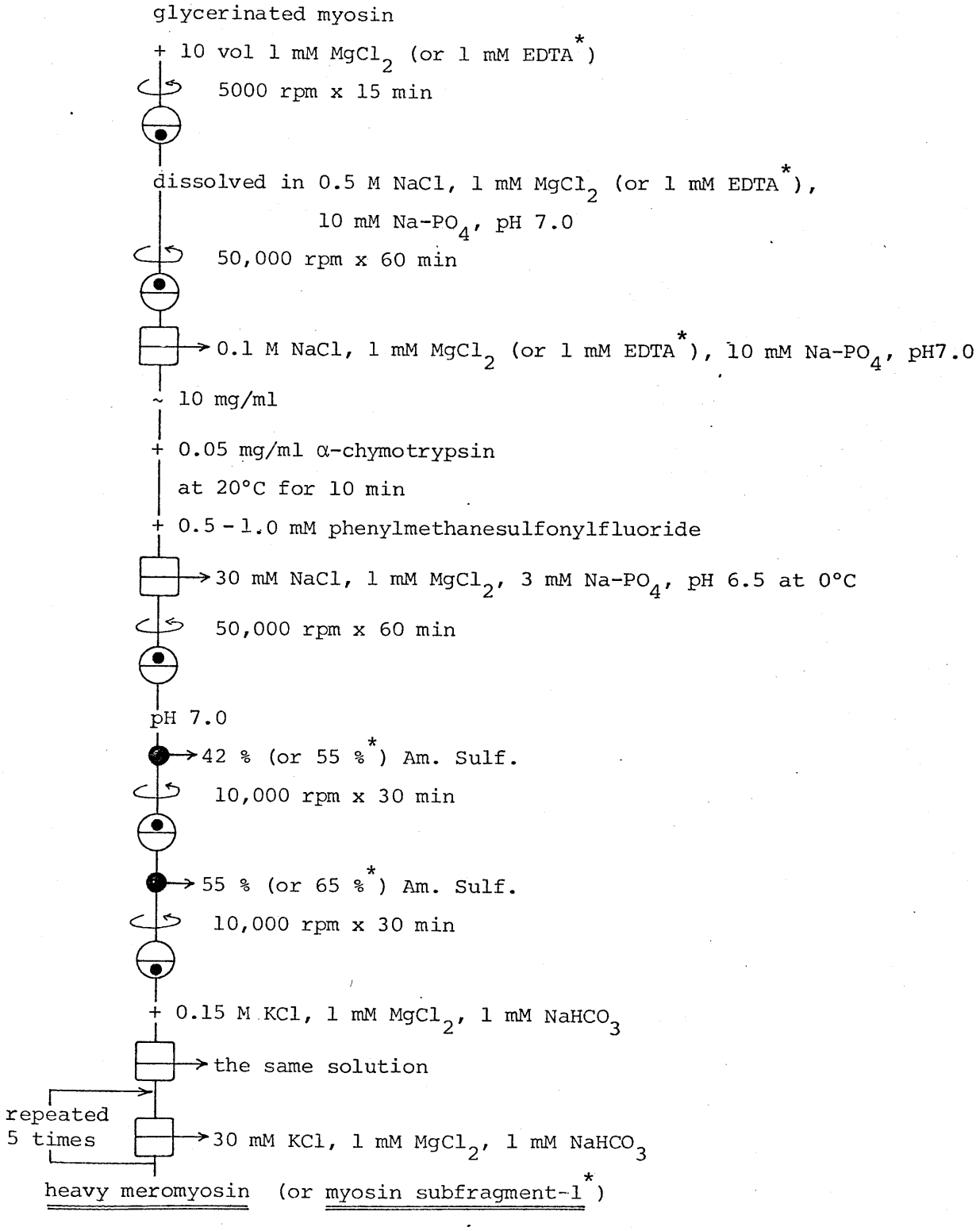

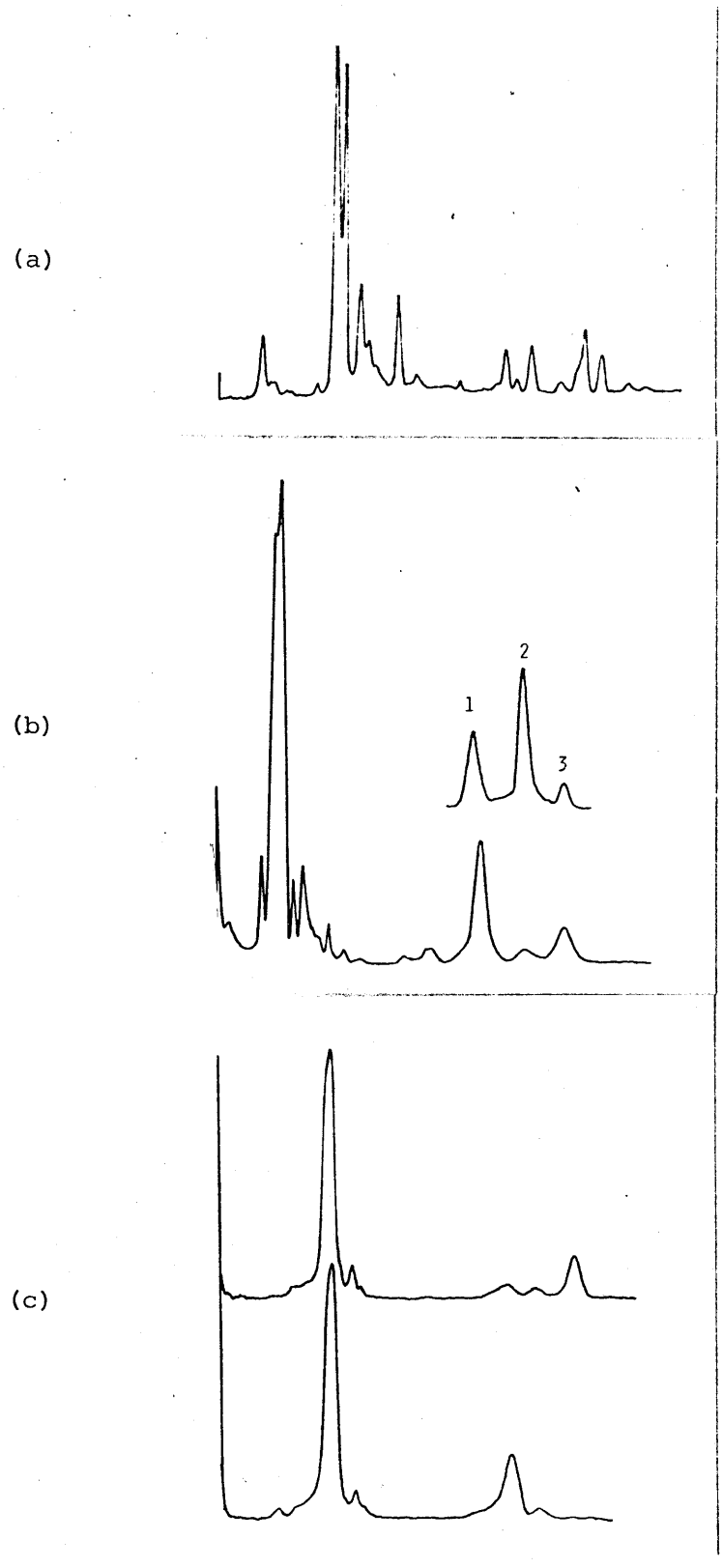

Fig. IV-7. SDS gel electrophoresis patterns of myosin subfragments. (a) heavy meromyosin obtained by tryptic digestion in the presence of 1 mM EDTA. (b) heavy meromyosin obtained by chymotryptic digestion in the presence of 1 mM $MgCl_2$; and light chains, g_1, g_2, g_3 of myosin (upper). (c) myosin subfragment-1 obtained by chymotryptic digestion in the presence of 1 mM EDTA; S1-A1 (lower) and S1-A2 (upper).

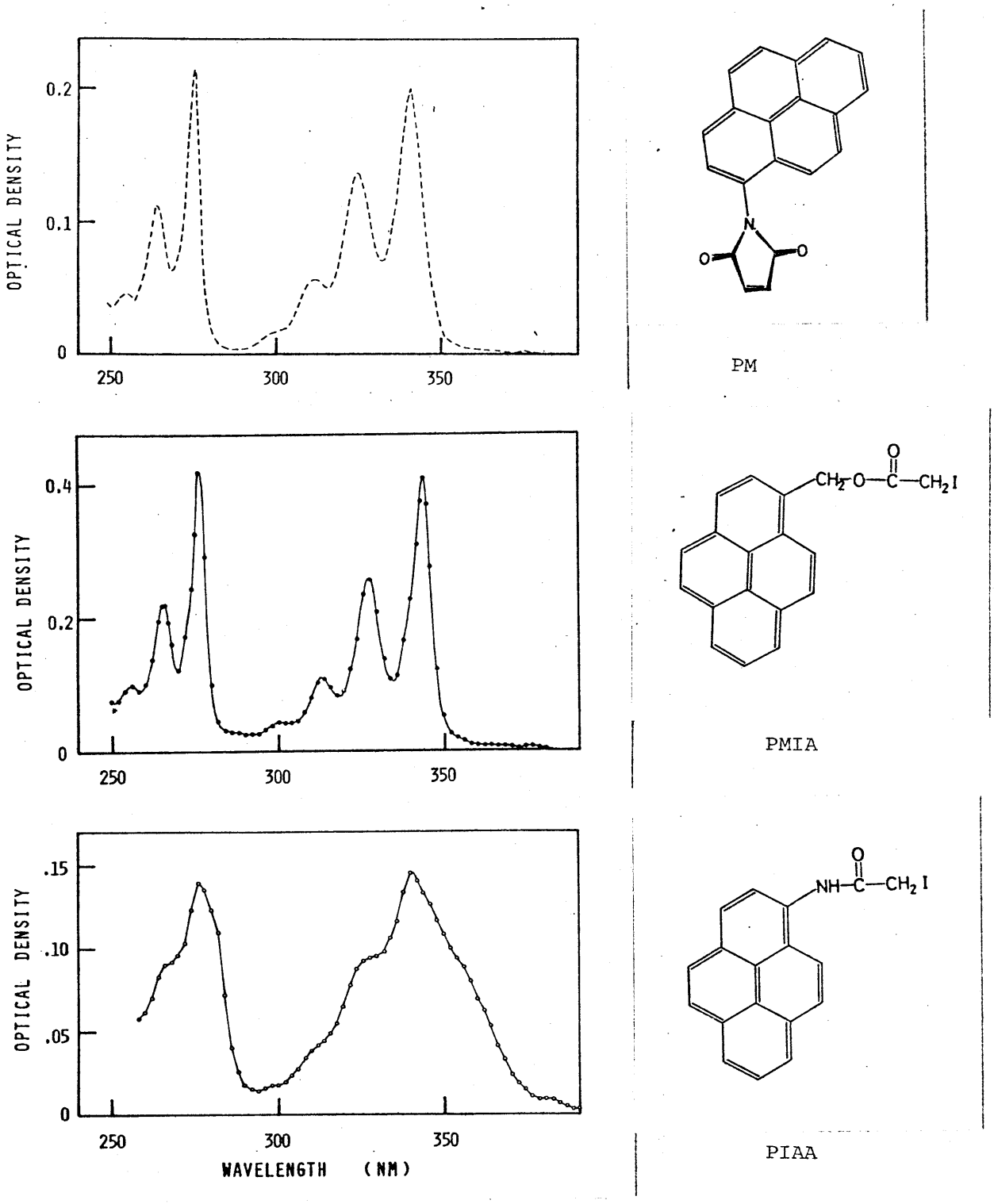

Fig. IV-8. Absorption spectra (left) and chemical structures (right) of N-(1-pyrenyl)maleimide [PM], N-(1-pyrenyl)methyliodoacetate [PMIA] and N-(1-pyrenyl)iodoacetamide [PIAA]. Absorption spectra were obtained under the following condition: 10 μM PM in cyclohexane(upper); 8 μM PMIA in cyclohexane(middle); 6.6 μM PIAA in ehtyleneglycol(lower).

Fig. IV-9

Preparation Method of Labelled Actin

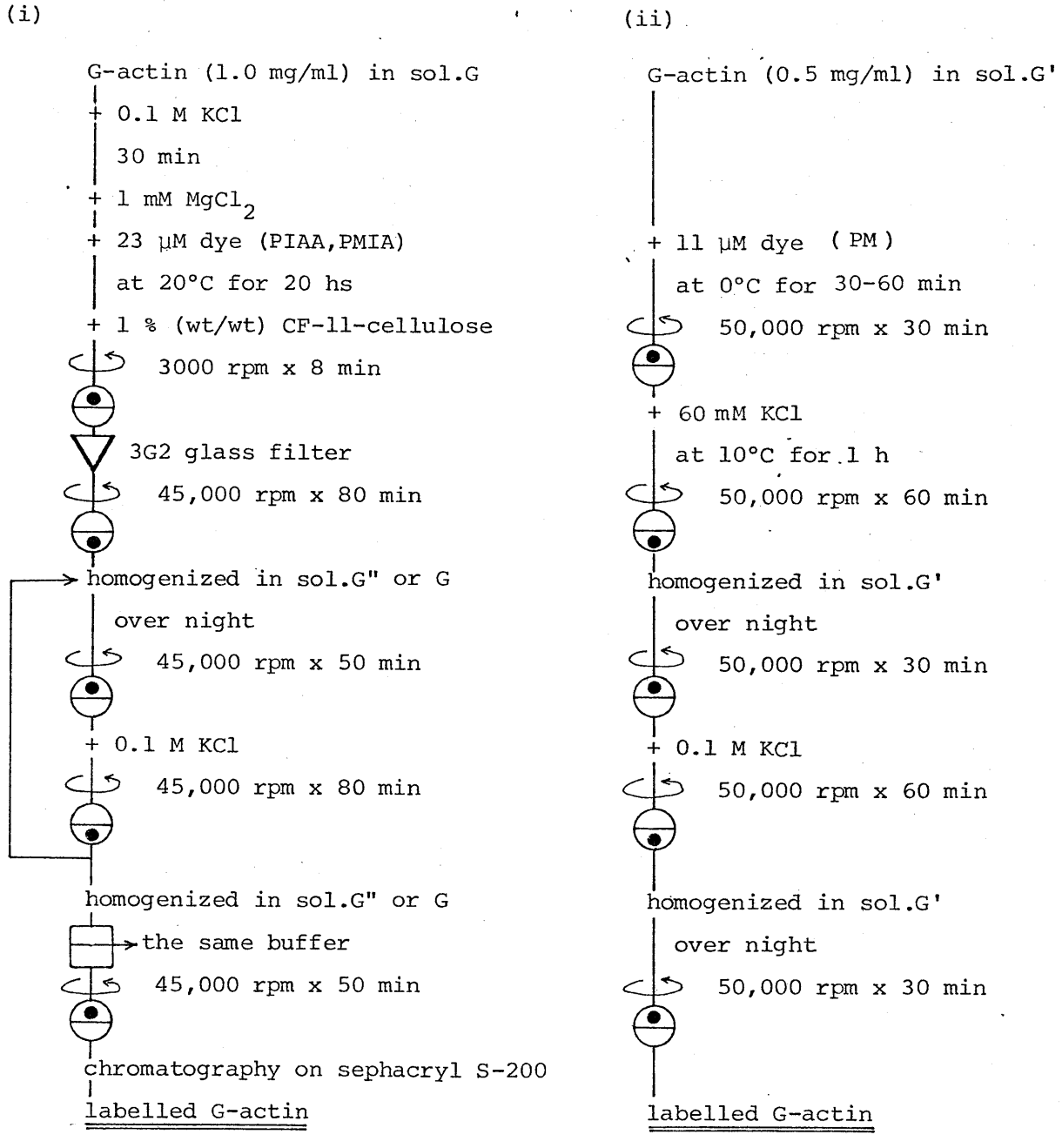

sol.G ; 0.2 mM ATP, 0.1 mM $CaCl_2$, 1 mM $NaHCO_3$, 1 mM NaN_3

sol.G' ; 0.2 mM ATP, 0.1 mM $MgCl_2$, 50 µM EGTA, 2 mM Imidazole-HCl(pH 7.0)

sol.G" ; 0.2 mM ATP, 0.1 mM $CaCl_2$, 2 mM Imidazole-HCl (pH 7.0),
1 mM NaN_3, 1 mM 2-mercaptoethanol

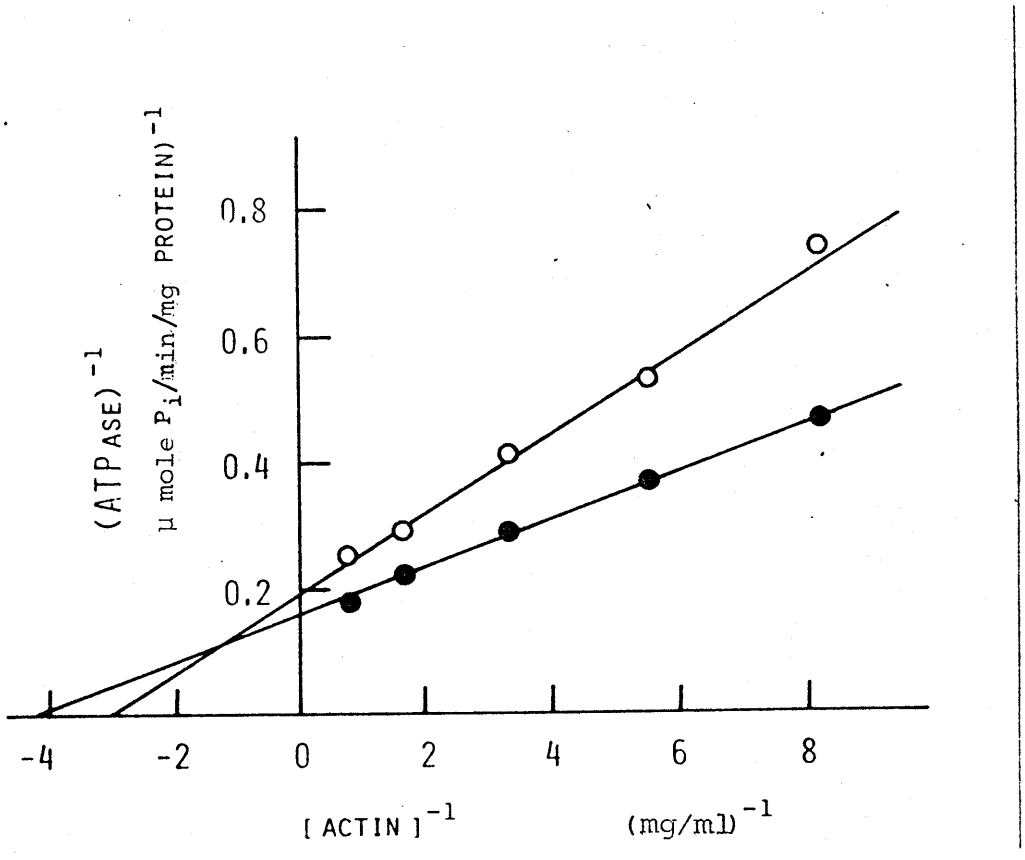

Fig. IV-10. Double reciprocal plot of the rate of acto-heavy meromyosin(CT) Mg-ATPase and the added actin concentration. ●—●, unlabelled F-actin; o—o, PM-labelled F-actin. Solvent condition: $MgCl_2$, 1.5 mM; KCl, 5 mM; ATP, 1 mM; Tris-HCl, 10 mM (pH 8.0), at 25°C. The concentration of heavy meromyosin was 0.036 mg/ml. The ATPase activity of heavy meromyosin(CT) only was 2.17 μM P_i/min/mg protein in the presence of 10 mM $CaCl_2$, 30 mM KCl, 1 mM ATP and 10 mM Tris-HCl (pH 8.0) at 25°C.

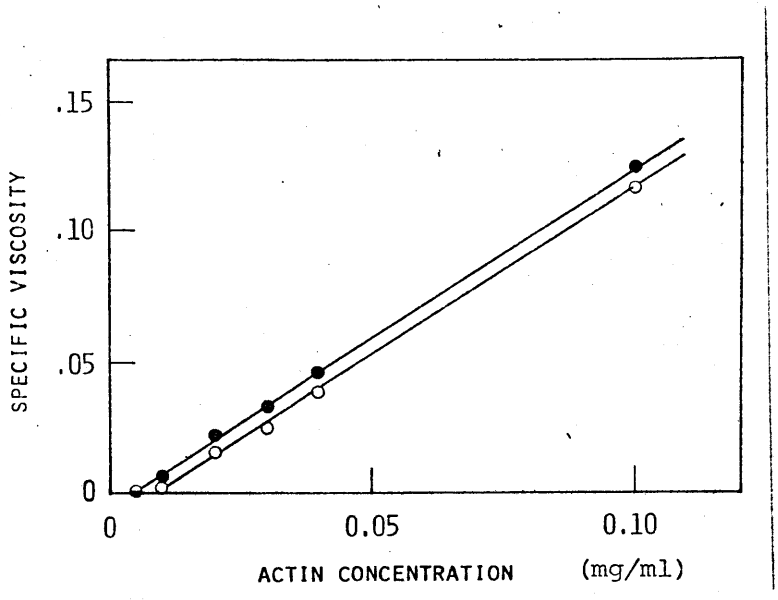

Fig. IV-11. Relationship between total actin concentration and specific viscosity η. o—o, PM-labelled actin; ●—●, unlabelled actin. Solvent condition: KCl, 0.1 M; $MgCl_2$, 1mM; ATP, 0.2 mM; phosphate buffer, 10 mM (pH 7.0); at 20°C.

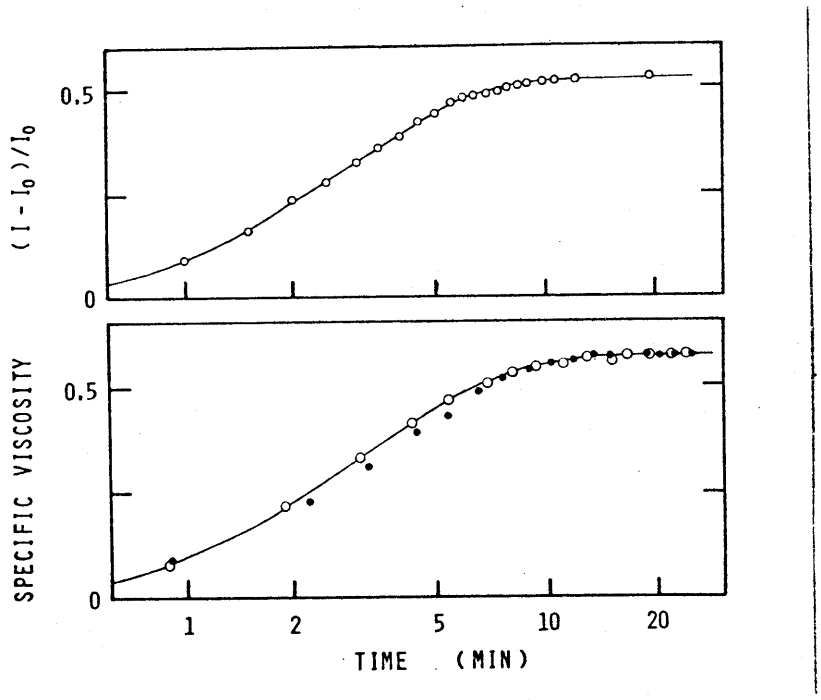

Fig. IV-12. Upper figure shows time course of increase in the fluorescence intensity of PM-labelled actin after the addition of KCl to 50 mM. Lower figure shows time course of increase in the specific viscosity during the polymerization of PM-labelled actin (open circle) or unlabelled actin (closed circle). Initial solvent condition was 0.1 mM ATP, 25 μM $MgCl_2$, 12 μM EGTA and 10 mM Tris-HCl (pH 8.0) and the concentration of actin was 0.5 mg/ml (at 20°C).

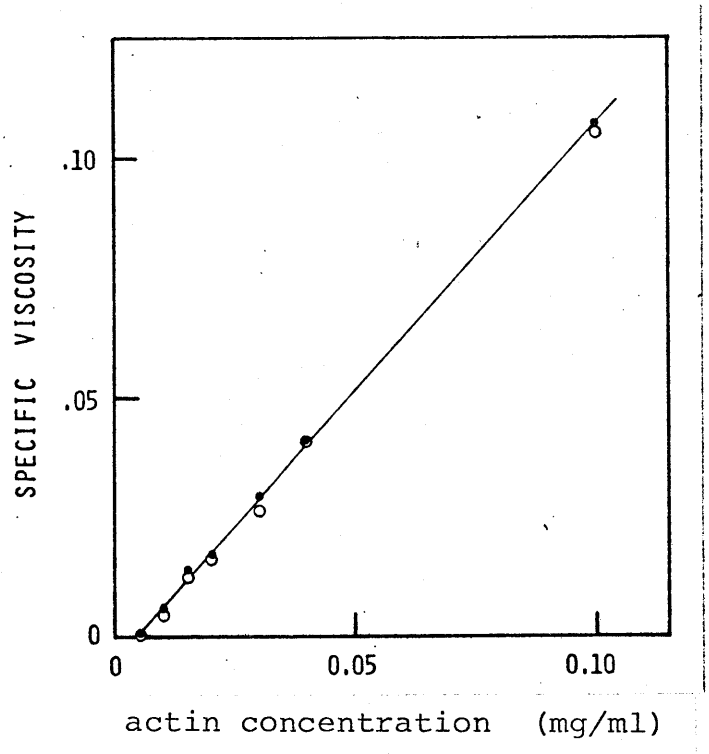

Fig. IV-13. Relationship between total actin concentration and specific viscosity. o—o, PMIA-labelled actin; ●—●, unlabelled actin. Solvent condition: KCl, 0.1 M; $MgCl_2$, 1 mM; $CaCl_2$, 0.1 mM; phosphate buffer, 10 mM (pH 7.0); ATP, 0.2 mM; NaN_3, 1 mM; at 20°C.

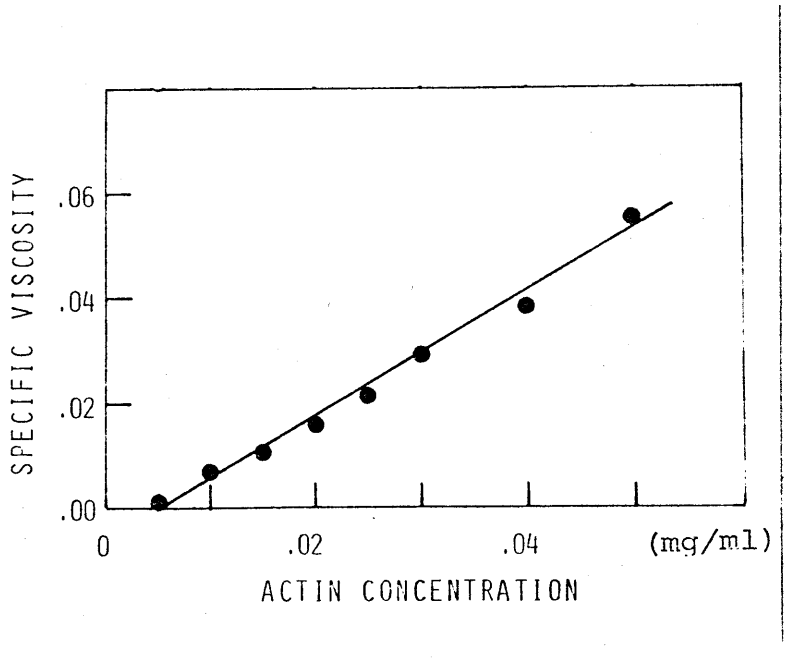

Fig. IV-14. Specific viscosity as a function of the total concentration of PIAA-labelled actin in the presence of 0.1 M KCl, 1 mM $MgCl_2$, 0.1 mM $CaCl_2$, 10 mM phosphate buffer (pH 7.0), 0.2 mM ATP, 1 mM 2-mercaptoethanol and 1 mM NaN_3 (at 20°C).

V BASIC PROBLEMS IN PULSE-FLUOROMETRY

In the study of fluorescence anisotropy decay by single-photoelectron counting, a long data accumulation time will be necessary if the measurement is performed at a low count rate where distortions due to multi-photoelectron effect can be neglected. This is a serious limitation to the application of this method to labile proteins. In this chapter, a method will be presented by which fluorescence anisotropy decay can be determined without any large distortion even when the measurement is performed at a high count rate. Then the data accumulation time can be reduced to less than 1 hour.

V-1 Introduction

Compared with the other techniques of fluorescence lifetime measurement [152,153], single-photoelectron counting method offers operation with excellent signal-to-noise ratio. This makes a direct measurement possible not only of fluorescence decay with multiple lifetimes, but also of anisotropy decay with multiple relaxation times [104-106]. On the other hand, practical problems have been raised on the application of this method to biological systems. The problem in determination of fluorescence anisotropy decay will be discussed in the section V-2 (cf. reference 154). The problem in analysis of experimental fluorescence decay curves will be discussed in the section V-3.

V-2 Determination of Fluorescence Anisotropy Decay by Single-Photoelectron Counting Method

V-2-1 Introduction

In single-photoelectron counting method, the time-to-amplitude converter is triggered when the nanosecond pulser emits a short duration of light which will excite fluorescent molecules; and, it is stopped when subsequent fluorescence induces ejection of a photoelectron from the photocathode

in the photomultiplier. Then the time lapse between these two events is converted into a proportional voltage pulse which is then stored in the corresponding channel of the multi-channel analyzer (MCA). After a great number of excitation cycles, the histogram of fluorescence intensity decay will be formed. If two or more photoelectrons are ejected during one excitation cycle, the timing information of only the first one is recorded in the MCA memory. Then the histogram recorded at a high count rate will be more or less distorted. This is called multi-photoelectron effects. Therefore data are usually recorded at a low count rate in order to minimize this effect. However the necessary time of data accumulation is often too long to apply this method to studies of fluorescence anisotropy decay of labile labelled proteins.

The techniques have been recently developed which diminished this difficulty [155,156]. Miehe et al. [157] reported the fluorescence lifetime measurement without distortion even at a high count rate, by using the photo-multiplier with high-gain first dynode which allows to distinguish single- and double-photoelectron events [158,159].

On the other hand, the basic problem in determination of fluorescence anisotropy decay by photoelectron counting system has not been discussed in detail. Even when the instrument is used which can select the single-photoelectron event, the definition of anisotropy decay which is usually used in the measurement at a low count rate is not appropriate for the measurement at a high count rate

The method of correction necessary for the performance at a high count rate is provided. The problem which arises from both fluctuation of fluorescence intensity and incompleteness of selection of single-photoelectron events will be also discussed.

V-2-2 Photoelectron counting

If photoelectron emission from the photocathod is independent statistical event from each other, the probability $\Phi(t)$ of emission of a photoelectron is proportional to the instantaneous light intensity $I(t)$: i.e., $\Phi(t)dt = \beta I(t)dt$, where β is the quantum efficiency of the photomultiplier [160]. From this relation, the probability distribution $p_k(t,t+T)$ of emission of k photoelectrons in a finite time interval between t and t+T is given by [161]

$$p_k(t,t+T) = (1/k!)\{\beta U(t,t+T)\}^k \exp\{-\beta U(t,t+T)\} \quad (V-1)$$

where $U(t,t+T)$ represents the time-integrated light intensity, namely,

$$U(t,t+T) = \int_t^{t+T} I(t')dt' \quad (V-2)$$

Now we shall consider a great number of excitation cycles in each of which a flash burst of exciting lights occurs at zero time and the subsequent fluorescence, whose intensity at time t is $I(t)$, induces emission of photoelectrons. In the measurement of fluorescence decay by photoelectron counting method, the practically interesting

quantity is the ensemble average of the probability $p_k(t_i,t_{i+1})$ which is taken over a great number of excitation cycles:

$$\bar{p}_k(t_i,t_{i+1}) = (1/k!)[\{\beta U(t_i,t_{i+1})\}^k \exp\{-\beta U(t_i,t_{i+1})\}] \qquad (V-3)$$

where the bracket [ ] means the ensemble average; t_i is the time after the instance of each flash burst of excitation and the time interval from t_i to t_{i+1} corresponds to the i-th channel of the MCA memory: (It is assumed to be independent of i, that is, $t_{i+1} - t_i = \varepsilon$ for all of i.) In the case where the fluorescence intensity does not fluctuate significantly among different excitation cycles and when β is constant over the wavelength, Eqn (V-3) reduces to [162]

$$\bar{p}_k(t_i,t_{i+1}) = (1/k!)\ \bar{x}_i^k \exp(-\bar{x}_i) \qquad (V-4)$$

where $\bar{x}_i = [\beta U(t_i,t_{i+1})]$ and this quantity means the average number of photoelectrons emitted at the time interval from t_i to t_{i+1} during one excitation cycle.

Let us consider the case that $\bar{x}_i << 1$. Then the probabilities of emission of one and more than one photoelectron can be approximated as follows:

$$\bar{p}_1(t_i,t_{i+1}) \simeq \bar{x}_i$$

$$\sum_{k>1} \bar{p}_k(t_i,t_{i+1}) = 1 - \bar{p}_0 - \bar{p}_1 \simeq \bar{x}_i^2/2 \qquad (V-5)$$

Therefore the probability $\bar{p}_{k>1}(t_i,t_{i+1})$ is negligible as compared to $\bar{p}_1(t_i,t_{i+1})$. The number N_i of photoelectrons

at the time interval t_i to t_{i+1} which are counted after a great number of excitation cycles N_c is :

$$N_i \simeq N_c \bar{p}_1(t_i,t_{i+1}) \simeq N_c\bar{x}_i = N_c[\beta U(t_i,t_{i+1})] \quad (V-6)$$

The number N_i is therefore proportional to the intensity of fluorescence at the time interval t_i to t_{i+1}. Nevertheless N_i does not represent the experimental count M_i stored in the MCA memory. Since the time-to-amplitude converter can detect the first photoelectron emitted in a given excitation cycle, M_i is given by the following formula:

$$M_i = N_i \prod_{j=0}^{i-1} \bar{p}_0(t_j,t_{j+1}) \simeq N_i\{1 - \sum_{j=0}^{i-1} N_j/N_c\} \quad (V-7)$$

The experimental count M_i can give the true decay curve of fluorescence when the following condition is satisfied:

$$\sum_{j=0}^{i-1} N_j/N_c < N_a/N_c << 1 \quad (V-8)$$

where N_a is the total count of photoelectrons. This condition is that the count rate of photoelectron is so low that no more than one photoelectron is emitted per excitation cycle.

Miehe et al. have considered the system with the electronic instrumentation which can select the excitation cycle with single-photoelectron event. In this system, one count is recorded in the MCA memory when only one photoelectron is ejected from the photocathode during one excitation cycle. After a great number of excitation cycles N_c, the number M_i of counts stored in i-th channel of the MCA memory is :

$$M_i = \bar{p}_1(t_i,t_{i+1}) \prod_{j\neq i} \bar{p}_0(t_j,t_{j+1}) \cdot N_c \quad (V-9)$$

From Eqn (V-4)

$$M_i = N_c \bar{x}_i \exp(-\sum_j \bar{x}_j) = N_c \bar{x}_i \exp(-\bar{X}) \qquad (V\text{-}10)$$

where $\bar{X}$ means the average number of photoelectron emitted over one excitation cycle. The operation without any distortion in the observed histogram of fluorescence intensity decay is possible at much higher count rate in the system with "selection instrument" than the system without it[163].

V-2-3 Selection instrument

In our experimental system, the signals from the last dynode of the phototube are driven to the preamplifier through which each pulse-like signal is converted to the signal whose decay time is 50 μsec. When two or more photoelectrons are ejected from the photocathode during one excitation cycle, the time interval between these events is the order of the magnitude of the fluorescence lifetime which is apparently much shorter than 50 μsec. Therefore, the corresponding outputs from the last dynode will be converted only to a single-pulse through the preamplifier.

The pulse-height of signal from the last dynode varies statistically in a manner characterized by the photomultiplier [164]. Let f(V) be the statistical distribution of the each signal. Now imagine when only one photoelectron is always ejected during one excitation cycle. Then the pulse-height spectrum of the output signal of the preamplifier will be given by

$$h_1(V) = f(V/\alpha) \qquad \text{(V-11)}$$

where α gives the degree of multiplication of the preamplfier. If two photoelectrons are always ejected during one excitation cycle, then the pulse-height spectrum $h_2(V)$ can be given as follows:

$$h_2(V) = \int_0^V h_1(V-V')h_1(V')dV' \Big/ \int_0^\infty \int_0^V h_1(V-V')h_1(V')dV'dV \qquad \text{(V-12)}$$

where $h_1(V)$ and $h_2(V)$ are normalized so that their integrations over pulse-height become unity. This relation can be driven from the ref. [165]. Similarly, the pulse-height spectrum $h_n(V)$ for n-photoelectrons is given by

$$h_n(V) = \int_0^V h_1(V-V')h_{n-1}(V')dV' \Big/ \int_0^\infty \int_0^V h_1(V-V')h_{n-1}(V')dV'dV \qquad \text{(V-13)}$$

The number n of photoelectrons ejected during one excitation cycle also varies statistically. Under the assumption made in Eqn (V-4), its distribution function is given by a Poisson distribution, that is,

$$P_n(\bar{X}) = (1/n!)\ \bar{X}^n \exp(-\bar{X}) \qquad \text{(V-14)}$$

where $\bar{X}$ gives the average number of this phenomenon. Therefore, the observed pulse-height spectrum becomes

$$H(V;\bar{X}) = \sum_n P_n(\bar{X})\ h_n(V) \qquad \text{(V-15)}$$

For an instant, we shall assume that $h_1(V)$ is a Gaussian distribution whose center lies on V_0 and whose half width is ΔV. Then $h_n(V)$ will be approximated by a Gaussian curve whose center lies on nV_0 and whose half width is $\sqrt{n}\Delta V$. Thus only when ΔV is much smaller than V_0, the observed pulse-height spectrum $H(V;\bar{X})$ will show several well-defined peaks which correspond to single-, double-photoelectron events and so on. This condition is well satisfied by RCA 8850 photomultiplier tube which contains high-gain first and second dynodes. An example of $H(V;\bar{X})$ is given in Fig. V-1. The decompsed pulse-height spectra $h_n(V)$ $(n = 1,2,3)$ were calculated from the $H(V;\bar{X})$ which was recorded at a small value of $\bar{X}$ ($\bar{X} \simeq 0.01$). They are shown in Fig. V-2.

The strobe circuit shown in the block diagram of the nanosecond pulse fluorometer (Fig. IV-1) plays a role of selection of single-photoelectron events. The signals from the last dynode of the phototube *via* the preamplifier are analysed by the single-channel analyser in which the lower and upper discrimination levels are set as shwon in Fig. V-2. Only when the output of the preamplifier has an energy within the range of amplitude corresponding to single-photoelectron events, this circuit allows the time-to-amplitude converter to furnish the timing information to the MCA memory.

V-2-4 Measurements of fluorescence anisotropy decay

Total and difference fluorescence decays are related

to the two principal components of polarized transient fluorescence:

$$S(t) = I''(t) + 2\, I^{\perp}(t)$$
$$D(t) = I''(t) - I^{\perp}(t) \qquad \text{(V-16)}$$

Let us define the time-integrated intensities $\bar{U}_S(t_i,t_{i+1})$ and $\bar{U}_D(t_i,t_{i+1})$ of total and difference fluorescence decays according to Eqn (V-2). These intensities are computed from the experimental numbers M''_i and $M^{\perp}_i$ using the following formulae(From Eqn (V-10)):

$$\bar{U}_S(t_i,t_{i+1}) = \{M''_i \exp(\bar{X}'') + 2\, M^{\perp}_i \exp(\bar{X}^{\perp})\}/N_c\beta$$
$$\bar{U}_D(t_i,t_{i+1}) = \{M''_i \exp(\bar{X}'') - M^{\perp}_i \exp(\bar{X}^{\perp})\}/N_c\beta \qquad \text{(V-17)}$$

where M_i represents the count stored in i-th channel after the excitation cycles N_c, and $\bar{X}$ represents the average number of photoelectrons ejected over one excitation cycle; the symbols " and $^{\perp}$ mean the vertical and horizontal components, respectively. Exponents appearing in Eqn V-17 result from the fact that all of the timing signals corresponding to photoelectron emission are not stored in the MCA memory and the probability of the storage is dependent on the count rate.

If $\bar{X}''$ and $\bar{X}^{\perp} \ll 1$, the above equations may be approximated:

$$\bar{U}_S(t_i,t_{i+1}) = (M''_i + 2\, M^{\perp}_i)/N_c\beta$$
$$\bar{U}_D(t_i,t_{i+1}) = (M''_i - M^{\perp}_i)/N_c\beta \qquad \text{(V-18)}$$

The maximum count rate to be allowed to use Eqn (V-18) is as low as the one at which the true fluorescence decay can be obtained in the counting system having no instrument for selection of single-photoelectron events. Because of this restriction, the long measurement time is necessary.

On the other hand, to use Eqn (V-17), we must determine the values of $\bar{X}$" and $\bar{X}^{-1}$ experimentally. Two methods are afforded to determine $\bar{X}$. The first one is to measure the count frequency of the signal from the preamplifier which has the amplitude over the noise level. Since the signal is counted as one whenever one or more photoelectrons are ejected during one excitation cycle and zero otherwise, the ratio R of this frequency to the frequency of flash of the lamp is given by the following expression:

$$R = \sum_{k=1} P_k(\bar{X}) = 1 - P_0(\bar{X}) = 1 - \exp(\bar{X}) \qquad \text{(V-19)}$$

From this experimental value we can determine $\bar{X}$.
The second method is to compare the probability that one and two photoelectrons are ejected during one excitation cycle. The pulse-height distribution of the signal from the preamplifier has the information about these values as expected from Eqn (V-15). Since $h_1(V)$, $h_2(V)$ and $h_3(V)$ are already known, $P_1(\bar{X})$ and $P_2(\bar{X})$ can be determined. The ratio R' of these is given by, from Eqn (V-14)

$$R' = P_2(\bar{X})/P_1(\bar{X}) = \bar{X}/2 \qquad \text{(V-20)}$$

Therefore, we have two methods to determine $\bar{X}$.

We have assumed provisionally in Eqn (V-4) that $U(t_i,t_{i+1})$ does not vary significantly among different excitation cycles. Now we can justify this assumption from comparison of the values of $\bar{X}$ determined from R and R'. One of the main reasons of the fluctuation in $U(t_i,t_{i+1})$ is that the number of photons emitted from one flash burst of the lamp fluctuates. If there are large variations in the intensity of exciting light, the above assumption will become incorrect, and, therefore, Eqs (V-4) and (V-14) must be replaced by , respectively

$$\bar{p}_k(t_i,t_{i+1}) = (1/k!) \int_0^\infty (x_i)^k \exp(-x_i)\, w_i(x_i)\, dx_i$$

and (V-21)

$$P_k(\bar{X}) = (1/k!) \int_0^\infty X^k \exp(-X)\, W(X)\, dX$$

Here $w_i(x_i)$ and $W(X)$ are distribution functions of x_i and X respectively, reflecting fluctuation of the lamp intensity. Apparently from Eqn (V-21), the difference between the values of $\bar{X}$ determined from R and R' becomes larger as $W(X)$ has a broader distribution. Inversely, if we obtain similar values of $\bar{X}$ from R and R', then we have reason to consider that the above assumption is useful.

Fig. V-3 shows the relationship between the values determined from R and R'. This result was obtained when the lamp was under the stable condition; that is, the signals from the Pickoff unit of the light pulser gave a sharp pulse-height distribution. At small values of $\bar{X}$

($X < 0.1$), the values determined from R were about 10 % larger than those determined from R'. This discrepancy may have resulted from neglection of the contribution of the dark pulse whose rate is about 90 counts/sec at room temperature. Apart from the region of small value of $\bar{X}$, a good coincidence between the values determined from R and R' was obtained. Needless to say, difference more than 10 % was observed where $0.1 < \bar{X} < 1.0$ when the condition of the lamp was not good.

V-2-5 Discussion

Equation V-17 was introduced under the assumption of complete selection of single-photoelectron events. However, it is apparent from Fig. V-2 that the time-to-amplitude converter sends the timing information to the MCA memory not only for the cycles with single-photoelectron events, but also for the cycles with double-photoelectron events. Therefore Eqn (V-10) must be replaced by

$$M_i = N_c[A_1\bar{p}_1(t_i,t_{i+1}) \sum_{j\neq i} \bar{p}_0(t_j,t_{j+1}) + A_2\{\bar{p}_1(t_i,t_{i+1}) \sum_{j>i} \bar{p}_1(t_j,t_{j+1}) \prod_{k\neq i,j} \bar{p}_0(t_k,t_{k+1}) + \bar{p}_2(t_i,t_{i+1}) \prod_{j\neq i} \bar{p}_0(t_j,t_{j+1})\}] \qquad (V\text{-}22)$$

Here A_1 and A_2 mean the integrated areas, between the two discrimination levels of the single-channel analyser, of $h_1(V)$ and $h_2(V)$: (Fig. V-2). When fluroescence intensity does not fluctuate largely among different excitation cycles,

this may reduce to the following formula, similarly with Eqn (V-10)

$$M_i = N_c\{A_1 + A_2(\bar{x}_i/2 + \sum_{j>i} x_j)\}\, x_i \exp(-\bar{X}) \qquad (V\text{-}23)$$

Since $A_1 = 0.45$ and $A_2 = 0.05$ under the set of discrimination levels as shown in Fig. V-2, the term containing A_2 is not small enough to be neglected when $\Sigma_{j>i}\, \bar{x}_i$ (or $\bar{X}$) becomes large. Distortion due to this term will appear in the initial time region of the experimental decay curve of fluorescence where the number of counts collected in each channel is larger than what would be when $A_2 = 0$. Though it is possible to correct this distrotion by calculation, the necessary procedure is not simple. If the stop-signals from the anode of the phototube are well time-resolved from each other, then the accurate decay curve can be obtained without this difficulty. In such a case, the signals with small pulse-height which contributes to the tailing of $h_2(V)$ in the region of low pulse-height can be non-effective by discriminater in the stop sircuit. If the resoving time of the stop circuit is shorter than the flurescence lifetime, the distortion due to the term containing A_2 in Eqn (V-23) will be small. Let us consider when real anisotropy decay has relaxation times much longer than the lifetime and $r(t) = r_c$ for the interesting time. In the extreme case in which the above condition is not satisfied, the experimental curve $\bar{U}_D(t_i,t_{i+1})/\bar{U}_S(t_i,t_{i+1})$ has the following approximated form:

$$\bar{U}_D(t_i,t_{i+1})/\bar{U}_S(t_i,t_{i+1})$$

$$\simeq r_c\{1 + (A_2/A_1)(1-r_c)(\bar{x}_i/2 + \sum_{j>i}\bar{x}_j)\} \qquad (V-24)$$

Fig. V-4 shows the experimental curves $\bar{U}_D(t_i,t_{i+1})/\bar{U}_S(t_i,t_{i+1})$ which were obtained from the polarized fluorescence decays of PM-labelled F-actin. It can be seen that the experimental curves do not largely depend on the count rate, indicating that the distortion is not so large as predicted by Eqn V-24.

In summary, by the correction method presented here, the operation without large distortions in the observed decay curve can be obtained even at the maximum frequency of data accumulation $f_{max} = f_c A_1 \exp(-1)$ (where f_c is the frequency of the flash burst of the lamp). If total count of 10^6 is necessary for each component of polarized fluorescence to analyse fluorescence anisotropy decay with sufficient accuracy, then the measurement time can be, in principle, reduced to only about one hour.

V-3 Analysis of Experimental Fluorescence Decay Curves

V-3-1 Introduction

Analysis of fluorescence decay curve is complicated by the finite duration of the exciting light pulse and the response time of the detection system. In the detection system which responds linearly to the light intensity, the fluroescence decay F(t) is given by the following convolution product[166]:

$$F(t) = \int_0^t g(t')\, f(t-t')\, dt' = g(t)*f(t) \qquad (V-25)$$

where g(t) is the response function of the excitation light flash and f(t) is the fluorescence decay which would be obtained if the excitation pulse is of a negligible duration and the detection system had a negligible response function. Difficulties in recovering f(t) from the experimental curve F(t) may arise from (i) the dependence of g(t) on excitation and emission wavelengths and (ii) the mathematical treatment of Eqn (V-25). Here, the practical problems in analysis of fluorescence decay curve will be discussed.

V-3-2 Determination of the response function g(t)

The observation that the response function of the apparatus is wavelength dependent has been made by Lewis et al. [167] and by Wahl et al. [168] independently. The response function g(t) itself must be considered as the following double-convolution product [168]:

$$g(t) = g_{FL}(\lambda_{ex}, t) * g_{PM}(\lambda_{em}, t) * K(t) \qquad (V-26)$$

where $g_{FL}(\lambda_{ex}, t)$ is the distribution function of the light intensity of exciting flash; $g_{PM}(\lambda_{em}, t)$ is the response function of the photomultiplier; K(t) is the response function of the series of the electronic devices. The function g_{FL} may depend on the wavelength λ_{ex} used for excitation; while g_{PM} may depend on the wavelength λ_{em} chosen at the fluorescence emission.

For examination of the characteristics of the response function of the photomultiplier RCA 8850 used in the present study, the fluorescence solution was replaced by a solution containing scatterers and the scattered light was viewed with the photomultiplier. Then we could obtain the following function:

$$g^{ex}(t) = g_{FL}(\lambda_{ex}, t) * g_{PM}(\lambda_{ex}, t) * K(t) \qquad (V-27)$$

Here $g_{PM}(\lambda_{em}, t)$ appearing in Eqn (V-26) is replaced with $g_{PM}(\lambda_{ex}, t)$. The curves $g^{ex}(t)$ which were obtained at various excitation wavelengths are presented in Fig. V-5. The excitation light flash was produced by the nanosecond light pulser ORTEC 9352 which was operated in air (1 atm). It can be seen that the raising of the $g^{ex}(t)$ curve is more delayed at the longer wavelength. Fig. V-6 shows the full width at half-maximum intensity (FWHM) of the $g^{ex}(t)$ curve as a function of the wavelength. The FWHM decreased monotonically with the increasing wavelength. These behaviours must be interpreted as follows: The time of flight of the photoelectron from the photocathode to the first dynode is proportional to the square root of the kinetic energy of the photoelectron at the surface of the photocathode; the kinetic energy distribution (or the time of flight) of the photoelectron depends on the energy of the incident photon $h\nu$. When the wavelength increases, the average kinetic energy decreases (or the average time of flight increases), and the distribution of the kinetic energy (or of the time of flight) becomes narrower [168].

In order to examine how $g_{FL}(\lambda_{ex}, t)$ contributes to $g^{ex}(t)$, the air in the spark chamber of the light pulser was exchanged with N_2 gass. Then, a change in the shape of $g^{ex}(t)$ was detected in the tailing region; that is, the $g^{ex}(t)$ curve decayed more slowly in N_2 gass than in air. This behaviour can be explained by considering that quenching processes of excited N_2 molecules are reduced in the pure N_2 gass. Thus, if there exists the significant dependence of $g_{FL}(\lambda_{ex}, t)$ on wavelength, it would come from the wavelength dependence of the lifetime of excited N_2 molecule. On the other hand, when the light pulser was operated in air, no significant variation with wavelength was detected in the shape of the tailing of $g^{ex}(t)$ (Fig. V-5), indicating that the wavelength dependence of $g_{FL}(\lambda_{ex}, t)$ can be negligibly small as compared with that of $g_{PM}(\lambda_{ex}, t)$ at least in the wavelength region examined (from 317 nm to 450 nm). Therefore, the response function g(t) which is necessary in analysis of fluorescence decay curves can be approximated with the $g^{ex}(t)$ curve obtained at the same wavelength as that of fluorescence emission. The approximations similar to this are used by several workers [169].

V-3-3 Numerical analysis of the data

A variety of deconvolution methods have been devised for the analysis of fluorescence decay curves:

a) Phase plane method [170]

b) Method of least squares [119, 171-173]

c) Method of moments [174-176]

d) Laplace transforms [177]

e) Method of modulating functions [178]

f) Exponential series method [179]

g) Fourier transforms [180]

In recent publications [181-183], these methods have been compared from each other, and it has been shown that the least-square and modulating function methods have the greatest ability in resolving closely spaced decay times. In analysis of the data which will be presented in Chapers VI and VII, the method of least square is used with slight modifications, because it can used to fit any chosen section of the decay curve. Here, the method used will be presented.

V-3-3-1 The method of least squares

Most of the deconvolution methods require an assumption that f(t) in Eqn (V-25) is a mathematical function which is characterized by several parameters. The problem is then to determine these parameters. In the method of least squares, the convolution integral (Eqn (V-25)) is firstly computed for a set of the parameters; and, the computed curve $F^{cal}(t)$ is plotted and compared with the experimental curve. Until the best fitting is obtained between the calculated and experimental curves, a search of the parameters may be continued. The fitting is judged by the magnitude of the sum of the weighted squares of the residuals [184]:

$$\chi^2 = \frac{1}{n} \sum_{i=0}^{n} \omega_i \cdot \{ F_i^{cal} - F_i^{ex} \}^2 \qquad \text{(V-28)}$$

where F_i^{cal} is the time-integrated intensity at the time interval from t_i to t_{i+1} (Eqn (V-2)); that is,

$$F_i^{cal} = U_F^{cal}(t_i, t_{i+1}) = \int_{t_i}^{t_{i+1}} F^{cal}(t)\, dt \qquad (V\text{-}29)$$

and F_i^{ex} is the count collected at the i-th channel. Since the statistical error of counting is Poisson distributed, approaching to Gaussian distribution at a large number of counts, the weighting factor ω_i appearing in Eqn (V-28) is given by the inverse of the number of counts at the i-th channel [181]:

$$\omega_i = (F_i^{ex})^{-1} \qquad (V\text{-}30)$$

The values of the parameters which gave the minimum of χ^2 have the best chance of being the correct ones which describe the experimental data [184].

When the fluorescence decay f(t) is a sum of exponential functions as described in the following equation, the numerical equations for the calculation of the fluorescence decay $F^{cal}(t)$ may be simplified:

$$f(t) = \sum_{k=1}^{p} A_k \exp(-t/\tau_k) \qquad (V\text{-}31)$$

The parameters to be estimated from the experimental curves are the decay times τ_k and the amplitudes A_k ($k = 1,2,\ldots,p$). When the time increment ε per one channel is much smaller than any of the decay times τ_k, fluorescence intensity at time t_i, $F^{cal}(t_i)$, can be approximated as follows:

$$F^{cal}(t_i) \simeq \sum_{k=1}^{p} A_k \{ \sum_{j=0}^{i} g_j \exp[-(i-j)\varepsilon/\tau_k] \} \qquad (V-32)$$

where

$$g_j = \int_{t_{j-1}}^{t_j} g(t)\, dt \qquad (V-33)$$

Thus

$$F_i^{cal} \simeq \frac{\varepsilon}{2} \{ F^{cal}(t_i) + F^{cal}(t_{i+1}) \}$$

$$= \varepsilon \sum_{k=1}^{p} A_k \{ \sum_{j=o}^{i} g_j \exp[-(i-j)\varepsilon/\tau_k] + 0.5\, g_i \}$$

$$= \varepsilon \sum_{k=1}^{p} A_k f_k(i) \qquad (V-34)$$

The time necessary for numerical computation of $f_k(i)$ may be considerably reduced by use of the following recurrence [171]:

$$f_k(i) = \{ f_k(i-1) + 0.5 \cdot g_{i-1} \} \exp(-\varepsilon/\tau_k) + 0.5 \cdot g_i \qquad (V-35)$$

V-3-3-2 The method of moments

Isenberg and his co-workers [175,176] extented the method of moments, which had been firstly considered by Bay [174], to the form applicable to multi-exponential analysis of fluorescence decay data. Let the s-th moments of F(t) and g(t) be defined by the following equations:

$$\mu_s = \int_0^{\infty} t^s F(t)\, dt \qquad (V-36)$$

and

$$m_s = \int_0^\infty t^s \, g(t) \, dt \qquad \text{(V-37)}$$

When the fluorescence decay is the multi-exponential function as described by Eqn (V-31), then the following equations are satisfied:

$$\frac{\mu s}{s!} = \sum_{u=1}^{s+1} \frac{\Gamma_u \, m_{s-u+1}}{(s-u+1)!} \qquad \text{(V-38)}$$

where

$$\Gamma_u = \sum_{k=1}^{p} A_k \, (\tau_k)^u \qquad \text{(V-39)}$$

Using Eqn (V-38), one can obtain the values Γ_1, Γ_2, ... from the moments of the experimental curves $F^{ex}(t)$ and $g(t)$. Knowing Γ_1, Γ_2, ... , Γ_{2p}, one can obtain the decay times τ_k ($k = 1, 2, \ldots, p$) as the roots of the polynomial equation:

$$\begin{vmatrix} 1 & \tau & \tau^2 & & \tau^p \\ \Gamma_1 & \Gamma_2 & \Gamma_3 & \cdots & \Gamma_{p+1} \\ \Gamma_2 & \Gamma_3 & \Gamma_4 & \cdots & \Gamma_{p+2} \\ \vdots & \vdots & \vdots & & \vdots \\ \Gamma_p & \Gamma_{p+1} & \Gamma_{p+2} & \cdots & \Gamma_{2p} \end{vmatrix} = 0 \qquad \text{(V-40)}$$

Then, using Eqn (V-39), one obtains the amplitudes A_k ($k = 1, 2, \ldots, p$).

V-3-3-3 The method of least squares with cut-off moments

When one evaluates the moments of the experimental curves $F^{ex}(t)$, one must give a following attention: The experimental data are available only up to a certain time t_c. The moments given in Eqn (V-36) must be approximated by the integrals from zero time to time t_c. The errors produced then are significant for the moments of $F^{ex}(t)$, especialy for the higher moments which are necessary for multi-exponential analysis. Under some experimental conditions, these errors may cause incorrect estimation of the decay parameters. On the other hand, the method of least squares is free from this problem. Disadvantage of the method of least squares as compared to that of momemts is in its long computation time. When the fluorescence decay consisting of a sum of p exponential terms is analysed by the method of least squares, the 2p decay parameters must be adjusted at the same time before the best fitting being obtained.

The number of the adjustable parameters may be reduced by use of the method of least squares with cut-off moments [119]. Firstly, a set of the decay constants τ_1, τ_2, ..., τ_p is tried; and, for each set of the τ_k values, $f_k(i)$ in Eqn (V-34) are evaluated which are functions of the decay constants only. Then the s-th cut-off moments of $f_k(i)$ are obtained:

$$\nu_s(k) = \varepsilon^{s+1} \sum_{i=0}^{n_c} i^s f_k(i) \qquad \text{(V-41)}$$

where $n_c = t_c$. Let μ_s' be defined as follows:

$$\mu_s' = \varepsilon^s \sum_{i=0}^{n_c} i^s \cdot F_i^{ex} \qquad \text{(V-42)}$$

From Eqn (V-34),

$$\mu_s' = \sum_{k=1}^{p} A_k \, \nu_s(k) \qquad \text{(V-43)}$$

Given the cut-off moments μ_0', μ_1', ..., μ_{p-1}' and $\nu_0(k)$, ..., $\nu_{p-1}(k)$ $(k = 1, 2, \ldots, p)$, one can obtain the amplitudes A_k $(k = 1, 2, \ldots, p)$ from Eqn (V-43) ; then, F_c^{cal} are calculated from Eqn (V-34). The set of τ_k being the most probable may be attained after a search of the set of τ_k which minimizes χ^2.

Under some experimental conditions, fluorescence decays contain significant scatter components. Even in such a case, the decay parameters may be evaluated by the method of least squares with cut-off moments with a following modification, provided that any of the decay constants τ_k are sufficiently long as compared with the duration of exciting flash. The sums in Eqs (V-28), (V-41) and (V-42) are taken from t_c' to t_c, where $t_c' = n_c'$ is the time from which the contribution of scattered exciting light to the decay curve can be negligible. Eqn (V-28), (V-41) and (V-42) should be replaced by:

$$\chi^2 = \frac{1}{(n_c - n_c' - 1)} \sum_{i=n_c'}^{n_c} \omega_i \cdot \{ F_i^{cal} - F_i^{ex} \}^2 \qquad \text{(V-29')}$$

$$\nu_s(k) = \varepsilon^{s+1} \sum_{i=n_c'}^{n_c} i^s \cdot f_k(i) \qquad \text{(V-41')}$$

$$\mu_s' = \varepsilon^s \sum_{i=n_c'}^{n_c} i^s \cdot F_i^{ex} \qquad \text{(V-42')}$$

Even when the method presented above is used, a long computation time may be necessary in analysis of the fluorescence decay which is a sum of more than two exponential functions. However, if one or more of these exponenential functions have much longer decay constants than those of the other exponential functions (and if they are much longer than the full width of half maximum of the response function g(t)), the computation time can be reduced remarkably by use of a following procedure. Firstly, the assumption is made so that the tail region of the experimental fluorescence decay could be approximated with a sum of two exponential functions; then the two decay constants τ_p and τ_{p-1} can be estimated using the modified least square method mentioned above. Secondly, a convolution product $g(t)*[A_p \cdot \exp(-t/\tau_p)]$ is subtracted from the experimental fluorescence decay; the tail region of the subtracted fluorescence decay is again analysed with double-exponential decay and the decay parameters τ_{p-1}, τ_{p-2}, A_{p-1} and A_{p-2} will be estimated. If coincidence is not obtained between the values of τ_{p-1} estimated from the first and second double-exponential analyses, the above procedure must be re-examined; the time regions used in the analyses should be altered. If the coincidence is obtained, the above procedure may be applied to determination of the shorter decay constants.

V-3-3-4 Analysis of total and difference fluorescence decay curves by the method of least squares

Total and difference fluorescence decay curves are computed from the experimental numbers M''_i and $M^{\perp}_i$ (Eqn (V-17)). Let S_i^{ex} and D_i^{ex} be defined as follows:

$$S_i^{ex} = M''_i \exp(X'') + 2\, M^{\perp}_i \exp(X^{\perp})$$
$$D_i^{ex} = M''_i \exp(X'') - M^{\perp}_i \exp(X^{\perp}) \qquad \text{(V-44)}$$

In the analysis of these curves by the method of least squares, the fitting between the calculated and experimental curves is judged from the following quantities:

$$\chi_S^2 = \frac{1}{n} \sum_{i=0}^{n} \omega_{Si} \{ S_i^{cal} - S_i^{ex} \}^2 \qquad \text{(V-45)}$$

$$\chi_D^2 = \frac{1}{n} \sum_{i=0}^{n} \omega_{Di} \{ D_i^{cal} - D_i^{ex} \}^2 \qquad \text{(V-46)}$$

where S_i^{cal} and D_i^{cal} are the calculated time-integrated intensities at the time interval corresponding to the i-th channel (Eqn (V-2)). Since M''_i and $M^{\perp}_i$ obey the Poisson distributions, the weighting factors ω_{Si} and ω_{Di} are given by the following formulae:

$$\omega_{Si} = M''_i \exp(2X'') + 4\, M^{\perp}_i \exp(2X^{\perp}) \qquad \text{(V-47)}$$

$$\omega_{Di} = M''_i \exp(2X'') + M^{\perp}_i \exp(2X^{\perp}) \qquad \text{(V-48)}$$

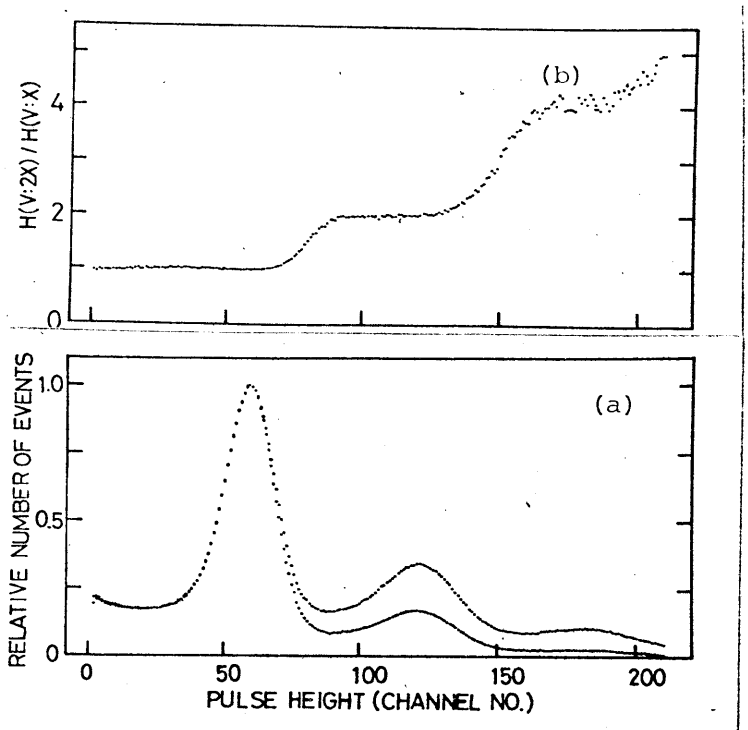

Fig. V-1. (a) the pulse-height spectra of the output signals of the preamplifier in the strobe circuit, lower curve was recorded when fluorescence intensity was half as compared with when the upper curve was recorded. (The signal was amplified 730 fold. 1 channel=0.039 V) (b): the ratio at each channel of the count number of two spectra.

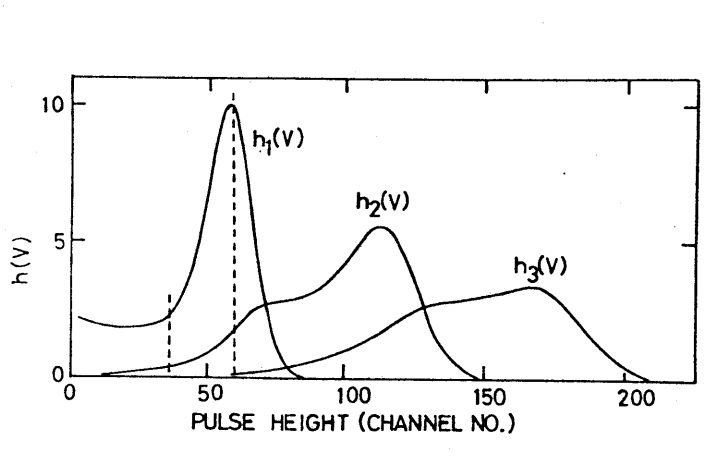

Fig. V-2. Pulse-height spectra of the output signals of the preamplifier which would be recorded if one, two or three photoelectrons are always ejected from the photocathode during one excitation cycle, respectively. Vertical dashed lines show the lower and upper discrimination levels of the single-channel analyser in the strobe circuit. (The scale of the abscissa is the same as the one in Fig. V-1.).

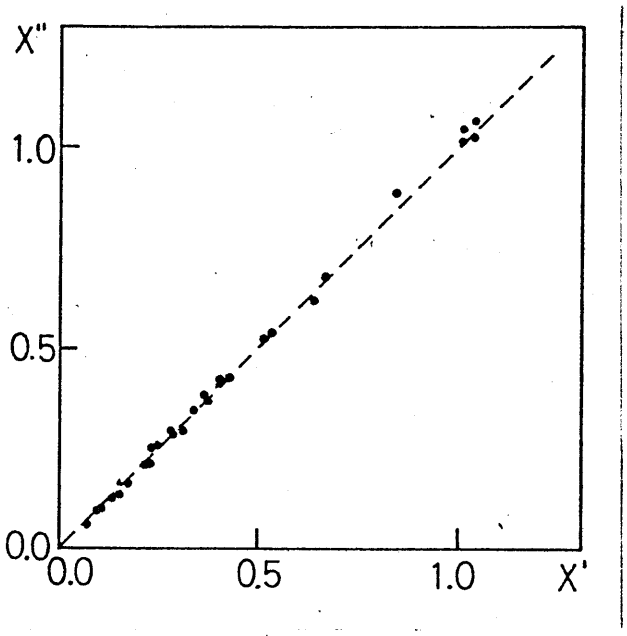

Fig. V-3. A typical observation on the relationship between the values $\bar{X}'$ and $\bar{X}''$ which were determined using Eqs (V-19) and (V-20), respectively. ---- represents the ideal case where fluorescence intensity will not fluctuate among different excitation cycles. Fluorescence from quinine sulfonate in 0.1N H_2SO_4 was observed through the cut-off filter which passed above 400 nm.

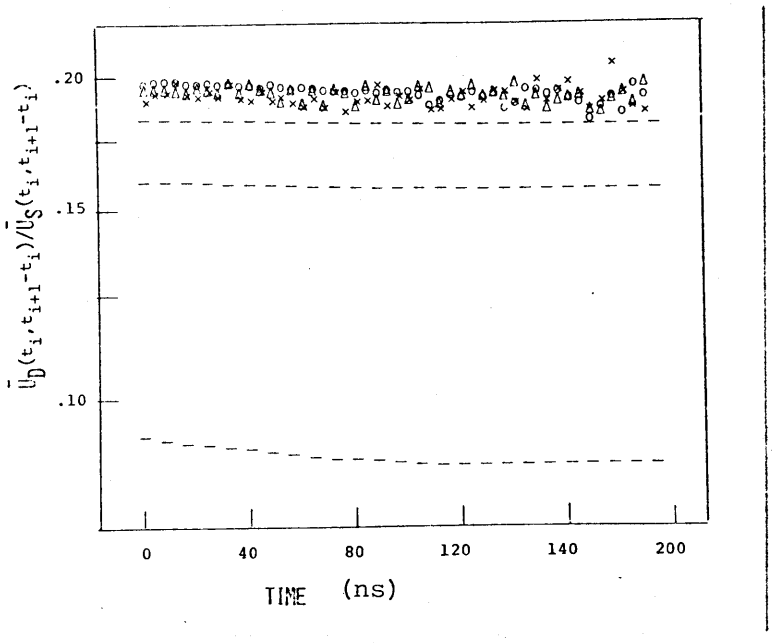

Fig. V-4. Curves of $\bar{U}_D(t_i, t_{i+1} - t_i)/\bar{U}_S(t_i, t_{i+1} - t_i)$ of fluorescence from PM-labelled F-actin which were recorded at three different count rates; o—o: $\bar{X}''$ =0.71, Δ—Δ: $\bar{X}''$ =0.234, ×—×: $\bar{X}''$ =0.046. Dashed lines represent the results if Eqn (V-18) was used (from upper, $\bar{X}''$ =0.046, 0.234, 0.71)

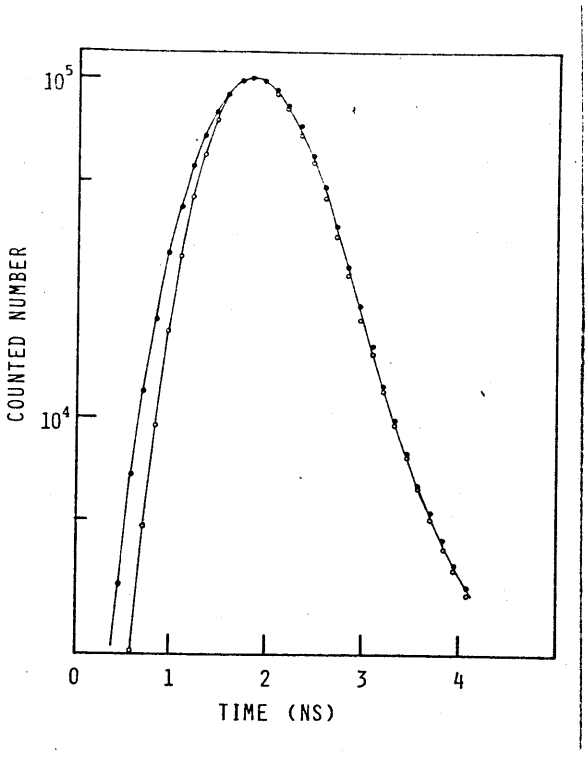

Fig. V-5. The response functions $g^{ex}(t)$ observed at 400 nm (open circle) and at 317 nm (closed circle).

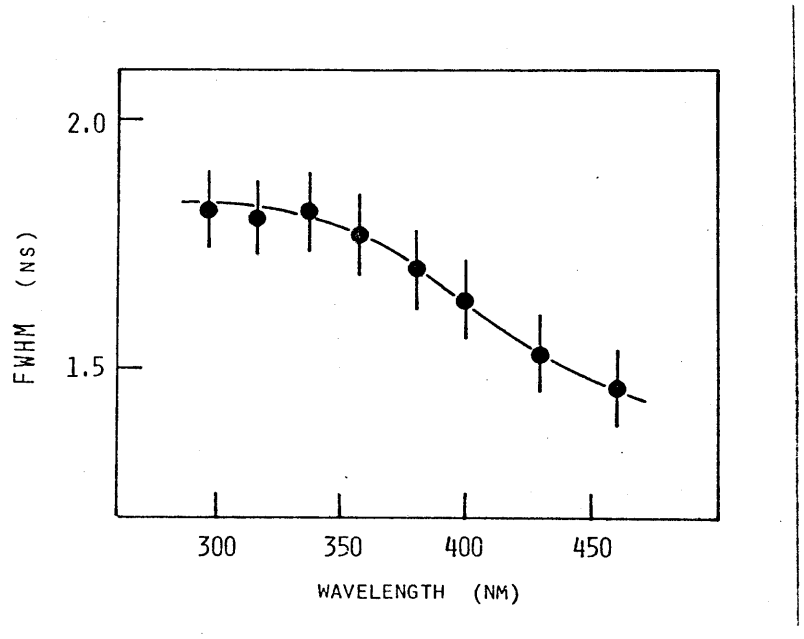

Fig. V-6. Full width of half magnitude (FWHM) of the response function $g^{ex}(t)$ as a function of wavelength.

VI CONFORMATIONAL CHANGE OF ACTIN DURING THE POLYMERIZATION

In this chapter, the behaviour of fluorescence and absorption of the conjugates of actin with PM, PMIA and PIAA were examined during polymerization of actin: These fluorescent probes are labelled to the same site (Cys-373) of the actin molecule. From comparison of the data obtained, it was found that the structure near the C-terminal region of the actin molecule is not significantly altered by increase in ionic strength. A large conformational change at this site is induced after the association of G-actin monomers.

VI-1 Introduction

G-actin polymerizes into a double-stranded polymer at high ionic strength. Up to date, a great number of physico-chemical studies have been made on thermodynamic characteristics of G-F transformation of actin. It was shown by Oosawa et al [20] that polymerization of acitn is described in terms of condensation phenomenon. However, only a little amount of information has been obtained as to what kind of change will occur of the local structure of actin protomer during the polymerization. For an instance, it has not been well documented as to when the structural change of actin protomer will occur, on increasing of ionic strength or on association of protomers.

In order to elucidate the conformational change of actin in the present study, a series of fluorescent probes of pyrene moiety of different length of reactive group were labelled to actin and the fluorescence changes associated with the polymerization of labelled actin were investigated. The probes used were N-(1-pyrenyl)maleimide [PM], N-(1-pyrenyl)methyliodoacetate [PMIA], and N-(1-pyrenyl) iodoacetamide [PIAA]. Although the conjugation of PM with actin has been previously investigated by Kawasaki et al. [185], a more systematic study of the time-resolved fluorescence of PM-labelled actin was made in the present work (Section VI-2). PMIA and PIAA are the sulfhydryl

reagents which have been recently produced by Molecular Probes (U.S.A.). The conjugation of PMIA and PIAA to actin may be firstly examined in the present work (Section VI-3 and VI-4, respectively). All these three probes were found to be labelled to the same site of actin (Cys-373); therefore, the results obtained using these probes can be compared with each other and from this comparison a more reliable information of the labelling site will be obtained.

VI-2 Polymerization of PM-labelled Actin

VI-2-1 Changes in fluorescence decay curve of PM-labelled actin with the polymerization

Fluorescence decay curves of PM-labelled actin were investigated in a solution containing 0.1 M KCl, 1 mM $MgCl_2$, 0.2 mM ATP and 10 mM phosphate buffer (pH 7.0). Depending on the concentration of PM-labelled acitn in the range from 0.003 to 0.86 mg/ml, a significant change in the fluorescnce decay curve was observed (Fig. VI-1). Since no F-actin was present at actin concentration of 0.003 mg/ml, which is below the critical concentration, all the labelled actin exists in monomeric form. On the other hand, at the highest concentration investigated (o.86 mg/ml), the majority exists in F-state. Kawasaki et al. [85] showed that the average fluorescence lifetime of actin-PM conjugate increased when the labelled G-actin was polymerized by increasing ionic strength. An important point found in

The present study is that the polymerization which was induced by increasing actin concentration without any change in ionic strength also bring about a large increase in the average lifetime.

It is possible that excitation energy transfer occurs between the fluorescent probes on two neigbouring actin protomers in F-actin, since PM-labelled actin has a weak absorption band around 376 nm where the emission spectrum has the maximum [186]. If the energy transfer of a high efficiency occurs, the fluorescence decay of PM-labelled actin protomer might depend on whether it is surrounded by the labelled actin protomers or by unlabelled actin protomers. In order to examine this possibility, F-actin was labelled with PM at various molar ratios of dye to protein (0.06 to 1.0) However, we found no detectable dependence of the fluorescence decay on the molar ratio of dye to protein, indicating that the energy transfer at high efficiency does not occur which would affect on the fluorescence decay. It is therefore apparent that a change in the local structure around the labelling site of actin protomer associated with polymerization must alter the emission mechanism of the probe.

VI-2-2 Investigation on the multiple-lifetime of PM-labelled F-actin

In contrast to the fluorescence decay, no appreciable change in shape of either absorption or fluorescence spectra

of PM-labelled actin was detected associated with the G-F transformation (Fig, VI-2). Fig. VI-3 shows typical excitation and emission spectra of fluorescence from PM-labelled G-actin and F-actin. The excitation spectrum (observed at 376 nm) had a fine strucutre of vibrational mode with peaks at 316, 329 and 344 nm. The emission spectrum (excited at 344 nm) also had a fine structure with peaks at 376, 386 and 418 nm. However, excitation at a wavelength away from the peaks (e.g., at 356 nm) brought about an additional small peak at 385 nm in the emission spectrum. Conversely, the excitation spectrum observed at 385 nm had a shoulder around 356 nm. Corresponding to these, the histogram depended on both emission and excitation wavelengths (Fig. VI-4). It is apparent from the fluorescence decay curves shown in Fig. VI-4 that the average fluorescence lifetimes observed at 385 nm and 409 nm were shorter than that observed at 374 nm. It was also found that excitation at 358 nm gave a much shorter average lifetime than excitation at 337 nm.

For determination of the factors which might cause the multiplicity of the fluorescence lifetime, a solution of the labelled F-actin containging 5 mM borate buffer (pH 8.0) was incubated at 35 °C for 40 hours [149]. It was found that the flurescence emission peaks at 376, 396 and 418 nm diminished or disappeared and, instead, new emission peaks appeared at 385 and at 406 nm (Fig. VI-3). Associated with the change in the emission spectrum, the componennts with longer decay constants (> 60 nsec) in the fluorescence decay curve diminished and the components with shorter decay components

(< 30 nsec) became dominant. It is worth noting that the red shift in the emission spectrum (Fig. VI-3) is similar to that observed by Wu et al. [187] in a system where a secondary reaction between the succinimide ring of protein-bound PM and a nearby amino group occurs. Therefore, the present finding suggests that the fluorescence decay of PM-labelled F-actin consists of, at least, two chemically distinct adducts of the dye; a main adduct which has fluorescence emission with the maximum at 376 nm and a small amount of contaminated adducts which have fluorescence emission with the maximum at 385 nm.

VI-2-3 Analysis of the fluorescence decay curves of PM-labelled F-actin

Although the contribution of the contaminated adducts may be negligible in steady-excitation fluorometry, it may be not samll enough to be neglected in measurements of fluorescence lifetime. This is because the components with short decay constants will affect the analysis of fluorescence lifetime strongly. Variations in the fluorescence decay curves were observed among several samples of PM-labelled F-actin even though the measurement condition was practically the same. The variation appeared only in the initial part during the decay (0 to 100 nsec after excitation); while a good coincidence in the later part was obtained. The variation in the initial part is likely indicating the presence of different amount of the contaminated adducts.

Since the detailed process of formation of the contaminated

adduct on the protein surface is still obscure, it is hard to determine exactly the way in which the contaminated adduct contributes to the fluorescenence decay and, therefore, to know the decay of fluorescence from the main adduct directly. It is therefore necessary to undertake the following approximation analysis. It is assumed first that the fluorescence decay s(t) of PM-labelled F-actin consists of $s_m(t)$ of the main adduct and $s_c(t)$ of the contaminated adduct:

$$s(t) = s_m(t) + s_c(t) \qquad \text{(VI-1)}$$

It is secondly assumed that $s_m(t)$ could be approximated by a sum of two exponential functions:

$$s_m(t) = A_1 \exp(-t/\tau_1) + A_2 \exp(-t/\tau_2) \qquad \text{(VI-2)}$$

where $\tau_{1,2}$ are the decay constants and $A_{1,2}$ the amplitudes of the exponential terms. In the following, we will use the relative amplitudes defined as follows:

$$B_{1,2} = A_{1,2}/(A_1 + A_2) \; ; \quad B_1 + B_2 = 1 \qquad \text{(VI-3)}$$

It was also assumed that the flurescence lifetimes of the contaminated adducts were sufficiently shorter than $\tau_{1,2}$ and therefore $s_c(t)$ was negligibly small as compared with $s_m(t)$ except for the initial part of the decay; i.e.,

$$s_c(t) \ll s_m(t) \qquad \text{for } t > t_0 \qquad \text{(VI-4)}$$

where t_0 indicates the time after that the observed fluorescence decay curves can be analysed by double-exponential

functions. The decay parameters $\tau_{1,2}$ and $A_{1,2}$ were determined by the method of least squares (Section V-3-3-3). Several sets of the decay constants were tried. For each set of the decay constants, the corresponding amplitudes $A_{1,2}$ were determined by the formula of cut-off moments (Eqs (V-41') and (V-42')) and the convoulution product of $s_m(t)$ and $g(t)$ was calculated (Eqn (V-25)); The corresponding calculated curve $(S_m)_i^{cal}$ was plotted (Eqn (V-29)) and compared with the experimental curve S_i^{ex}. The best fit between the calculated and experimental curves at $t > t_0$ was attained after a search for the set of $\tau_{1,2}$ which gives the minimum of the mean weighted residues χ_S^2.

$$\chi_S^2 = \frac{1}{(n_2-n_1-1)} \sum_{i=n_1}^{n_2} \{ (S_m)_i^{cal} - S_i^{ex} \}^2 \cdot \omega_{Si} \qquad \text{(VI-5)}$$

Here the sum was taken in the period of $t > t_0$; in most cases, $t_0 = t_{n_1} = 160$ nsec and $t_{n_2} = 850$ nsec after excitation were taken. ω_{Si} in Eqn (VI-5) is the statistical weighting factor (Eqn (V-47)). Only the data gave the minimum of χ_S^2 less than 1.2 were used in the following analyses.

Fig. VI-5 shows an example of the analysis. Closed circles show an experimental fluorescence decay curve S_i^{ex} of PM-labelled F-actin and the smooth line shows the corresponding calculated decay curve $(S_m)_i^{cal}$. The decay curve shown by open circles is the difference between S_i^{ex} and $(S_m)_i^{cal}$; on the other hand, dashed line shows the fluorescence decay curve observed with PM-labelled F-actin after incubation at 35 °C for 40 hours. Thus we then cosider that the coincidence

of these two curves is justifing the assumptions made above. Since the precision of the determined parameters even after these corrections for the contaminated adducts has a limitation, we have made efforts to reduce the amount of the contamination in preparations as far as possible. This was done by preparing protein-dye conjugate at low temperature (0 - 5 °C) and at low pH (not higher than pH 7.0) where the production of the contaminated adduct was found to be reduced considerably.

For the purpose of estimation of the effect of coexistence of the labelled G-actin with the labelled F-actin on the decay parameters, the fluorescence decays obtained at various actin concentrations were analysed. The results are summerized in Table VI-1. Both τ_1 and τ_2 increased by amounts of about 20 % when the concentration of actin was raised from 0.003 mg/ml to 0.86 mg/ml. It was also found that the relative amplitude of the longer decay component B_1 increased appreciably. At an intermediate concentration of actin (0.011 mg/ml), analysis with two exponential decays was not so satisfactory (e.g., $\chi_S^2 = 1.5$) as at the extreme concentrations (0.86 mg/ml or 0.003 mg/ml) where χ_S^2 was very close to unity. This is presumably due to the presence of approximately equal amount of G-acitn and F-actin.

VI-2-4 Dependence of fluorescence decay of labelled F-actin on the emission wavelength

In order to see the emission spectra of the decay components with time constants of τ_1 and τ_2, the time-resolved

emission spectrum of the labelled F-actin was measured after excitation at 337 nm. Then we found that the time-resolved emission spectrum obtained under the time window set between 0 and 30 nsec was more weighted around 385 and 409 nm than that obtained under the time window set between 100 and 850 nsec (Fig. VI-6). This is compatible with our observation mentioned above that the contaminated adducts had shorter lifetimes (< 30 nsec) than the main adduct and gave emission peaks around 385 and 406 nm (Fig. VI-3). Therefore we proceeded to analyse the fluorescence decay curves observed at various wavelengths (shown in Fig VI-4) according to the following scheme of three-components:

$$\Phi_1(\lambda) = h(\lambda)\ B_1(\lambda)\ \tau_1$$

$$\Phi_2(\lambda) = h(\lambda)\ B_2(\lambda)\ \tau_2 \qquad \text{(VI-6)}$$

$$\Phi_3(\lambda) = h(\lambda) \sum_{i=0}^{n_c} \{ S_i^{ex} - (S_m)_i^{cal} \} / \{ A_1(\lambda) + A_2(\lambda) \}$$

where λ is the emission wavelength and $h(\lambda)$ was determined from the time-resolved emission spectra. The values of τ_1 equal to 177 nsec and τ_2 equal to 93 nsec (at 2.5 °C) were obtained from the fluorescence decay in which emission above 370 nm was collected altogether. Strictly speaking, the lifetime thus determined were somewhat averaged in this range of wavelength. However, we also found that when the emission wavelength was selected at 375 nm with $\Delta\lambda = 5$ nm, the decay curve was described with two exponential terms satisfactorily whose time constants were 172 $\pm$ 6 nsec and 89 $\pm$ d nsec.

It is apparent that the lifetimes of τ_1 and τ_2 are approximately constant above 370 nm. Fig. VI-7 shows the three components of emission spectra $\Phi_i(\lambda)$ thus determined. One can see that the shapes of $\Phi_1(\lambda)$ and $\Phi_2(\lambda)$ are very similar to each other except for a slight red-shift of $\Phi_2(\lambda)$ as compared with $\Phi_I(\lambda)$.

VI-2-5 Temperature dependence of fluorescence decay of PM-labelled F-actin

The effect of temperature on the fluorescence decay of PM-labelled F-actin was examined between 2 and 20 °C where the results were reversible with respect to temperature. In this study, excitation was at 337 nm and emission above 370 nm was collected. The average fluorescence lifetime decreased with increase in temperature. The double-exponential analysis using Eqn VI-2 revealed that this is due to changes not only in the decay constants but also in the relative amplitude. The results are summerized in Fig. VI-8.

VI-2-6 Fluorescence anisotropy decay of PM-labelled actin

Fluorescence anisotropy decay curves of PM-labelled actin were investigated at low and high ionic strengths. Fig. VI-9 shows the typical ones, in which the experimental curves $R^{ex}(t_i) = D_i^{ex}/S_i^{ex}$ are plotted. The open circles represent the anisotropy decay curves obtained under the solvent condition of 0.2 mM ATP, 0.1 mM $CaCl_2$, 2 mM imidazole-HCl (pH 7.0) and 0.2 mM DTT (at 20.7 °C), where all the labelled actin (0.68 mg/ml) exists in G-state; while, the

closed circles represent the one obtained in the presence of 0.1 M KCl, 1 mM $MgCl_2$, 0.2 mM ATP and 10 mM phosphate buffer (pH 7.0), where the majority exists in F-state. It can be seen that the correlation time of rotation of PM-labelled actin increased on polymerization. The correlation time of labelled G-actin was 29 nsec at 20.7 °C and 49 nsec at 4.7 °C. The kinetic volume of actin is estimated using Einstein-Stokes equation $\theta^{-1} = kT/\eta V$, on the assumption that the actin molecule can be approximated with a rigid sphere. Then the correlation times obtained at the different temperatures predict the same kinetic volume which corresponds to a shperical molecule of radius 3.04 nm.

In the initial time region of the experimental curve $R^{ex}(t_i)$ of PM-labelled F-actin, a small decay component with the correlation time of about 1 μsec was detected. This component may be explained by the possible motions of the probe with respect to the F-actin filament. However, a serious problem appeared when the experimental curve was analysed; that is, it was found that the fundamental anisotropy of the contaminated adduct was different from that of the main adduct. The fundamental anisotropy observed after the incubation of PM-labelled F-actin at pH 8.0 and at 35 °C was approximately 1.1 times as large as that observed before the incubation. Thus it appeared that we had no way to obtain decisive conclutions about the flexibility of the labelling site.

VI-2-7 Discussion

The fluorescence of PM conjugated to F-actin exhibited multi-exponential decay. Wu et al. [187] have shown that PM adduct with protein often undergoes secondary reaction with amino groups of peptide of the protein through its succinimide ring (i.e., aminolysis and/or hydrolysis) (Fig. VI-10). It was found that the reaction was accompanied by a red shift of the emission spectrum. In the present study, the time-resolved emission spectra (Fig. VI-7) showed occurence of aminolysed (and/or hydrolysed) adduct in the preparation of F-actin-PM conjugate. One may consider that the multiplicity of fluorescence lifetime we observed is due to the presence of such a contaminated adduct of F-actin. Actually, analysis of emission spectra showed its existence. However we also found that even at the blue edge of the emission spectrum (372 nm) where the fluorescence intensity of the aminolysed (and/or hydrolysed) adduct is negligibly small relative to the normal adduct, the fluorescence decay is not single-exponential; it could be approximated with double-exponential function whose decay constants were 177 and 93 nsec (at 2.5°C). Among possible explanations of this multiplicity, the first possibility is that there are two different types of labelling sites. This is however unlikely since there was no detectable change in the fluorescence decay with variation of the molar ratio of dye to actin (0.06 to 1.0). It has been shown that, for several kinds of maleimide dyes, the first

mole of dye binds to the unique reactive cysteine of actin[8,188]. Thus one needs an alternative explanation. There have been several reports given recently that there is a fluorophore, which is bound to a single site within a single protein and exhibits multi-exponential fluorescence decay. For an instance, the enzyme-bound NADH is of double-exponential function [119,189,190]. Gafni and Brand [189] have attributed this to a reversible excited-state reaction which would transform the fluorescent chromophore to a non-fluorescent product. Whereas, Brochon et al. [190] gave an explanation assuming that the dehydronicotinamide moiety bound to the enzyme has a heterogeneity of local environment. In the fluorescence decay of the actin-bound PM shown in the present study, the relative amplitude of the long decay component varied with the emission wavelength; the emission spectrum $\Phi_2(\lambda)$ was slightly but distinctively red-shifted as compared with $\Phi_1(\lambda)$ (Fig. V-7). Therefore it is reasonable to conclude that there exists a heterogeneity of the excited state of the probe. Several possibilities are considered to explain this; i) two way of adsorption of the pyrene moiety to the actin molecule, or two local configurations of side chains of amino acid of actin around the labeling site, ii) existence of S1-S2 coupling of the excited states of the pyrene moiety [191]. At the present stage of the study, we are not able to decide on these possibilities. In either case, temperature dependence of ratio of amplitude B_2/B_1 of the two decay

components (Fig. VI-8) may be an indication of thermodynamic equilibrium between two possible configurations (or excited states).

As shown in Fig. VI-1, a remarkable change in the decay curve was associated with polymerization of PM-labelled actin. We found that the change is not due to increase in the ionic strength of the solution but due to the association of actin protomers (see also Table VI-1). On the other hand, occurence of local conformational change of G-actin due to increase in the ionic strength was detected by Rich and Estes [28] by proteolytic digesting method of G-actin and F-actin. According to their finding, when the ionic strength of G-actin solution is increased to 0.1 where the concentration of actin is below ciritical concentration, actin monomer becomes resistant to proteolytic digestion by trypsin and by chymotrypsin, while it is not at low ionic strength. They then proposed a state of "F-monomer" of actin, which is distinct from G-monomer at low ionic strength. Thus we can say that both G-monomer and F-monomer give essentially the same fluorescence decay of the probe used in the present study. It may be that the local structure around the probe (near the C-terminal region) is not significantly altered by increase in ionic strength, though the location of peptide which is susceptible to proteolysis at low ionic strength is not clear yet.

VI-3 Polymerization of PMIA-labelled actin

VI-3-1 Conjugation of PMIA to F-actin

The reactivity of actin-SH groups towards PMIA was investigated. F-actin was incubated with various concentrations of the dye at 20 °C for 12 hours. After removal of unreacted dye, the fluorescence intensity was measured at 397 nm after excitation at 348 nm. Fig. VI-11 shows the fluorescence intensity as a function of the molar ratio of the added dye to actin. It is apparent that PMIA reacted preferentially with a unique site of actin protomer.

VI-3-2 Absorption and fluorescence spectra of PMIA-labelled actin

Absorption and fluorescence spectra of PMIA-labelled actin (0.5 mg/ml) were investigated at room temperature. All of PMIA-labelled actin exists as G-actin in G-buffer [0.2 mM ATP, 0.1 mM $CaCl_2$, 1 mM bicarbonate and 1 mM NaN_3], while the majority exists as F-actin in F-buffer [0.1 M KCl, 1 mM $MgCl_2$, 0.1 mM $CaCl_2$, 0.2 mM ATP, 10 mM phosphate buffer (pH 7.0) and 1 mM NaN_3] as judged from the viscosity measurements (Section IV-3-3).

Fig. VI-12 shows the absorption spectrum of PMIA-labelled F-actin, which was very similar to that of PMIA-2-mercapto-ethanol conjugate, except a red-shift (Fig. IV-8). In Fig. VI-12, the difference absorption spectrum is shown of PMIA-labelled F-actin with reference of PMIA-labelled G-actin. It can be seen that polymerization of PMIA-labelled G-actin was accompanied with a red-shift of the absorption spectrum.

The maximum of absorption was located at 347.9 nm for F-acdtin and at 347.2 nm for G-actin (Table VI-2).

The excitation and emission spectra of fluorescence from PMIA-labelled actin are shown in Fig. VI-13. The shape of emission spectra of PMIA labelled G- and F-actin were very similar to each other, but polymerization of PMIA-labelled actin was accompanied with considerable increase in the fluorescence intensity.

VI-3-3 Time resolved fluorescence of PMIA-labelled actin

Polarized fluorescence decays of PMIA-labelled G- and F-actin (0.5 mg/ml) were observed above 370 nm after excitation at 337 nm.

(i) Total fluorescence decay of PMIA-laballed actin

The total fluorescence decay curves of both PMIA-labelled G- and F-actin exhibitied non-single exponential functions. For analysis of the experimental decay curves S_i^{ex}, the fluorescence decay s(t) is assumed to be a sum of exponential functions, and the method of least squares was used in which the amplitudes of the decay components was determined by use of cut-off moments (Eqs V-41 and 42). It was then found that the double-exponential decays could describe the experimental curves well. An example of the analysis is shown in Fig. VI-14, in which open circles show the experimental curve S_i^{ex} and the smooth line shows the calculated curve S_i^{cal}.

On the polymerization of PMIA-labelled G-actin, the two decay constants τ_1 and τ_2 increased by 30-40 %; at the same time, the relative amplitude B_1 of the long decay component increased considerably (Table VI-3).

The fluorescence decay of PMIA-labelled F-actin was observed at various temperatures between 5 and 39 °C. With increase in temperature, the average fluorescence lifetime decreased. This decrease was not only due to decrease in the each decay constant but also due to decrease in the relative amplitude of the long decay component. The result is summarized in Fig. VI-15.

(ii) Anisotropy decay of PMIA-labelled actin

The experimental anisotropy decay curve R_i^{ex} of PMIA-labelled G-actin is plotted which was obtained at 8.8 °C (Fig. VI-16). When log R_i^{ex} was approximated with a linear line, the inclination gave the correlation time 44 nsec. This value corresponds to the correlation time of rotation of a rigid spherical molecule whose radius is 3.10 nm (without any hydration).

The experimental curve R_i^{ex} of PMIA-labelled F-actin was obtained at various temperatures between 5 and 39 °C (Fig. V-17). At higher temperature, decay components with the correlation time shorter than 10 nsec were more pronounced. Since the contribution of PMIA-labelled G-actin co-existing with F-actin to the curves R_i^{ex} is negligible as judged from viscosity of the solution, these components of shorter correlation time are not due to the depolymerization of

PMIA-labelled F-actin. Thus we concluded that decays observed in R_i^{ex} result from rotational motions of the probe with respect to F-actin filament. Since PMIA has a long group (i.e., -NH-O-(C=O)-CH_2-), by which the pyrene moiety and the cysteine residue of the actin molecule are connected, it is probable that the rapid motion is due to the rotation presumably limited around C-N and C-O bonds in the aminoacetate group of the probe.

VI-3-4 Discussion

The fluorescence decays of PMIA-labelled actin were found to be described with double-exponential functions. Since PMIA was conjugated to the unique cysteine residue (Cys-373) of the actin molecule, this multiplicity indicates the existence of heteogeneity of environment in the excited state of the probe. It has been shown in Section VI-2-7 that actin-bound PM also has a heterogeneity of environment in its excited state. It is therefore very probable that such a heterogeneity is inherent to the labelling site of the actin molecule.

Red shift in the absorption spectrum was observed on the polymerization of PMIA-labelled G-actin. In order to elucidate the origin of this shift, absorption spectrum of the conjugate of PMIA with 2-mercaptoethanol was investigated in various organic solvents (between 300 nm and 400 nm). The solvents used were methanol, ethanol, cyclohexane and dioxane. The absorption spectra obtained in these solvents had similar shapes from each other, except slight red- or

blue- shifts. The wavelength of the absorption maximum was shown in Table VI-2. It is clear that the absorption spectrum of PMIA-2-mercaptoethanol is more red-shifted in the polar solvent than in the non-polar solvent. It is therefore unlikely that the red shift observed on the polymerization of PMIA-labelled actin is simply due to the decrease in polarity of the environment, which may be expected from the behaviour of the fluorescence quantum yield. One may note that the absorption spectra of PMIA-labelled actin in the both G- and F-states were considerably red-shifted as compared with those of PMIA-2-mercaptoethanol conjugate. When PMIA-labelled G-actin was denatured by addition of 0.1 % SDS, the wavelength of the absorption maximum was blue-shifted to 345.1 nm (Table VI-2). It is suggested that the red shift observed has resulted from the interaction of the actin-bound PMIA with a particular side chain of the protein. In the presence of 0.1 % SDS, the fluorescence decay was able to be approximated with single-exponential function (Table VI-3). It appears that the double-exponential fluorescence decays observed for the native actin are related to the specific interaction between the probe and the side chain of the protein.

VI-4 Polymerization of PIAA-Labelled Actin

VI-4-1 Conjugation of PIAA to F-actin

The reactivity of actin-SH groups towards PIAA was

investigated. F-actin (4.7 μM) was incubated with various concentrations of the dye in the presence of 0.1 M KCl, 1 mM $MgCl_2$, 0.1 mM $CaCl_2$, 0.2 mM ATP, 1 mM bicarbonate (pH 7.6) and 1 mM sodium azide. The conjugation reaction was continued in the dark at 20 °C for 20 hours and then Whatmann CF-11-cellulose was added at the final concentration of 1 % (wt/wt). After removal of the cellulose adsorbing unreacted dye, the fluorescence intensity was measured: Excitation was at 347 nm and emission was at 386 nm. As seen from Fig. VI-18, PIAA reacted preferentially with a unique site of actin protomer. In order to determine the SH group reacted, we examined the reactivity of the dye towards NEM-treated F-actin prepared as follows: F-actin was firstly reacted with NEM at 7 °C for one day; the molar ratio of NEM to actin was 1.3 : 1.0. Then this F-actin was reacted with the dye under the same condition as described above. It can be seen from Fig. VI-18 that the reaction of the dye towards to F-actin was almost completely inhibited after NEM-treatment. Since Elzinga and Collins [8] have shown that NEM reacts preferentially to Cys-373 of actin, it can be concluded that PIAA has been conjugated to Cys-373 of F-actin in the absence of NEM.

VI-4-2 Absorption and fluorescence spectra and quantum yield of PIAA-labelled actin

Absorption and fluorescence spectra of PIAA-labelled actin were investigated at 20 °C. The concentration of the labelled actin was 0.2 mg/ml. At this concentration, all

of PIAA-labelled actin exists as G-actin in G-buffer, while the majority exists as F-actin in F-buffer as judged from viscosity of the solution.

The absorption spectra of PIAA-labelled actin in G- and F-buffers (Fig. VI-19) show that polymerization of G-actin was accompanied by appearance of peaks at 365 nm and 383 nm.

The emission spectrum of PIAA-labelled F-actin showed a fine structure of vibration with peaks at 386, 407 and 430 nm, while they are less sharp in G-actin (Fig. VI-20).

Measurements of the quantum fluorescence yields of PIAA-labelled actin were made after excitation at 342 nm. The effect of the rotational Brownian motion of the fluorophore on the quantum yields was corrected. The quantum yields obtained at 13 °C were 0.083 for G-actin and 0.41 for F-actin, respectively. It should be noted that the increase in the quantum yield on polymerization of G-actin corresponds to an increase in the fluorescence intensity by 20 to 25 times when it is observed at the emission peaks (i.e., 386 or 407 nm) after excitation at 365 nm. Owing to this high sensitivity, the determination of the small amount of F-actin which co-exists with G-actin becomes much easier than viscosity measurement (Fig. VI-21). It can be seen from Fig. VI-21 that the critical concentration of actin can be determined more accurately than viscosity measurement. An important conclusion drawn from this is that the change in the fluorescence intensity observed on polymerization of actin is not due to the change in the ionic strength of

the solution but due to the association of actin monomers. In this respect, the absorbance at 365 nm was found to increase gradually with time after the addition of salts to PIAA-labelled G-actin solution. These results indicate that a change of the local conformation near the Cys-373 of G-actin is induced only after the time of association of actin monomer.

VI-4-3 Time-resolved fluorescence of PIAA-labelled F- and G-actin

VI-4-3-1 Fluorescence decays of PIAA-labelled F- and G-actin

Polarized fluorescence decay of PIAA-labelled actin was measured in G- and F-buffers at 13 °C. The total and difference fluorescence decays are shown in Fig. VI-22. Both of PIAA-labelled G- and F-actin exhibited multi-exponential fluorescence decays. The experimental decay curves $S^{ex}(t)$ were analysed as shown in the last of the section V-3-3-3. Then we found that five exponential terms are necessary in order to obtain the best fits between calculated and experimental curves. The necessity of the fourth and fifth term was realized when we extended the time range of analysis longer than 100 ns. The decay parameters obtained are given in Table VI-4. The time constant of the major term is 1.78 and 11.0 nsec for G-actin and for F-actin, respectively. The average fluorescence lifetime, which may be proportional to the fluorescence quantum yield, was calculated from the decay parameters obtained:

$$\langle\tau\rangle = \sum_{i=1}^{5} C_i \tau_i \qquad \text{(VI-7)}$$

where C_i are the relative amplitudes of the exponential decay components. The average fluorescence lifetime of PIAA-labelled G-actin was 3.99 nsec; on the other hand, it was 10.0 nsec for PIAA-labelled F-actin.

VI-4-3-2 Anisotropy decay of PIAA-labelled F-actin

At first, the following experimental cruve $R^{ex}(t)$ was examined:

$$R^{ex}(t) = D^{ex}(t)/S^{ex}(t) \qquad \text{(VI-8)}$$

As seen in Fig. VI-23, the experimental curve $R^{ex}(t)$ of PIAA-labelled F-actin has plateau in the initial (0-20 nsec) and tail (200-500 nsec) time regions; between 80 nsec and 150 nsec, $R^{ex}(t)$ decreased remarkably. This can not be explained by assuming that, for all of k, $r_k(t)$ in Eqn III-42 are represented with the same function. Instead, A_{ki} in Eqn III-41 is needed to vary with k. For simplification of analysis of $D^{ex}(t)$, it was assumed that the anisotropy decay of PIAA-labelled F-actin could be characterized with a single correlation time Θ_F; furthermore, it was assumed that $r_{i0} = r_{a0}$ for i = 1,2,3 and $r_{i0} = r_{b0}$ for i = 4,5 (Eqn (III-41)):

$$r_{1,2,3}(t) = r_{a0} \exp(-t/\Theta_F)$$
$$r_{4,5}(t) = r_{b0} \exp(-t/\Theta_F) \qquad \text{(VI-9)}$$

Then the parameters r_{a0}, r_{b0}, Θ_F were determined according

to the way shown in Eqn (V-44). The values obtained are shown in Table VI-5. There is a large difference between the values of r_{a0} and r_{b0}. The value of θ_F is of the order of μsec. The smooth line in Fig. VI-23 is the R(t) curve calculated from the parameters obtained. It is obvious that the anomalous behaviour of the experimental curve $R^{ex}(t)$ could be explained with the difference between the fundamental anisotropies r_{a0} and r_{b0}.

VI-4-3-3 Anisotropy decay of PIAA-labelled G-actin

When the experimental curve log $R^{ex}(t)$ of PIAA-labelled G-actin was approximated with a linear line in the time region between 0 and 10 nsec, the inclination gave the correlation time 25 nsec (at 13 °C). This value is much shorter than the rotational correlation time of actin monomer (32 nsec) which is estimated from the previous reports [192]; therefore, we considered that the fluorophore has a freedom of rotation on actin. For simplification of analysis of $D^{ex}(t)$, it was assumed that, for i = 1,2,3, $r_i(t)$ were represented with the following equation;

$$r_i(t) = r_{G0}\{\beta_f \exp(-t/\theta_f) + (1-\beta_f) \exp(-t/\theta_G)\} \quad \text{(VI-10)}$$

where θ_f is the correlation time of the rotation of the fluorophore on actin and θ_G corresponds to the rotation of actin monomer. We analysed the curve $D^{ex}(t)$ between 0 and 30 nsec, in order to obviate the possibility that the assumption for $r_{4,5}(t)$ would strongly affect the estimation

of the parameters in Eqn (VI-10). Then the parameters r_{G0}, θ_f, θ_G were obtained which are shown in Table VI-5. The fundamental anisotropy r_{G0} was almost equal to r_{a0} obtained for F-actin. The correlation time of the rotation of the fluorophore was about 1.5 nsec. Existence of such a rotation may be the origin of obscurity of the emission spectrum of PIAA-labelled G-actin.

VI-4-4 Discussion

The reslut of the fluorometric titration of SH groups of F-actin with PIAA indicates that a single SH group is preferentially reactive with the dye, i.e. Cys-373. On the other hand, fluorescence decays of PIAA-labelled actin were found to be multi-exponential functions (Table VI-4). The possibility may be considered that the experimental decay components with small amplitudes are due to the reagents which are conjugated to the amino acid residues different from Cys-373 or due to impurity of the original reagent. It is, however, unlikely that the dominant exponential decay components also come from such heterogeneities. Fluorescence decays with multi-lifetime have been found for several fluorescent reagents which were conjugated to Cys-373 of actin [151,193]. It is resonable to consider that multiplicity of fluorescence lifetime of PIAA-labelled actin is mainly due to a heterogeneity of the local environment which is inherent to the labelling site of the actin molecule. The question is raised as to whether this heterogeneity is pre-existing in the ground

state of the dye or appears only in its excited state. With this respect, one may note from comparison of the absorption and excitation spectra of PIAA-labelled actin (Figs VI-19 and VI-20) that the fluorescence quantum yield is dependent on the excitation wavelength; for PIAA-labelled F-actin, the quantum yield observed after excitation around 365 nm is about 1.3 times as large as that observed after excitation around 345 nm. One may ask whether the electronic transition corresponding to the absorption band around 345 nm is different from the one corresponding to the absorption band around 365 nm or not. In order to examine this possibility, we investigated the excitation polarization spectrum of PIAA-labelled F-actin (Fig. VI-20). The time-averaged anisotropy was almost independent on the excitation wavelength in the region between 330 and 370 nm. It may be suggested from this result only that the two peaks of the excitation spectrum at 345 nm and at 365 nm comes from the same electronic but different vibrational excitation transitions. Both the results about the quantum yield and the polarization spectrum can be explained as follows. The fluorophore has a heterogeneity of the local environment even in its ground state; and, some fraction of the fluorophore exists in a state of low quantum yield and another fraction exists in a state of high quantum yield; in the former state, the absorption spectrum is relatively similar to that of PIAA-labelled G-actin; while, in the latter state, the absorption spectrum exhibits a strong vibronic band at 365 nm and whose shape may be approximated with the excitation spectrum

obtained for PIAA-labelled F-actin. The change in the absorption spectrum induced on the polymerization of actin appears to be due to the change in these fractions.

Another interesting question is what kind of the change in the local environment can result in the large change in the absorption spectrum observed on the G-F transformation. When the absorption spectra of PIAA-2-mercaptoethanol conjugate were measured in various organic solvents with different polarities (i.e., hexane, dioxane, chlorofolm, ethanol), all of them are relatively similar to the absorption spectrum of PIAA-labelled G-actin and none have a strong vibronic absorption band around 365 nm as seen in the one of PIAA-labelled F-actin. It is therefore unlikely that the possible change in local polarity only results in the large change in the absorption spectrum of PIAA-labelled actin. Presumably a specific interaction between the fluorophore and a side chain of F-actin causes a strong vibronic band around 365 nm.

VI-5 General Discussion

According to the helical polymer model proposed by Oosawa and Kasai [24], a conformational change occurs in the actin monomer when it joins to F-actin nuclei or to growing helical polymer. Recently, Rich and Estes showed by proteolytic digesting method that the addition of 0.1 M KCl induces a rapid change in the conformation of G-actin to form "F-actin monomer" prior to the formation of the

nuclei. Therefore, one must consider at least two kinds of conformational change during the polymerization process of actin. In the present work, we examined the behaviour of fluorescence and absorption of the conjugate of actin with PM, PMIA and PIAA during polymerization of actin: These fluorescent probes are labelled to the same site (Cys-373) of the actin molecule. Then we found:

1) The polymerization of PM-labelled G-actin was accompanied with a remarkable change in the fluorescence decay; this change is shown to be not due to a change in the ionic strength but due to the association of G-actin monomer.

2) The polymerization of PMIA-labelled G-actin was accompanied with a red shift in the absorption spectrum. This shift could not be explained by the possible change in the polarity of environment of the labelling site; and the specific interaction of the probe with a side chain of the protein is suggested.

3) The polymerization of PIAA-labelled G-actin was accompanied with conspicious change in the absorption and fluorescence spectra, which are found to be induced only after the association of G-actin monomers. It is suggested that the appearance of a strong absorption band at 365 nm after the polymerization is due to formation of the specific interaction of the probe with a side chain of the protein.

4) The fluorescence decays of PM- and PMIA-labelled actin could be approximated with double-exponential functions, and the relative amplitude of the long decay component was

found to increase on the polymerization of labelled aftin. The multiplicity of the fluorescence lifetime was also found for PIAA-labelled actin. These multiplicities appear to result from the heterogeneity of environment which is inherent to the labelling site.

From these results, it is apparent that the structure near the C-terminal region of the actin molecule is not significantly altered by increase in ionic strength. A large conformational change at this site is induced after the association of G-actin monomers and, then, the actin molecule takes a conformation which is favourable to the specific interaction of the probe with a side chain of the protein; this interaction is characterized by anomalous red-shift of the absorption spectrum of PMIA-labelled actin, or by appearance of the strong absorption band at 365 nm of PIAA-labelled actin. The heterogeneity of local environment of the probe which is an origin of the multiplicity of fluorescence lifetime of labelled actin is conceivably related to this interaction. In this respect, temperature dependence of the relative amplitude of the fluorescence decay components was observed for PM- and PMIA-labelled F-actin, suggesting the existence of a thermal equilibrium between the possible local conformations. It appears that the conformational change of actin induced after the association of actin monomers accompanies a shift in this equilibrium.

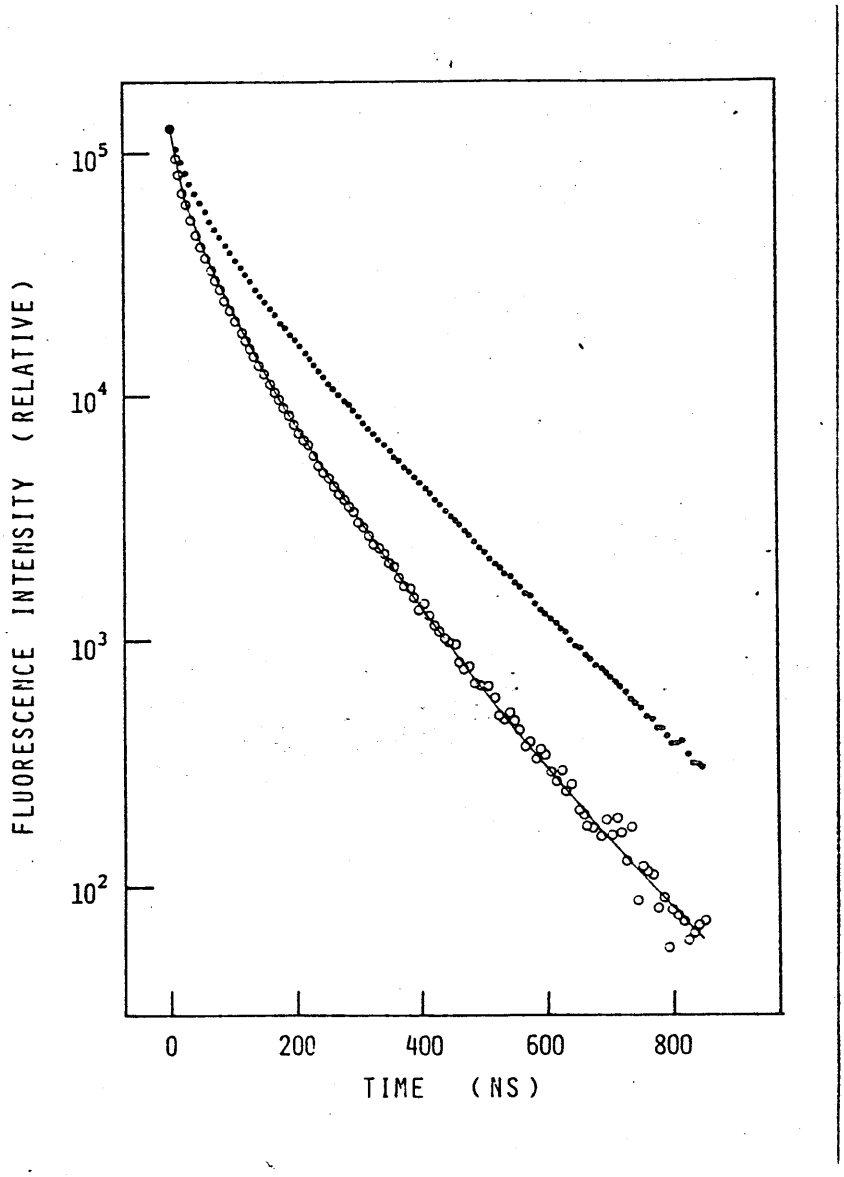

Fig. VI-1. Fluorescence decay curves of PM-labelled actin at different actin concentrations. Actin concentrations were 0.86 mg/ml (●) and 0.003 mg/ml (o). Solvent condition: KCl, 0.1 M; $MgCl_2$, 1 mM; ATP, 0.2 mM; phosphate buffer (pH 7.0), at 3°C. Smooth line shows the fluorescence decay curve observed at low ionic strength: i.e., ATP, 0.2 mM; $MgCl_2$, 0.1 mM; EGTA, 0.05 mM; Imidazole-HCl, 2 mM (pH 7.0); actin, 0.96 mg/ml.

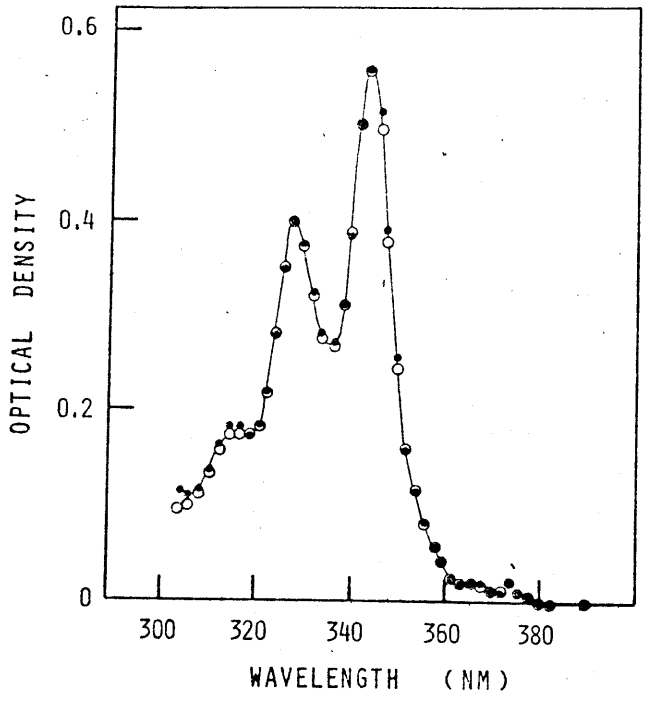

Fig. VI-2. Absorption spectra of PM-labelled actin at high (●) and low (o) ionic strengths. Solvent condition: 0.1 M KCl, 1 mM $MgCl_2$, 0.2 mM ATP and 10 mM phosphate buffer (pH 7.0) (●), or 0.2 mM ATP, 0.1 mM $MgCl_2$, 0.05 mM EGTA and 2 mM Imidazole-HCl (pH 7.0) (o). Actin concentration was 2.0 mg/ml.

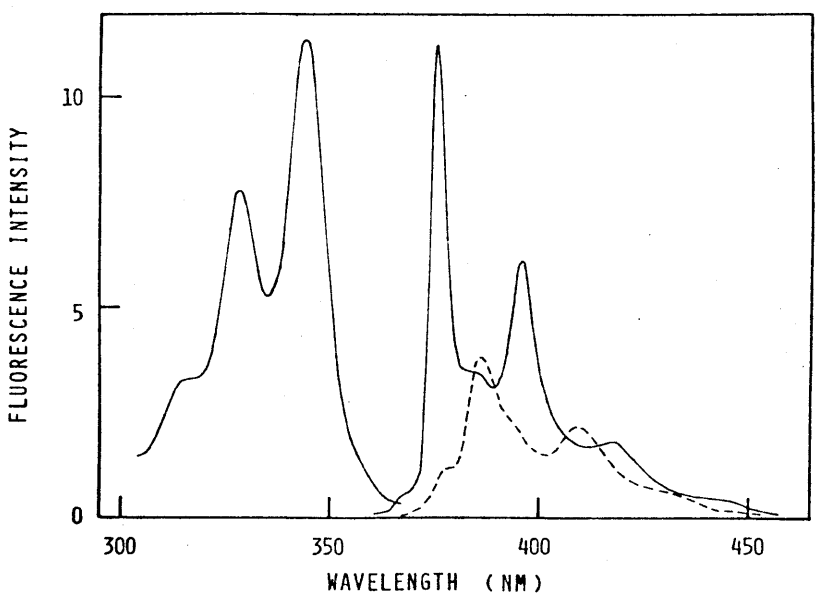

Fig. VI-3. Fluorescence spectra of PM-labelled F-actin (smooth lines). The excitation spectrum (left) was observed at 376 nm; the emission spectrum (right) was obtained after excitation at 344 nm; the slit width was 3 nm. Solvent condition: 0.1 M KCl, 1 mM $MgCl_2$, 0.2 mM ATP, 10 mM phosphate buffer (pH 7.0) and 0.2 mg/ml actin. Dotted line shows the fluorescence emission spectrum of the PM-labelled F-actin which had been incubated at pH 8.0, at 38°C for 40 hrs (in this experiment, actin which had been denatured during the incubation was removed by performing a cycle of polymerization and depolymerization before fluorescence measurement).

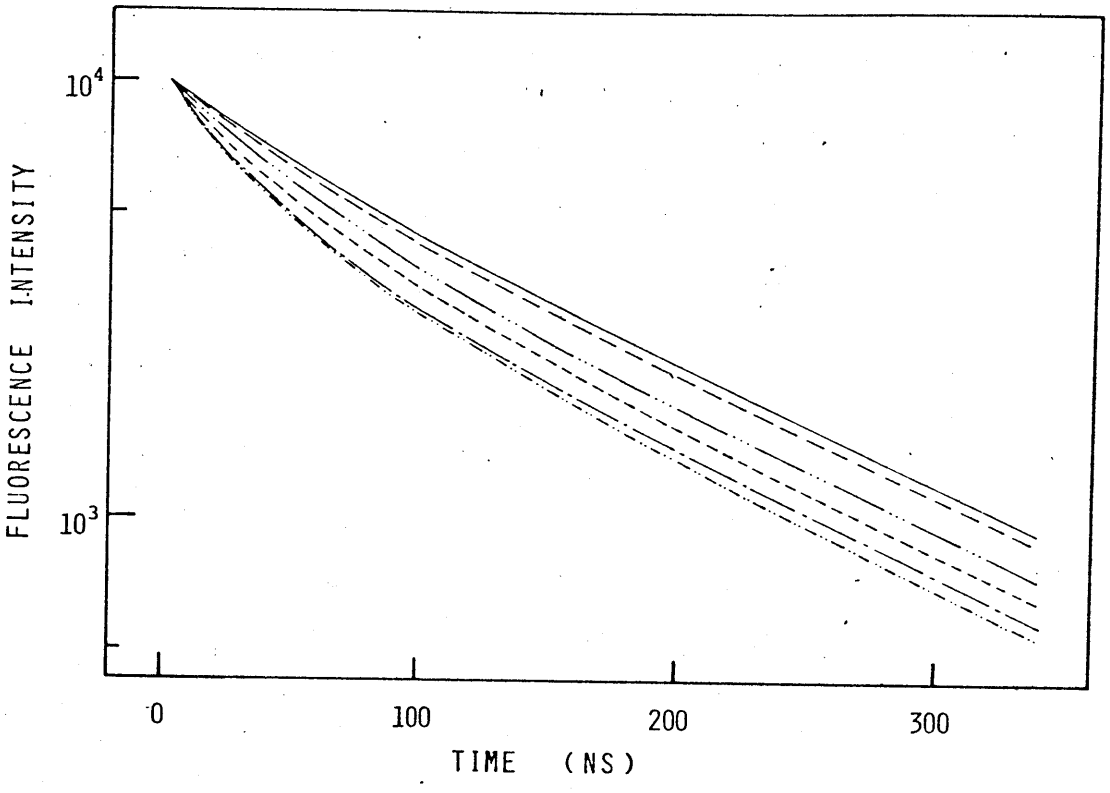

Fig. VI-4. Dependence of the fluorescence decay of PM-labelled F-actin on the emission wavelength. Emission was at 372 nm (———), 374 nm (— — —), 386 (— · · · —), 380 nm (----), 385 nm (—·—), and 409 nm (—·—·—); excitation was at 337 nm. Solvent condition: actin, 1.4 mg/ml; KCl, 0.1 M; $MgCl_2$, 1 mM; ATP, 0.2 mM, phosphate buffer, 10 mM (pH 7.0), at 2.5°C.

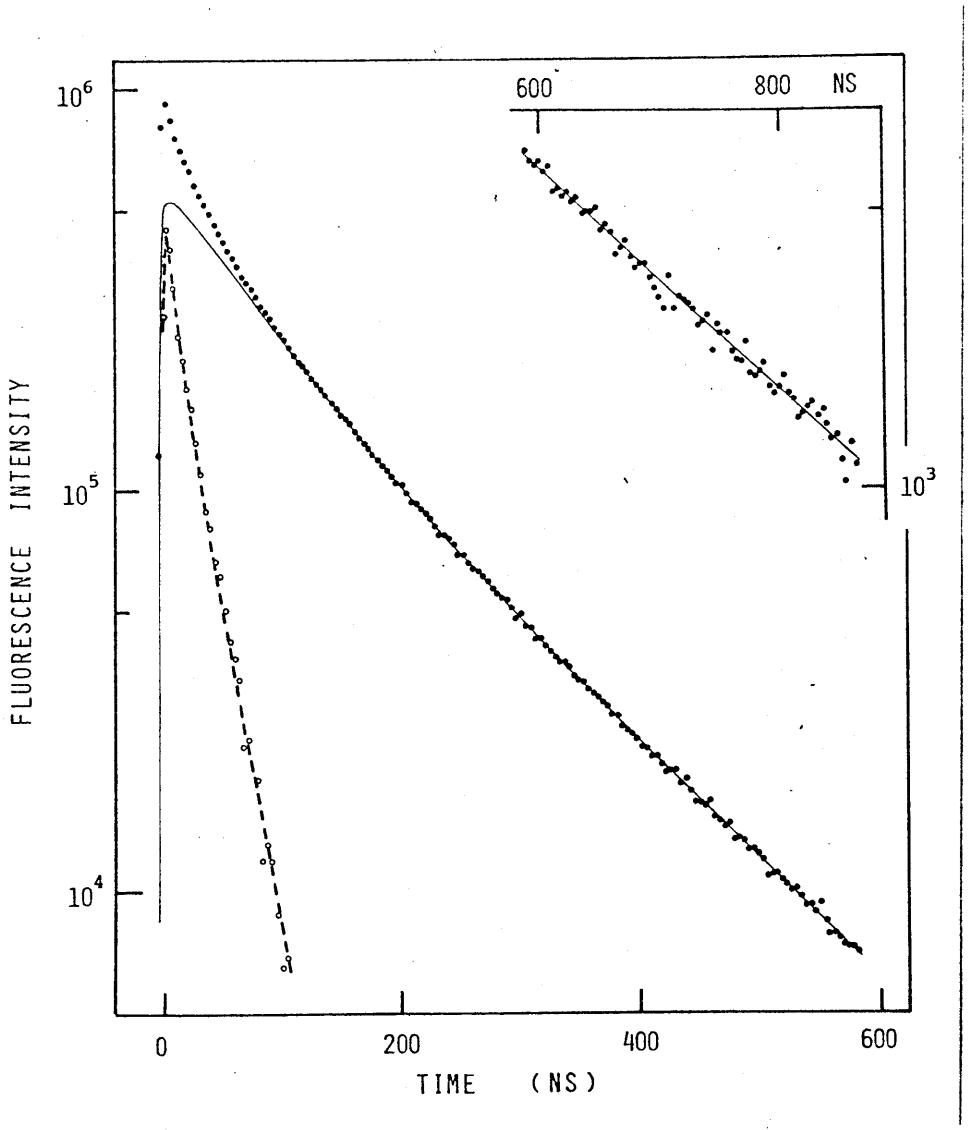

Fig. VI-5. An experimental fluorescence decay curve (closed circle) and the result of a double-exponential analysis (smooth line) of PM-labelled F-actin (0.2 mg/ml) in the presence of 0.1 M KCl, 1 mM $MgCl_2$, 10 mM phosphate buffer (pH 7.0) and 0.2 mM ATP at 1°C: Excitation was at 337 nm and emission above 370 nm was collected. The dashed line shows difference between the experimental and calculated decay curves. The curve represented by open circles shows the fluorescence decay of PM-labelled F-actin which was obtained after the labelled F-actin solution being incubated at pH 8.0, at 35°C for 40 hrs: Excitation was at 358 nm and emission above 400 nm was collected.

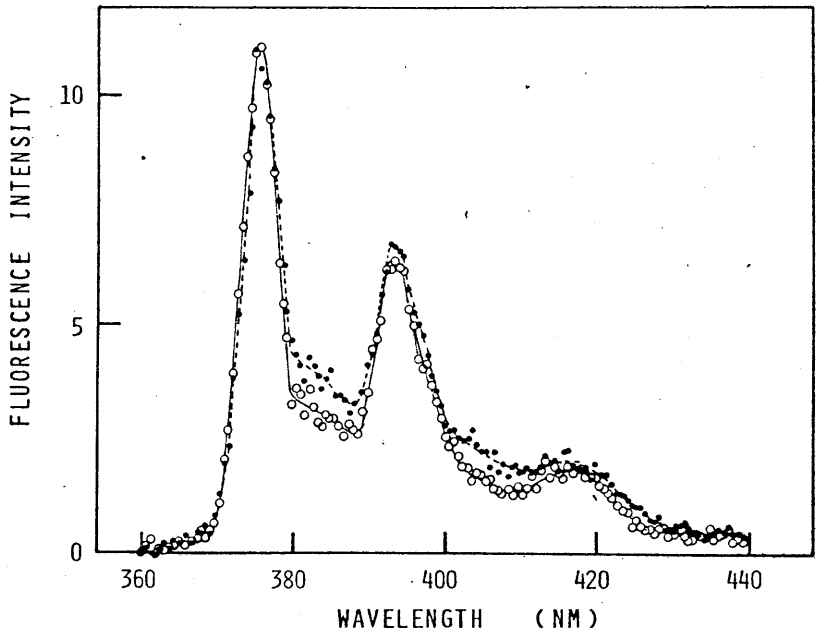

Fig. VI-6. Time-resolved fluorescence emission spectra (corrected) of PM-labelled F-actin. The time window during the fluorescence decay was set between 0 and 30 nsec (closed circle), or between 100 and 850 nsec (open circle) after excitation. The slit width was 2 nm and excitation was at 337 nm. Solvent condition was the same as that shown in Fig. VI-5.

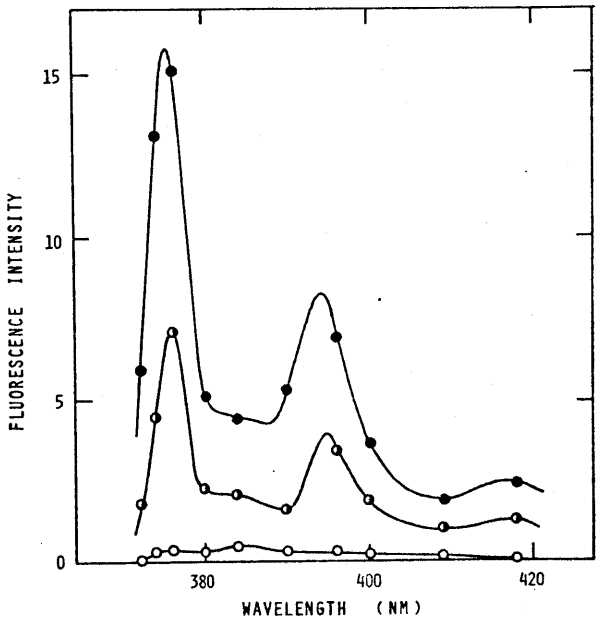

Fig. VI-7. Decomposition of the emission spectrum of PM-labelled F-actin into three decay components. ●—●, $\Phi_1(\lambda)$; ◑—◑, $\Phi_2(\lambda)$; ○—○, $\Phi_3(\lambda)$.

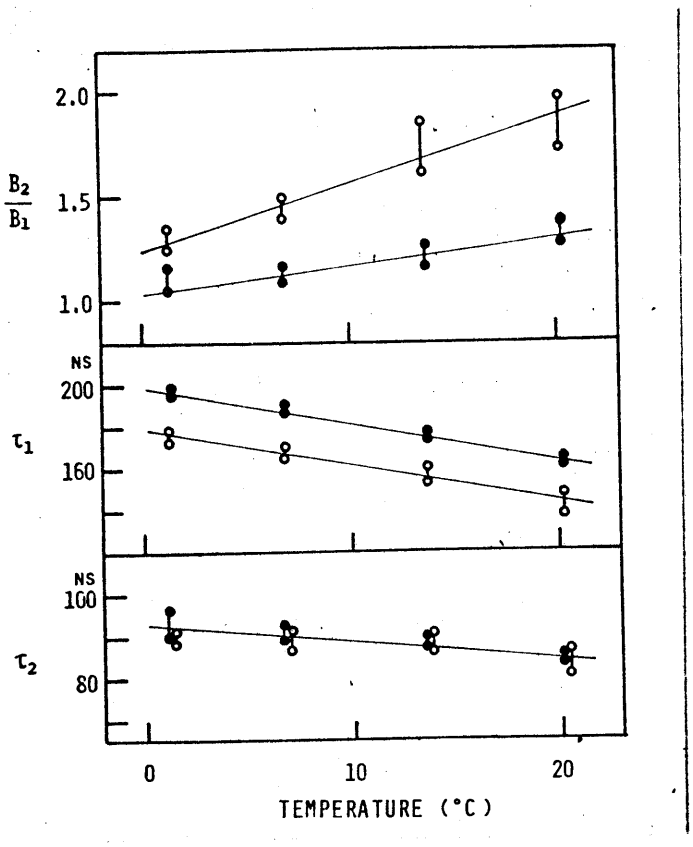

Fig. VI-8. Temperature dependence of the decay parameters of fluorescence from PM-labelled F-actin. ●—●, PM-labelled F-actin alone (0.2 mg/ml); o—o, in the presence of heavy meromyosin ([heavy meromyosin]$_{mol}$/[actin]$_{mol}$ = 1/2). Solvent condition: 0.1 M KCl, 1 mM $MgCl_2$, 10 mM phosphate buffer (pH 7.0); ATP (in the absence of heavy meromyosin) or ADP, about 20 μM.

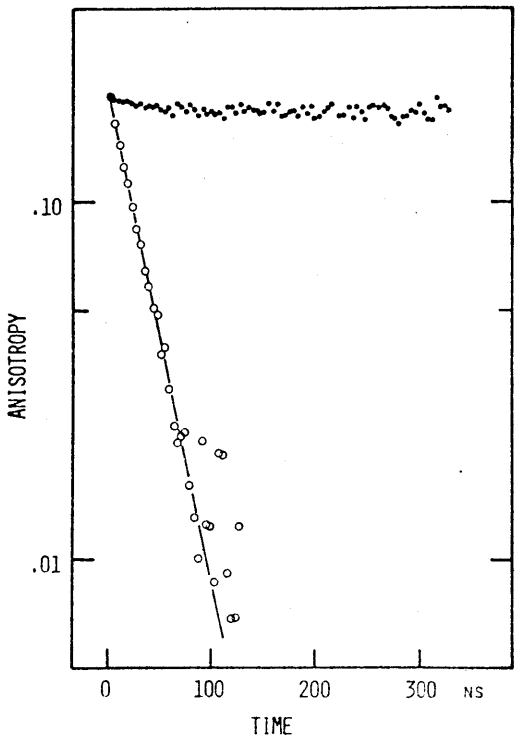

Fig. VI-9 Experimental fluorescence anisotropy decay curve of PM-labelled G-actin (open circle) at 20.7°C. Excitation was at 337 nm and emission above 380 nm was collected. Solvent condition: 0.2 mM ATP, 0.1 mM $MgCl_2$, 2 mM Imidazole-HCl (pH 7.0), 0.2 mM NaN_3 and 0.2 mM DTT.
The curve shown by closed circles is the anisotropy decay curve of PM-labelled F-actin.

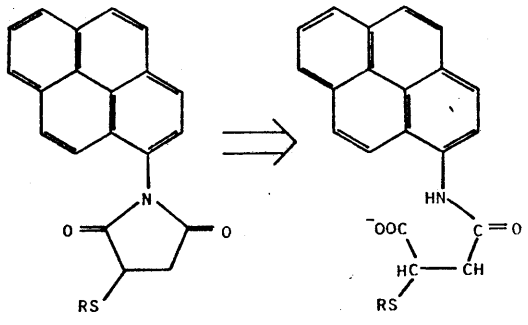

Fig. VI-10. Hydrolytic opening of the imide ring of PM adduct with actin.

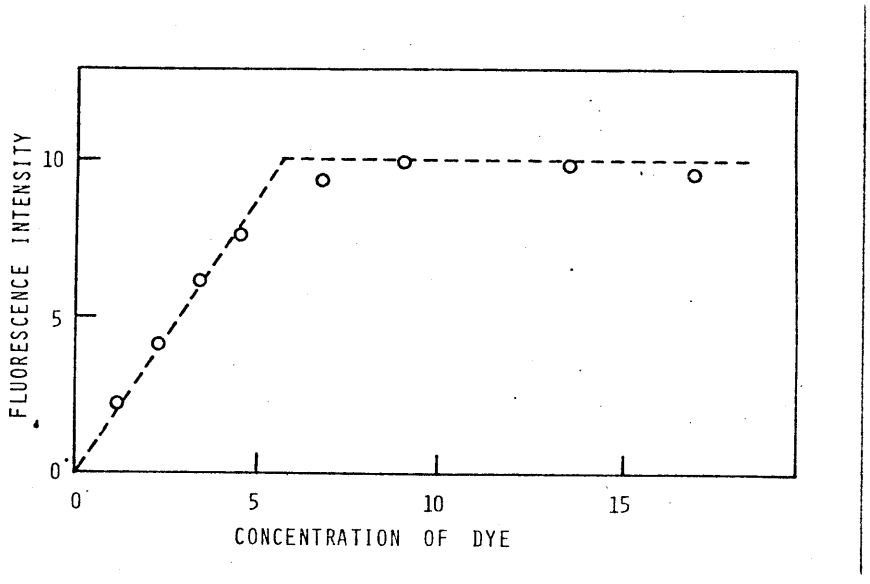

Fig. VI-11. Fluorometric titration of actin-SH groups with PMIA. F(Ca)-actin (6.2 μM) was incubated with various concentrations of PMIA in the presence of 0.1 M KCl, 1 mM $MgCl_2$, 0.1 mM $CaCl_2$, 0.2 mM ATP, 1 mM bicarbonate and 1 mM sodium azide. The conjugation was continued in the dark at 20°C for 12 hrs and then CF-11-cellulose was added at the final concentration of 1 % (wt/wt). The cellulose adsorbing unreacted dye was sedimentated by centrifugation at 3,000 rpm for 10 min. The fluorescence intensity of the supernatant was measured at 397 nm after excitation at 348 nm.

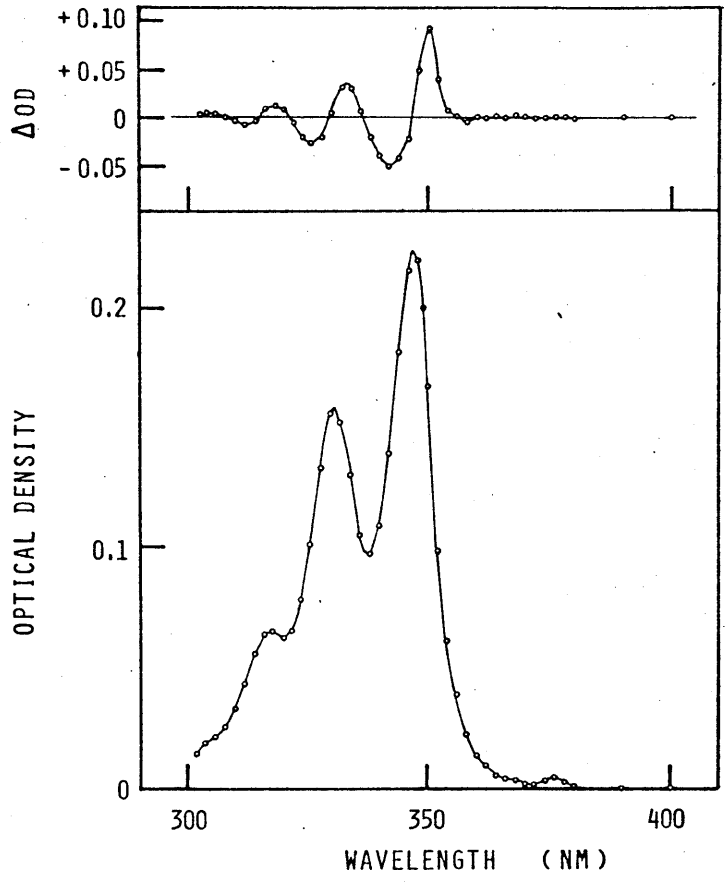

Fig. VI-12. Absorption spectrum of PMIA-labelled F-actin (lower). Actin concentration was 0.5 mg/ml. Solvent condition: KCl, 0.1 M; $MgCl_2$, 1 mM; $CaCl_2$, 0.1 mM; ATP, 0.2 mM; phosphate buffer, 10 mM (pH 7.0); NaN_3, 1 mM. Upper figure shows the difference absorption spectrum of PMIA-labelled F-actin with reference of PMIA-lavelled G-actin: The concentrations of both F- and G-actin were 0.5 mg/ml. The G-actin solution contains 0.2 mM ATP, 0.1 mM $CaCl_2$, 2 mM Imidazole-HCl (pH 7.0) and 1 mM NaN_2.

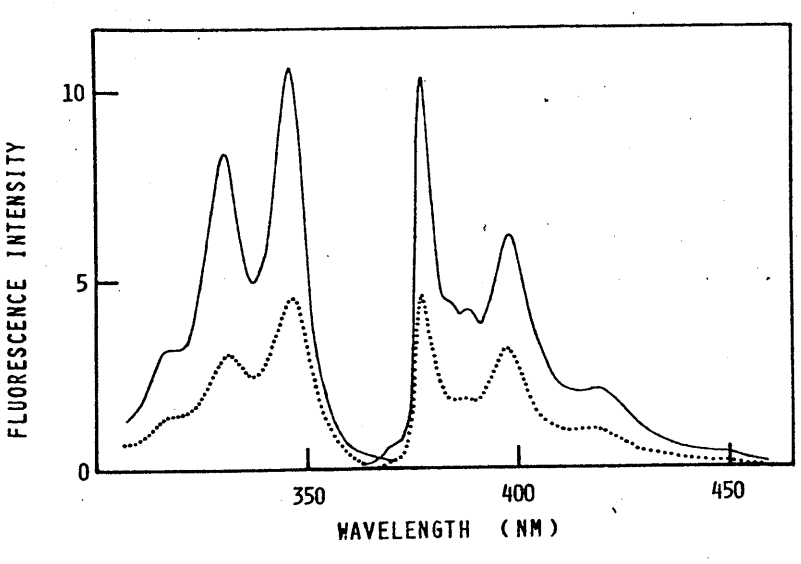

Fig. VI-13. Fluorescence spectra of PMIA-labelled G- (dashed lines) and F-actin (smooth lines). The excitation spectra (left) were observed at 376 nm; the emission spectra were obtained after excitation at 348 nm. The solvent conditions are shown in Fig. VI-13.

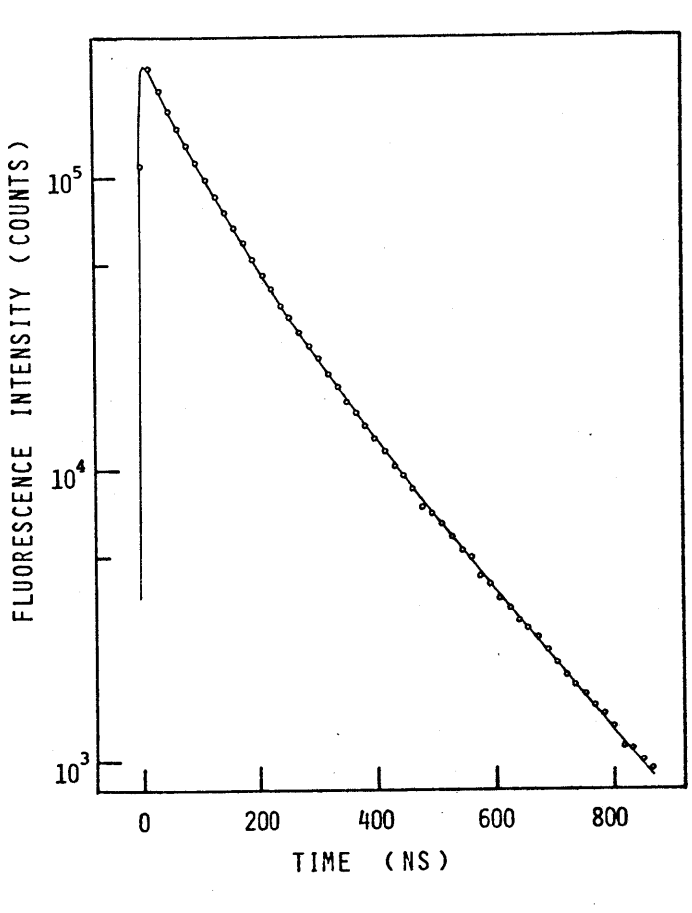

Fig. VI-14. An experimental fluorescence decay curve (closed circle) and the result of a double-exponential analysis (smooth line) of PMIA-labelled F-actin (0.5 mg/ml) in the presence of 0.1 M KCl, 1 mM $MgCl_2$, 0.1 mM $CaCl_2$, 0.2 mM ATP, 10 mM phosphate buffer and 1 mM NaN_3 at 8.8°C.

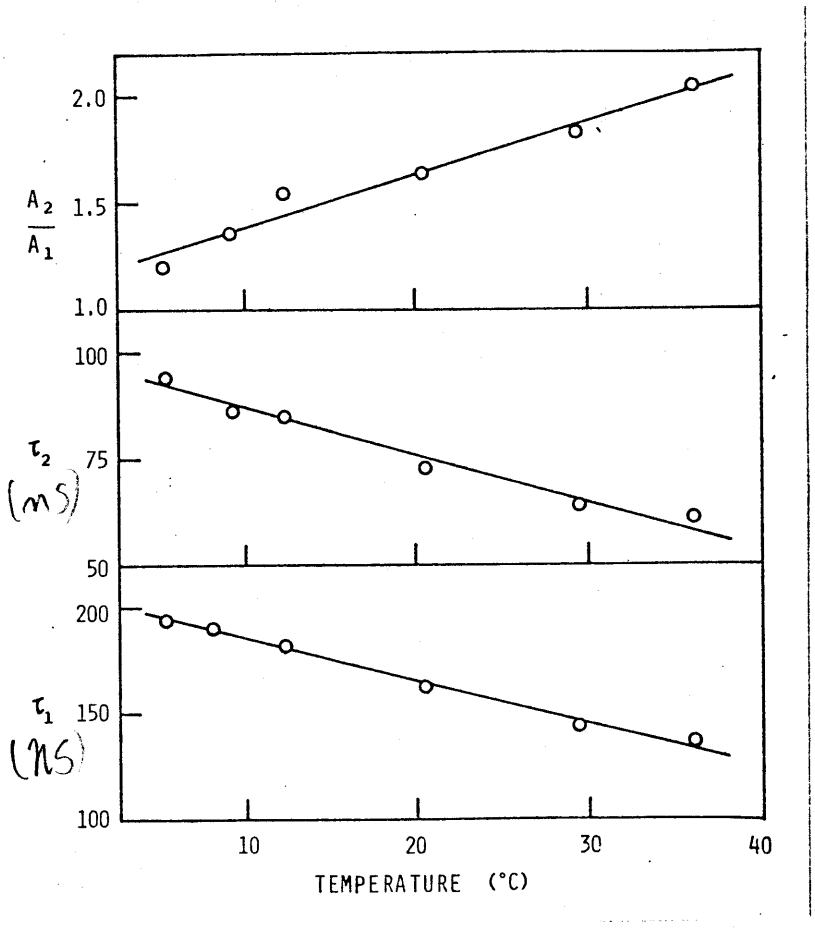

Fig. VI-15. Temperature dependence of the decay parameters of fluorescence from PMIA-labelled F-actin. Solvent condition: KCl, 0.1 M; $MgCl_2$, 1 mM; $CaCl_2$, 0.1 mM; ATP, 0.2 mM; phosphate buffer, 10 mM (pH 7.0); NaN_3, 1 mM; actin, 0.5 mg/ml.

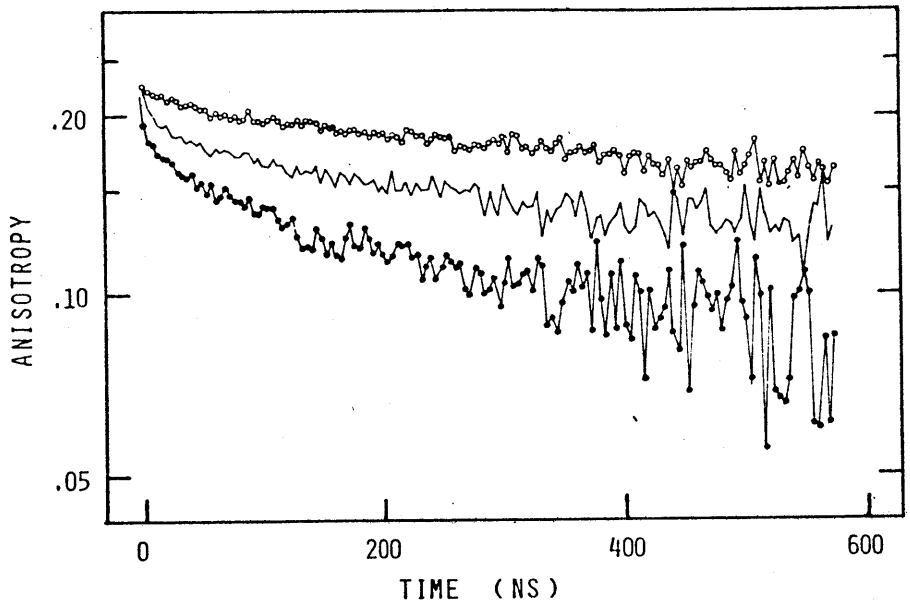

Fig. VI-16. Experimental fluorescence anisotropy decay of PMIA-labelled F-actin (0.5 mg/ml). Temperature of the solution was 5.2°C (o—o), 20.5°C (——), or 36.0°C (●—●). Excitation was at 337 nm and emission was collected between 370 and 400 nm.

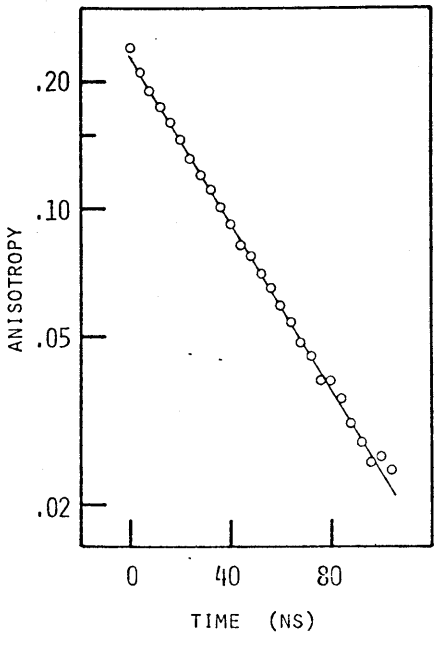

Fig. VI-17. Experimental fluorescence anisotropy decay of PMIA-labelled G-actin (0.5 mg/ml) at 8.8°C. Fluorescence measurement was made under the same condition as that shown in Fig. VI-16.

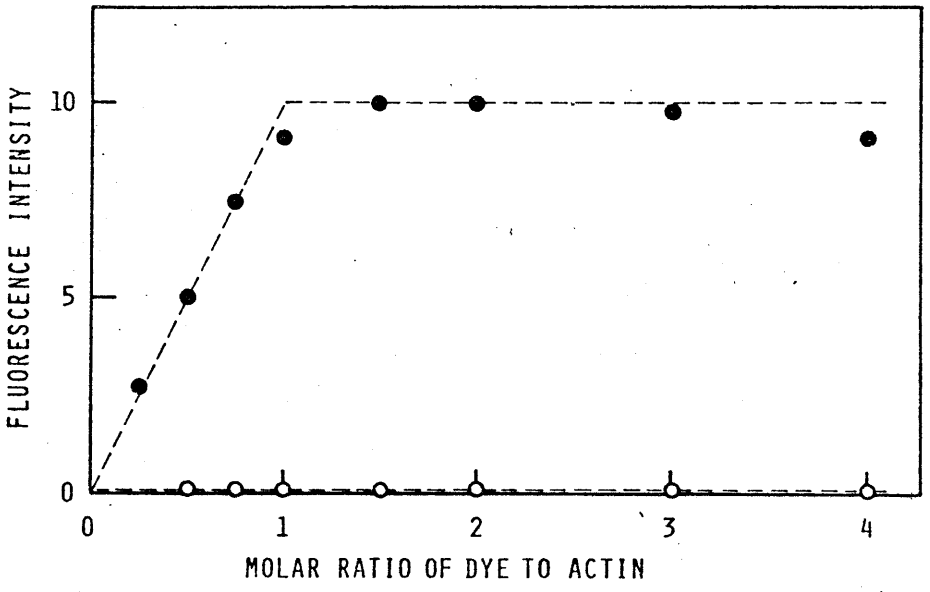

Fig. VI-18. Fluorometric titration of actin-SH groups with PIAA. Native (closed circle) and NEM-treated F-actin (open circle) were reacted with various concentrations of PIAA in the presence of 0.1 M KCl, 1 mM $MgCl_2$, 0.1 mM $CaCl_2$, 0.2 mM ATP, 1 mM bicarbonate and 1 mM sodium azide at 20°C for 20 hrs. After unreacted dye being removed, the fluorescence intensity was measured at 386 nm after excitation at 347 nm.

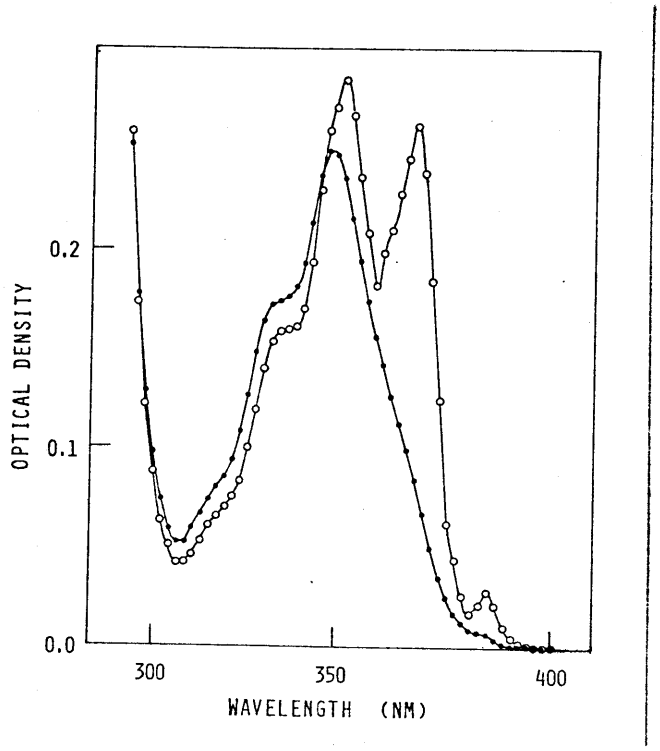

Fig. VI-19. Absorption spectrum of PIAA-labelled G- (closed circle) and F-actin (open circle). Solvent condition was 0.2 mM ATP, 0.1 mM $CaCl_2$, 2 mM Imidazole-HCl (pH 7.0), 1 mM NaN_3 and 1 mM 2-mercaptoethanol for G-actin; or 0.1 M KCl, 1 mM $MgCl_2$, 0.1 mM $CaCl_2$, 0.2 mM ATP, 10 mM phosphate buffer (pH 7.0), 1 mM NaN_3 and 1 mM 2-mercaptoethanol for F-actin. The concentration of actin was 0.5 mg/ml.

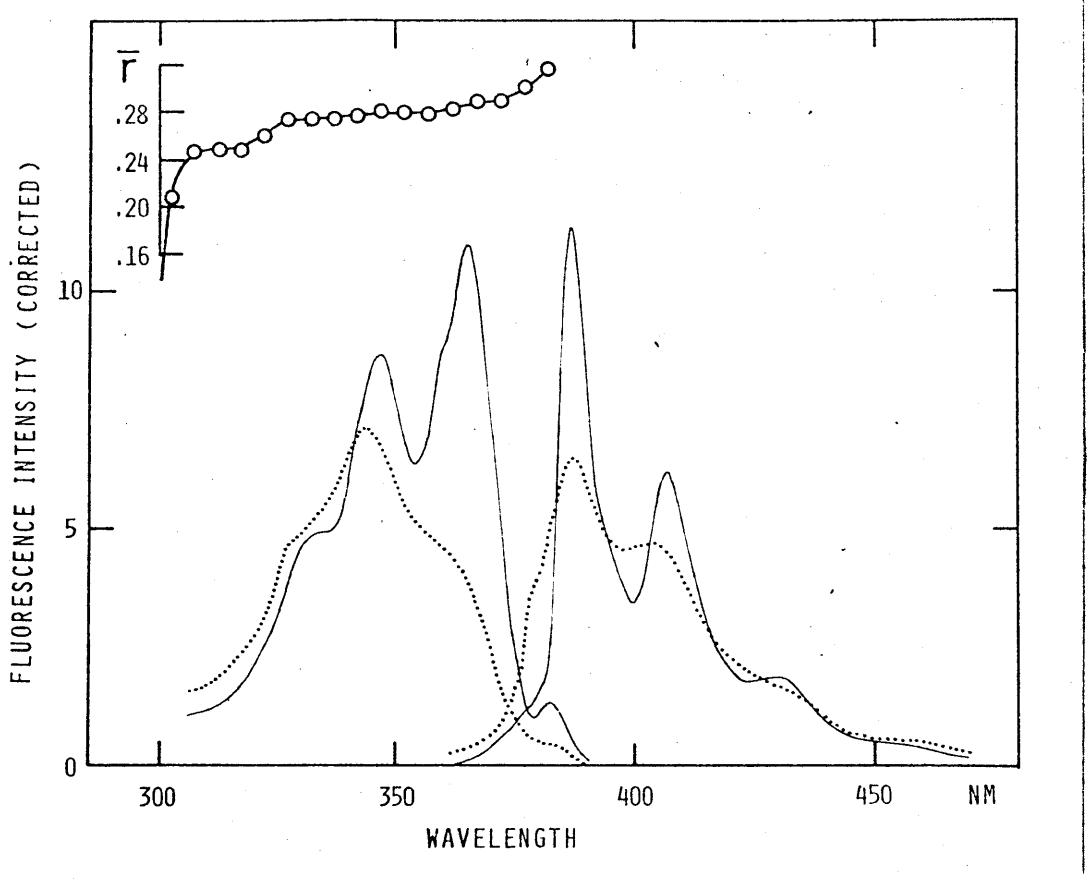

Fig. VI-20. Fluorescence spectra (corrected) of PIAA-labelled G- (dotted line) and F-actin (smooth line). The excitation spectra (left) were observed at 407 nm and the emission spectra (right) were obtained after excitation at 342 nm, where the slit width was 3 nm. The excitation spectra are normalized so as to have the same intensity at 342 nm and the two emission spectra are normalized so as to give the same integrated intensity. The excitation polarization spectrum of PIAA-labelled F-actin is shown in the upper side: The slit width was 3 nm and emission was observed at 407 nm. The solvent conditions for G- and F-actin are shown in Fig. VI-19.

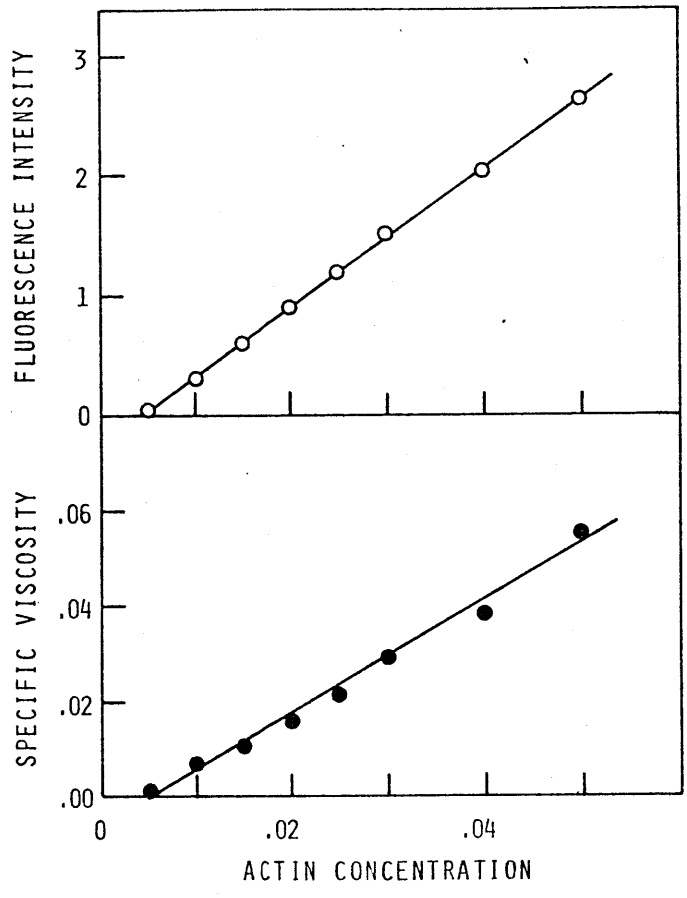

Fig. VI-21. Fluorescence intensity (upper) and specific viscosity (lower) of PIAA-labelled actin as a function of the total concentration of actin. Fluorescence intensity was measured at 365 nm after excitation 407 nm: The slit width was 3 nm. Solvent condition: KCl, 0.1 M; $MgCl_2$, 1 mM; $CaCl_2$, 0.1 mM; ATP, 0.2 mM; phosphate buffer, 10 mM (pH 7.0), NaN_3, 1 mM; 2-mercaptoethanol, 1 mM; at 20°C.

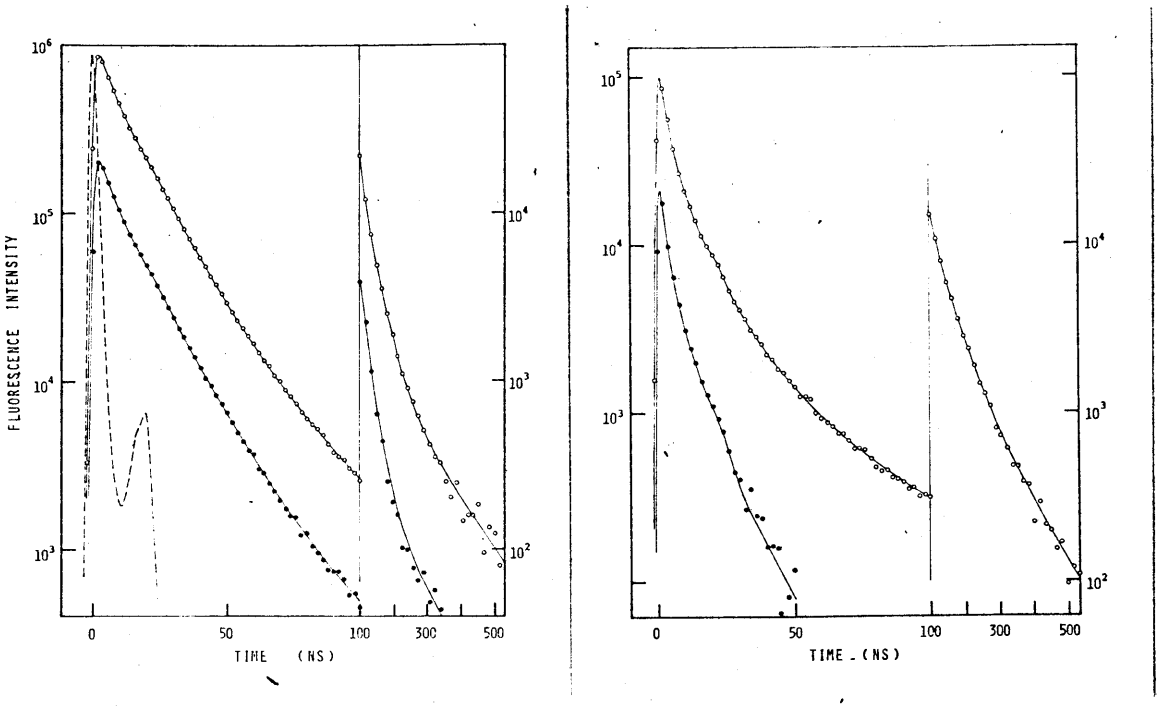

Fig. VI-22. Fluorescence decays of PIAA-labelled G- (right) and F-actin (left). Open and closed circles show the experimental total and difference fluorescence decay curves, respectively. The calculated decay curves are shown by smooth lines. Exitation was at 358 nm and emission above 400 nm was collected. Temperature of the solution was 13°C. The solvent conditions for G- and F-actin are shown in Fig. VI-19.

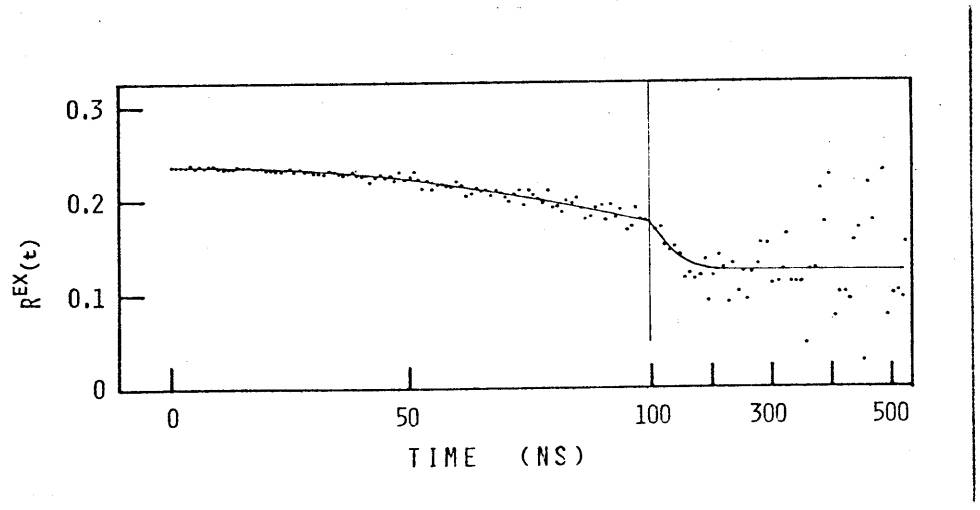

Fig. VI-23. An experimental fluorescence anisotropy decay curve (closed circle) and the result of analysis (smooth line) of PIAA-labelled F-actin.

Table VI-1 Double-exponential analysis of fluorescence decay of PM-labelled actin.

c*	solvent	temperature	τ_1	τ_2	B1	R
mg/ml	salt[a]	°C	nsec	nsec		
1.4[b]	+	2.5	172	89	0.67	1.13
0.86	+	3.0	173	86	0.469	0.94
0.011	+	3.0	175	89	0.351	1.50
0.003	+	3.0	151	75	0.256	1.21
0.96	-	3.0	150	75	0.242	1.07

a) (+) indicates that the solution contained 0.1 M KCl, 1 mM $MgCl_2$, 200 µM ATP, and 10 mM phosphate buffer (pH 7.0); and (-) indicates 100 µM $MgCl_2$, 50 µM EGTA, 200 µM ATP and 2 mM Imidazole-HCl (pH 7.0).

b) Emission was at 375 nm and the slit width was 5 nm; in other cases, emission above 370 nm was collected altogether.

Table VI-2 The wavelength of the absorption maximum of PMIA conjugate with actin or 2-mercaptoethanol in various solvent conditions.

conjugate	solvent	concentration	λ_m (nm)
G-actin-PMIA	0.2 mM ATP [a]	0.5 mg/ml [d]	347.2
F-actin-PMIA	0.1 M KCl [b]	"	347.9
actin-PMIA	0.1 % SDS [c]	"	345.1
2-SHOH-PMIA	methanol	8 μM [e]	342.6
"	ethanol	"	342.5
"	cyclohexane	"	343.6
"	dioxane	"	344.5

a) 0.2 mM ATP, 0.1 mM $CaCl_2$, 2 mM Imidazole-HCl (pH 7.0) and 1 mM NaN_3. b) 0.1 M KCl, 1 mM $MgCl_2$, 0.1 mM $CaCl_2$, 10 mM phosphate buffer (pH 7.0), 0.2 mM ATP and 1 mM NaN_3. c) 0.1 % SDS, 0.1 M phosphate buffer (pH 7.0). d) the concentration of protein. e) the concentration of dye.

Table VI-3 Double-exponential analysis of fluorescence decay of PMIA-labelled actin (0.5 mg/ml).

solvent	temp 0°C	τ_1 ns	τ_2 ns	A_1	A_2	χ_s^2
F-buffer	8.8	87	195	0.431	0.569	1.49
G-buffer	8.8	67	130	0.375	0.625	1.97
0.1% SDS[a]	25.0	47	110	0.144	0.856	1.76

(a) 0.1% SDS, 0.1 M phosphate buffer (pH 7.0)

Table VI-4 Fluorescence decay parameters of PIAA-labelled actin (at 13°C).

	G-actin		F-actin	
i	τ_i (ns)	C_i (×100)	τ_i (ns)	C_i (×100)
1	1.78	64.0	2.80	31.2
2	7.0	29.2	11.0	52.1
3	18.4	6.0	19.0	15.7
4	55	0.74	41	1.0
5	154	0.042	149	0.026
$\langle\tau\rangle$	3.99		10.0	

Table VI-5 Anisotropy decay parameters of PIAA-labelled actin (at 13°C)

(i) F-actin

r_{a0}	r_{b0}	θ_F (ns)	χ_D
0.238	0.125	5×10^3	1.46

(ii) G-actin

r_{G0}	β_f	θ_f (ns)	θ_G (ns)	χ_D
0.235	0.19	1.5	38	1.08

VII CONFORMATIONAL CHANGE OF F-ACTIN UNDER INFLUENCE OF BINDING OF HEAVY MEROMYOSIN OR SUBFRAGMENT-1.

Fluorescence behaviours of PM- and PIAA labelled F-actin were examined in the presence of heavy meromyosin or subfragment-1. From the results obtained;

1) it is strongly suggested that binding of myosin head to F-actin alters the conformation of the each protomer towards that of G-actin.

2) no evidence was obtained for the presence of the co-operative nature between the protomers in the actin filament on the binding of myosin head (in the system without ATP).

VII-1 Introduction

F-actin activates the Mg-ATPase activity of myosin by a factor of several hundreds. This activation is believed to be related to the molecular process of the force generation of muscle contraction. Offer et al. [66] have shown that the ability of G-actin to activate the ATPase activity of myosin subfragment-1 is cosiderably less than the activation obtained with F-actin under identical conditions. In order to explain this superiority of F-actin compared with G-actin, they considered the possibility that conformational change occurs in the subunits of F-actin during the interaction with myosin and the conformational change accelerates the rate-limiting step in the cycle of ATP hydrolysis by myosin. If so, the problem would be raised as to what kind of conformational change is induced in F-actin during the interaction with myosin. Although several reports [72-79,194,195] have been published about the conformational change in actin filament induced by binding of heavy meromyosin or subfragment-1, there have been controversies among their results and interpretations. Therefore a systematic study of actin-myosin interaction will be desired to clear up the situation.

In the present work, the fluorescence behaviours of PM- and PIAA-labelled F-actin were investigated in the presence of heavy meromyosin or subfragment-1. The results obtained using PM and PIAA will be presented in Section VII-2 and VII-3, respectively.

VII-2 Binding of Heavy Meromyosin to PM-Labelled F-actin

VII-2-1 Steady-excitation fluorometry of the complex of PM-labelled F-actin with heavy meromyosin or subfragment-1

To a concentrated solution of PM-labelled G-actin (about 2 mg/ml) containing 0.2 mM ATP, salts (0.1 M KCl, 1 mM $MgCl_2$, 10 mM phosphate buffer, pH 7.0) were added. Then the solution was left standing at 5 °C for 5 to 8 hours so that PM-labelled G-actin polymerized completely. This mother solution of PM-labelled F-actin was mixed with various amounts of heavy meromyosin or subfragment-1. After the ATP being hydrolysed, fluorescence measurements were done. In the steady fluorescence measurement, excitation and emission were fixed at 344 nm and 396 nm, respectively. Scattered light of exciting beam was eliminated using a dilute $NiSO_4$ solution filter and optical cut-off filters.

VII-2-1-1 Binding of heavy meromyosin(TR)

The fluorescence intensity of polarized fluorescence of PM-labelled F-actin was investigated in the presence of heavy meromyosin(TR) which was prepared by tryptic digestion. At low saturation of binding of heavy meromyosin(TR) to F-actin, anomalous phenomena of the solution were found; when the solution was poured into the sample cuvette ($1 \times 1 \times 4$ cm^3), the fluorescence intensity began to decrease and settled to a level in a few minutes; then, if the solution

was agitated mechanically, the fluorescence intensity increased abruptly; and after the mechanical agitation being ceased, the fluorescence intensity began to decrease again (Fig. VII-1). The magnitude of the fluctuation in the fluorescence intensity was dependent on the degree of binding saturation of heavy meromyosin(TR) to F-actin. The large fluctuation as shown in Fig VII-1 was not observed in the absence of heavy meromyosin(TR) or in the presence of the excess amount of heavy meromyosin(TR); it occured only at low saturation of binding of heavy meromyosin(TR) to F-actin. On the other hand, the fluctuation in the polarized fluorescence intensity was found to result from both fluctuations in the fluorescence anisotropy and in the total fluorescence intensity. Fig VII-2 shows the fluorescence anisotropy and the total fluorescence intensity as a function of the amount of heavy meromyosin(TR) added. When the polarized fluorescence intensities were observed at 8 - 10 min after the solution being poured into the sample cuvette, the biphasic changes with increasing amount of heavy meromyosin(TR) were found in both the fluorescence anisotropy and the total fluorescence intensity (open circles in Fig. VII-2); while, when the solution of acto-heavy meromyosin(TR) was agitated mechanically, these biphasic changes were diminished or disappeared (closed circles in Fig. VII-2).

VII-2-1-2 Binding of heavy meromyosin(CT)

Heavy meromyosin(CT), which was prepared by chymotryptic

digestion, was added to PM-labelled F-actin (0.2 mg/ml). The complex of PM-labelled F-actin and heavy meromyosin(CT) did not exhibited the large fluctuations in the polarized fluorescence intensity as observed in the presence of heavy meromyosin(TR). Although change in the total fluorescence intensity of the complex was observed after the mechanical agitation, the magnitude of the change was very small (Fig. VII-3). As for the fluorescence anisotropy of PM-labelled F-actin, no large dependence on the molar ratio of heavy meromyosin to F-actin was detected even without the mechanical agitation.

VII-2-1-3 Binding of subfragment-1

Subfragment-1 prepared by chymotryptic digestion was added to PM-labelled F-actin (0.5 mg/ml), and the polarized fluorescence intensity of the complex was measured at 8 - 10 min after the solution being poured. When the amount of subfragment-1 added was increased, the biphasic changes as shown in Fig. VII-2 were often observed in the fluorescence and in the total fluorescence intensity. But the magnitude of fluctuation varied between preparations of subfragment-1; and, sometimes, no large fluctuation was detected in the fluorescence intensity. One may consider the possibility that variation in the results obtained is related to heterogeneity of subfragment-1, since there have been known to exist two species of subfragment-1; the one with A1-light chain and the one with A2-light chain (S1-A1 and S1-A2, respectively) [146]. For examination

of this possibility, subfragment-1 was fractionated into S1-A1 and S1-A2. However, the result obtained using the fractionated subfragment-1 was the same as the one obtained using the subfragemnt-1 before fractionation. Therefore, another explanation was needed. On the course of the study, we found that the variation of the result occured even when the same sample was used; that is, after the acto-S1-A1 solution was left standing at 5 °C for 2 days, fluctuation in the polarized fluorescence intensity became larger than that observed before the store (Fig. VII-4). It is therefore suggested that the aging of proteins is at least one of origins of the anomalous fluctuation observed.

VII-2-2 Pulse-excitation fluorometry of the complex of PM-labelled F-actin and myosin head

In the pulse-excitation fluorometry, excitation was at 337 nm and emission above 370 nm was collected altogether. Measurements of fluorescence decay were started at 10 - 20 min after the solution being poured into the sample cuvette, and done without mechanical agitation.

VII-2-2-1 Total fluorescence decay of PM-labelled F-actin in the presence of heavy meromyosin or subfragment-1

Typical experimental decay curves of total fluorescence of PM-labelled F-actin (0.2 mg/ml) in the presence of heavy meromyosin(CT) are shown in Fig. VII-5. The average fluorescence lifetime decreased monotonically on increasing amount of heavy meromyosin(CT), and showed a saturation at

a molar ratio approximately equal to 0.5. The similar behaviour in the average lifetime was observed when heavy meromyosin(TR) was added to PM-labelled F-actin. The decrease in the average lifetime does not indicate depolymerization of F-actin by the presence of heavy meromyosin, since heavy meromyosin has an effect to shift the G-F equilibrium of actin towards F-state [196]; actually, in the presence of heavy meromyosin, the supernatant after centrifugation of PM-labelled F-actin solution contained less actin than in the absence of heavy meromyosin. Therefore the occurence of some conformational change in actin protomer is highly probable. In order to examine the change of lifetime in detail. Data shown in Fig. VII-5 were analysed on the basis of assumption that each fluorescence decay consists of a sum of two exponential functions (Eqn (VI-2)). Fig. VII-6 shows the result of this analysis. A decrease in the relative amplitude B_1 of the long decay component is an apparent determining factor of the decrease in the average lifetime.

The temperature depedence of the decay times $\tau_{1,2}$ and the ratio of amplitudes B_2/B_1 in the presence of heavy meromyosin(CT) is included in Fig VI-8. One may note that the change in the ratio B_2/B_1 was more remarkable at higher temperature, the reason of which is not clear at the present stage.

When subfragment-1 was added to PM-labelled F-actin (0.5 mg/ml), decrease in the average fluorescence lifetime was also found; the average lifetime decrease monotonically

with increasing amount of subfragment-1 added, and the decrease appeared to saturate at the molar ratio of subfragment-1 to actin approximately equal to 1.0. The behaviour of the average fluorescence lifetime observed on the binding of heavy meromyosin or of subfragment-1 was independent of preparations of proteins.

VII-2-2-2 Fluorescence anisotropy decay of PM-labelled F-actin in the presence of heavy meromyosin

In contrast to the total fluorescence decay, the behaviour of the fluorescence anisotropy decay of PM-labelled F-actin observed on the binding of heavy meromyosin was found to depend on the preparation method of heavy meromyosin used. Examples of the experimental fluorescence anisotropy decays in the presence of heavy meromyosin(TR and CT) were shown in Fig. VII-7 and 8, respectively: The curves represented with closed circles were obtained when the molar ratio of heavy meromyosin(TR or CT) to actin was 1:8. As expected from the result of steady fluorescence anisotropy, no significant change in the anisotropy decay of PM-labelled F-actin was observed on the binding of heavy meromyosin(CT) to F-actin. While, on the binding of heavy meromyosin(TR), a remarkable decrease in the fundamental anisotropy was observed. The biphasic change with increasing amount of heavy meromyosin(TR) was observed in the value of the fundamental anisotropy. The biphasic change observed in the steady fluorescence anisotropy was almost explained by this behaviour of the fundamental anisotropy.

VII-2-3 Discussion

VII-2-3-1 Biphasic changes in the fluorescence intensity and anisotropy with increasing amount of heavy meromyosin

In the presence of heavy meromyosin (TR), the fluorescence intensity of PM-labelled F-actin was found to fluctuate remarkably after the solution of acto-heavy meromyosin being poured into the sample cuvette and being agitated mechanically. The maximum fluctuation of the fluorescence intensity appeared at low saturation of binding of heavy meromyosin(TR) to F-actin (1/10 - 1/4). Under the stationary condition (i.e., at 8 - 10 min after the solution being poured), the total fluorescence intensity observed at the low saturation of binding of heavy meromyosin(TR) was 70 - 80 % of the intensity observed in the absence of heavy meromyosin(TR). While, the corresponding large decrease in the average fluorescence lifetime of PM-labelled F-actin was not observed. Thus it is suggested that the large decrease in the fluorescence intensity is not due to the change in the emission mechanism of fluorescence from the actin-bound PM, but due to the change in the mechanism of excitation of the probe. The change in the mechanism of excitation was also suggested from the behaviour of fluorescence anisotropy decay; that is, a large change was observed only in the fundamental anisotropy but not in the rotational correlation times. On the other hand, in the presence of the low amount of heavy meromyosin(TR), the scattered intensity

of the excitation light by the solution also fluctuated as well as the flurescence intensity. Fig. VII-9 shows an example of the time course of the fluctuation of the scattered intensity after the solution being poured into the sample cuvette. In this measurement, the same optical apparatus was used as in the measurement of fluorescence intensity except that the both excitation and emission wavelengths were set at 355 nm. It can be seen from Fig. VII-1 and -9 that the fluctuation of the scattered intensity correlated strongly to the one of the fluorescence intensity. This result may suggest that the fluctuation in the fluorescence intenstiy is related to formation of some macroscopic structure of the complex of F-actin and heavy meromyosin(TR).

Now we shall consider the problem as to what kind of macroscopic structure of acto-heavy meromyosin(TR) can cause the decrease in the probability of absorption of the polarized exciting light by the actin-bound probe. The following possibilities may be considered;

i) On partially saturation of actin filament with heavy meromyosin(TR), the actin filaments which exist on the optical path of the exciting light begin to orient in some particualr direciton; the direction of the absorption oscillator of the actin-bound probe will distribute anisotropically so that the effective concentration of absorber is reduced.

ii) The actin filaments form large clusters or aggregates in the sample cuvette. Then the effective concentration

of absorbers is reduced due to the so-called absorption flattening effect [197]; that is, when high dense regions of absorbers are formed here and there, the probability that an absorber exists in the shadow of the other absorbers from the exciting lights will increase as compared with the case of uniform distribution of absorber. The formation of such a macroscopic structure will also cause the decrease in the experimental fluorescence anisotropy. If the absorption flattening effect is significant, the orientation distribution of the excited molecule (at the instance of excitation will be no longer expressed by Eqn (III-18). Instead, $f(\theta, \psi) = \frac{3}{4} \cos^2\theta$ must be replaced with the following function;

$$f'(\theta, \psi) = \frac{3}{4} \cos^2\theta \cdot \xi(\theta) \qquad \text{(VII-1)}$$

where $\xi(\theta)$ is a function which is close to 1 at $\theta = \pi/2$ but has the smaller value when θ becomes smaller than $\pi/2$. Thus the apparent fundamental anisotropy has a smaller (absolute) value than the one observed under the uniform distribution of absorber; that is, Eqn (III-24) may be replaced with the following value:

$$r_0 = \frac{2}{5} \left(\frac{3}{2} \cos^2\beta - \frac{1}{2} \right) \cdot \gamma \qquad \text{(VII-2)}$$

where γ is a positive value less than 1.

In order to examine these possibilities, we prepared the conjugate of actin with N-(1-Anilinonaphthyl-4)maleimide (ANM). This fluorescent reagent has been known to have the two electronic absorption bands in the wavelength region

between 300 nm and 400 nm. In fact, ANM-labelled F-actin exhibited the excitation polarization spectrum in which the anisotropy varied from 0,26 to 0.32 in this region of wavelength (Fig. VII-10). It is therefore probable that the two absorption oscillators orient in the different directions with reference of the axis of the actin filament. If a particular anisotropic distribution of the orientation of the actin filament was induced on the binding of heavy meromyosin(TR), the behaviour of the changes in the fluorescence intensity and anisotropy would be dependent on the excitation wavelength. Decrease in these quantities may be observed in some case, but increase may be also observed in another particular case. In Fig. VII-10, the excitation polarization spectrum of ANM-labelled F-actin observed in the presence of heavy meromyosin(TR) is also shown (closed circles). This was obtained at the molar ratio of added heavy meromyosin (TR) to actin equal to 1:8. It can be seen that the fluorescence anisotropy of the complex of acto-heavy meromyosin had the smaller values at any excitation wavelengths than those of F-actin alone. Furthermore, with increasing saturation of ANM-labelled F-actin with heavy meromyosin(TR), biphasic changes both in the fluorescence intensity and anisotropy were observed, whose manners were very similar to those observed for PM-labelled F-actin. It seems therefore difficult to explain the decreases in the fluorescence intensity and anisotropy in terms of distribution of the some selected orientation of actin filament in the sample cuvette. On the other hand, these

behaviour can be explained well by considering the absorption flattening effect (Eqn VII-2). It appears probable that the binding of heavy meromyosin to F-actin promotes the formation of large clusters or aggregates of the actin filaments. In any case, such macroscopic structures of actin filamets may be so weak as to be broken by the mechanical agitation of the sample solution.

There are several reports of observation of biphasic response of physical parameters of acto-heavy meromyosin complex at low saturation of heavy meromyosin to actin. The first one was found in a measurement of flow birefringence by Tawada[51]. The present observation of fluorescence intensity and anisotropy would be related to the biphasic response of acto-heavy meromyosin complex so far reported [51, 72-75]. However, it is very important to decide on whether this is the intrinsic property of the complex of F-actin and heavy meromyosin or not, because there have been also reports which throw doubt on these observations [76-78, 195]. We found that with different proteolytic preparation of heavy meromyosin, fluorescence intensity and anisotropy of the complex responded differently to mechanical agitation. Discrepancy between the reports from several laboratories may have resulted from different preparation of heavy meromyosin. In the present study, it was also found that, after the solution of acto-subfragment-1 being stored at 5 °C for 2 days, a typical biphasic response was observed in the fluorescence anisotropy; this behaviour had been obscure before the store (Fig. VII-4).

This is suggesting that a kind of aging of the proteins is related to appearance of the biphasic behaviour. It has been known that heavy meromyosin(TR) contains many regions proteolytically digested in its heavy chains as compared with heavy meromyosin(CT) (Fig. IV-7). It seems probable that these regions are susceptible to aging of the protein. In this respect, it was found that the heavy meromyosin which was obtained by tryptic digestion of myosin in the presence of divalent cation (i.e., 1 mM $MgCl_2$, in which the number of regions of proteolytic digestion is smaller than those prepared in the absence of $MgCl_2$ [40]) scarcely induced biphasic response of fluorescence anisotropy.

VII-2-3-2 Conformational change of actin protomer on the binding of myosin head

The average fluorescence lifetime of PM-labelled F-actin was found to decrease monotonically with increasing saturation of binding of myosin head to F-actin. This behaviour was always observed when any kinds of myosin head were added to F-actin; i.e., heavy meromyosin(TR or CT), subfragment-1, S1-A1 and S1-A2. Furthermore the extent of the decrease which was observed at the complete saturation of binding of myosin head to F-actin was almost independent of the kind of myosin head used. These results may be explained as follows: In contrast to the fluorescence intensity observed after steady-excitation, which was shown to be sensitive to the macroscopic configuration of actin filaments, the fluorescence decay is sensitve only to the microenvironment

of the actin-bound probe. Therefore, information about the local conformation of the labelling site of the actin protomer may be obtained from the behaviour of the fluorescence decay.

Since the heavy meromyosin prepared according to Weeds and Pope [41] gave the best reproducibility so far as we studied, the data of the fluorescence decays which were obtained on the addition of this heavy meromyosin(CT) were mainly analysed with double-exponential functions (Eqn (VI-2)). It was then found that the relative amplitude B_1 of the long decay component decreased remarkably on the binding of heavy meromyosin(CT) to F-actin. In Section VI-2, it was shown that the polymerization of PM-labelled G-actin accompanies a increase in the relative amplitude of the long decay component. One may note that the decay parameters, e.g., the decay constants and the relative amplitudes, of fluorescence of PM-labelled F-actin under the influence of heavy meromyosin have intermediate values between those of G-actin and F-actin. This may indicate that the binding of heavy meromyosin breaks (or at least loosens) the bonding between actin protomers of F-actin. In this respect, we note the hypothesis proposed by Oosawa et al. [68] that the regularity of helical structure of F-actin filament is perturbed by the binding of myosin head. Such a conformational change in F-actin filament may play some important role in muscle contraction.

VII-3 Binding of Myosin Head to PIAA-Labelled F-Actin

VII-3-1 Absorption and fluorescence spectra of PIAA-labelled F-actin in the presence of heavy meromyosin

PIAA-labelled G-actin (2 - 4 mg/ml) was polymerized by addition of 0.1 M KCl, and ATP in the solution was removed by dialysis against the solution containing 0.1 M KCl, 1 mM $MgCl_2$ (or 0.05 M KCl, 2 mM $MgCl_2$), 10 mM phosphate buffer (pH 7.0), 1 mM 2-mercaptoethanol and 1 mM sodium azide. To this solution of PIAA-labelled F-actin, various amounts of heavy meromyosin(CT) were added: The final concentration of PIAA-labelled F-actin was 0.2 mg/ml. Under this solvent condition, the fluorescence intensity of the complex of PIAA-labelled F-actin and heavy meromyosin was found to be stable (no significant fluctuation was observed).

Fig. VII-11 shows the excitation spectra of PIAA-labelled F-actin in the presence of various amounts of heavy meromyosin: The fluorescence emission was observed at 406 nm. With increasing of the concentration of heavy meromysoin added, the shape of excitation spectrum changed; in particular, the peak at 365 nm was reduced more remarkable than the peak at 345 nm. On the other hand, the shape of emission spectrum obtained after excitation at 365 nm was almost independent of the amount of heavy meromyosin added, though the fluorescence intensity integrated over emission was reduced largely. A striking change in the absorption spectrum of PIAA-labelled F-actin was observed on addition

of heavy meromyosin. The open circles in Fig VII-12 show the absorption spectrum obtained when excess amount of heavy meromyosin (3.0 mg/ml) was added. Then the absorption peak at 365 nm disappeared, which was obvious in the absorption spectrum of PIAA-labelled F-actin alone. It should be noted that the absorption spectrum obtained at the complete saturation of binding of heavy meromyosin was very similar to that of PIAA-labelled G-actin (continuous line in Fig. VII-12).

Fig. VII-13 shows the fluorescence intensity of PIAA-labelled F-actin as a function of the molar ratio of heavy meromyosin to actin protomer. The fluorescence intensity was observed at 407 nm after excitation at 365 nm. The manner of the change in the fluorescence intensity on increasing amount of heavy meromyosin was found to depend on the labelling ratio of PIAA to actin molecule. The closed circles in Fig VII-13 were the data obtained when the labelling ratio was 95 %. The fluorescence intensity decreased linearly on increasing amount of heavy meromyosin added, and showed a saturation at the molar ratio approximately equal to 0.5. While, the open circles in Fig. VII-13 were the data obtained when the labelling ratio was 24 %; that is, PIAA-labelled G-actin (labelling ratio equal to 95 %) was diluted 4-fold with unlabelled G-actin and the mixture was polymerized. In this case, the fluorescence intensity did not decrease linearly; the slow decrease was found at the molar ratio of heavy meromyosin to F-actin between 0 and 0.3 and the rapid decrease was found at the molar ratio

between 0.3 and 0.5. The rate of decrease of the fluorescence intensity on increasing of the molar ratio of heavy meromyosin to actin (at the low saturation of the binding of heavy meromyosin) was decreased monotonically as the labelling ratio of PIAA to actin was decreased (Table VII-1). However, the molar ratio of heavy meromyosin to actin at which the saturation of the decrease of the fluorescence intensity occured was found to be independent of the labelling ratio; that is, it occured at the molar ratio approximately equal to 0.5. The ratio of the fluorescence intensity observed at the complete saturation of binding of heavy meromyosin to that observed in the absence of heavy meromyosin was also independent of the labelling ratio; it was always between 0.24 to 0.27. These behaviours can be explained by difference between the binding affinities of heavy meromyosin to PIAA-labelled and unlabelled actin protomers.

VII-3-2 Binding of subfragment-1 to PIAA-labelled F-actin

Binding of subfragment-1 to PIAA-labelled F-actin brought about the similar changes in the absorption and fluorescence spectra as observed on the binding of heavy meromysoin. Fig. VII-14 shows the fluorescence intensity observed at 407 nm after excitation at 365 nm and the absorbances at 345 nm and at 365 nm as a function of the concentration of subfragment-1 added. Actin concentration was 0.2 mg/ml and the labelling ratio of PIAA to actin

molecule was 80 %. The absorbance at 365 nm decreased remarkably on addition of subfragment-1. Corresponding to this, the fluorescence intensity decreased largely with increasing concentration of subfragment-1. The fluorescence intensity at complete saturation of F-actin with subfragment-1 was 25 % of that observed in the absence of subfragemnt-1.

When ATP was added to the solution of acto-subfragment-1 at the final concentration of 1 mM, the fluorescence intensity increased to about 90 % of the intenstiy observed in the absence of subfragemnt-1 (the closed triangle in Fig. VII-14). It is therefore indicated that the change in the fluorescence intensity was reversible.

VII-3-3 Discussion

It is interesting to note that the binding of subfragment-1 to PIAA-labelled F-actin was accompanied with a decrease in the fluorescence intensity by almost the same extent as observed on the binding of heavy meromyosin; that is, the fluorescence intensity observed at the complete saturation of myosin head (both heavy meromyosin and subfragment-1) was 24 - 27 % of that observed in the absence of myosin head. This result indicates that the divalent manner of binding of heavy meromyosin to F-actin does not make the actin-conformation change different from the one which is induced on the binding of monovalent myosin (or subfragment-1) (Fig. II-7).

It was found that when PIAA-labelled F-actin was saturated with myosin head, the absorption spectrum becomes

very similar to that of PIAA-labelled G-actin. One may consider the possibility that, on the binding of myosin head, the pyrene moiety which may be buried between neibouring actin protomers is displaced onto the surface of actin filament and becomes to contact with the solvent. On the other hand, the fluorescence quantum yield or the shape of emission spectrum (observed after excitation at 365 nm) of PIAA-labelled F-actin scarecely changed on the binding of myosin head, although conspicious change was found on the G-F transformation of PIAA-labelled actin (Section VI-4). Therefore, it appears unlikely that the change in the absorption spectrum is simply due to the displacement of the pyrene moiety from the buried region to the surface of the protein. Another explanation must be needed. It has been shown in the section VI-4 that PIAA labelled to actin has heterogeneity of local conformation in its ground state and the change in the absorption spectrum induced on the polymerization of actin is due to a shift in the equilibrium between the possible local conformations of the labelling site. It is probable that this equilibrium is also shifted on the binding of myosin head to F-actin and it becomes very similar to the equilibrium attained in G-state of actin. In this respect, it has been shown in the section VII-2 that the relative amplitude of the long decay component of fluorescence from PM-labelled F-actin decreases remarkably on the binding of heavy meromyosin to F-actin and it becomes close to the value obtained in G-state of actin. This result is compatible with the present result, since the multiplicity

of lifetime of fluorescence from PM-labelled F-actin can be be also explained if the heterogeneity of local environment is pre-existing in the ground state of the dye (Eqn (III-6)). These two results suggest that, on the binding of myosin head, the conformation of actin protomer in F-actin becomes similar to the one of G-actin. Such a conformational change of actin must be considered in elucidation of the molecular mechanism of force generation of muscle contraction.

VII-4 Concluding Remark

The following results were obtained in the present work.

i) When heavy meromyosin was bound to PM-labelled F-actin, a remarkable change in the fluorescence decay was observed. The decay parameters (e.g., the relative amplitude of the long decay component) changed monotonically on increasing saturation of binding of heavy meromyosin and it levelled-off around the molar ratio of heavy meromyosin to actin equal to 0.5. Decay parameters under the influence of heavy meromyosin had values intermediate between those of G-actin and of F-actin alone.

ii) When heavy meromyosin was bound to PIAA-labelled F-actin, conspicious changes in the absorption and fluorescence spectra were observed. These changes are saturated at the molar ratio of heavy meromyosin to actin approximately equal to 0.5. The absorption spectrum at the complete saturation of PIAA-labelled F-actin with heavy meromyosin

was very similar to that of PIAA-labelled G-actin: The strong absorption band at 365 nm, which is characteristic to F-actin alone, disappeared on the binding of heavy meromyosin. Binding of subfragment-1 to PIAA-labelled F-actin accompanied the same changes in the fluorescence and absorption spectra as those observed on the binding of heavy meromyosin.

From these results, it is strongly suggested that binding of heavy meromyosin to F-actin alters the conformation of the each protomer towards that of G-actin. Such a conformaitonal change should be taken into account when considering the superiority of F-actin to activate the myosin ATPase activity as compared to G-actin. It appears that the transformation of the structure of the protomer towards the one of G-actin is related to the molecular mechanism in which myosin ATPase is accelerated by F-actin.

From the results obtained in the present study, no evidance was obtained for the presence of the co-operative nature between the protomers in the actin filament on the binding of myosin head. Furthermore, essential difference between heavy meromyosin and subfragment-1 was not obtained in the action to the actin conformation. However, the present results, which were obtained in the system without ATP, do not necessarily mean that the co-operative nature is absent in the system containing ATP. The possibility may be considered that the myosin·ADP·P_i complex, which is a reaction intermediate with excess energy, affects on the actin filament with a manner different from the action of

myosin without the nucleotide. Formation of a transient conformation of the actin molecule immediately after the binding of myosin·ADP·P_i complex to F-actin appears to be necessary for actomyosin to undergo a cyclic reaction of ATP splitting. Up to date, no evidence of existence of such a transient conformation has been obtained, only because of lacking of a probe sensitive to actin conformation. It may be expected that PIAA is used as a probe suitable to study of the transient conformation of actin, since the fluorescence intensity of PIAA-labelled F-actin responds much remarkably to the binding of (nucleotide-free) myosin.

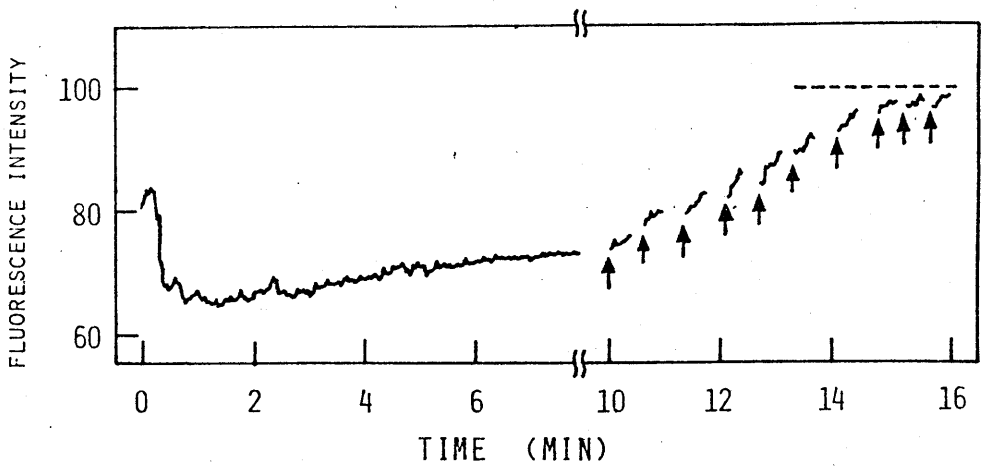

Fig. VII-1. Fluctuation in the fluorescence intensity of the complex of PM-labelled F-actin and heavy meromyosin (TR). The solution of acto-heavy meromyosin was poured into the sample cuvette ($4 \times 1 \times 1$ cm^3) at zero time; and the cuvette was tapped at the time shown by the arrows. The concentration of PM-labelled F-actin was 0.2 mg/ml and the molar ratio of heavy meromyosin to actin was 1 : 8. Solvent condition: KCl, 0.1 M; $MgCl_2$, 1 mM; phosphate buffer, 10 mM (pH 7.0); ATP (F-actin only) or ADP; about 20 μM; at 20°C. The fluorescence intensity was observed at 396 nm after excitation at 344 nm. Dashed line shows the fluorescence intensity observed in the absence of heavy meromyosin.

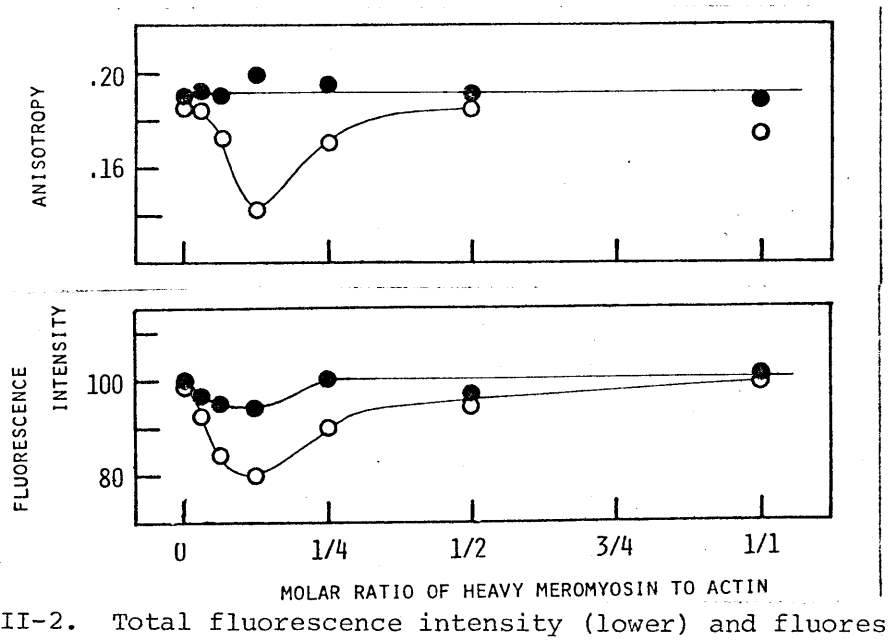

Fig. VII-2. Total fluorescence intensity (lower) and fluorescence anisotropy (upper) as a function of the saturation of PM-labelled F-actin with heavy meromyosin(TR). The data shown by open circles were obtained at 8 - 10 min after the solution being poured into the sample cuvette; while, the data shown by closed circles were obtained after the solution being agitated mechanically. Experimental condition was identical to that in Fig. VII-1.

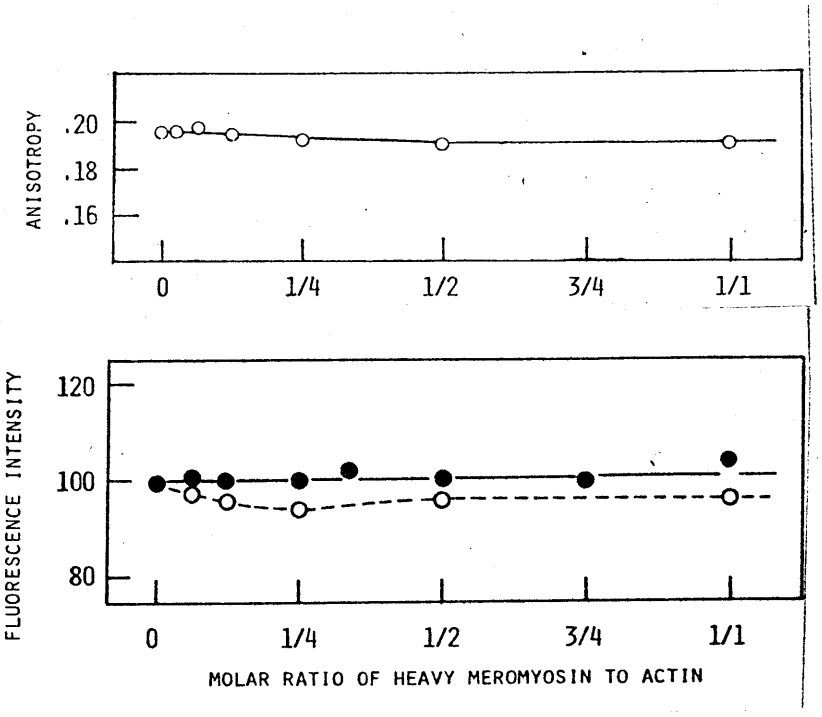

Fig. VII-3. Total fluorescence intensity and fluorescence anisotropy as a function of the saturation of PM-labelled F-actin with heavy meromyosin(CT). Experimental detail was the same as that shown in Fig. VII-2.

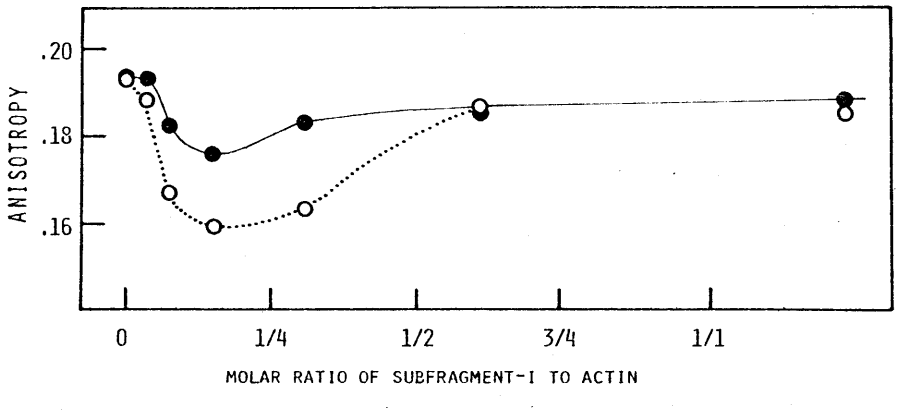

Fig. VII-4. Fluorescence anisotropy as a function of the saturation of PM-labelled F-actin with S1-A1. The data shown by closed circles were obtained at 2 hrs after S1-A1 being added to F-actin solution; while, the data shown by open circles were obtained after the same solution of acto-S1-A1 being left standing at 5°C for 2 days. The fluorescence intensity was observed at 8 - 10 min after the solution being poured into the sample cuvette. Experimental condition was identical to that in Fig. VII-2.

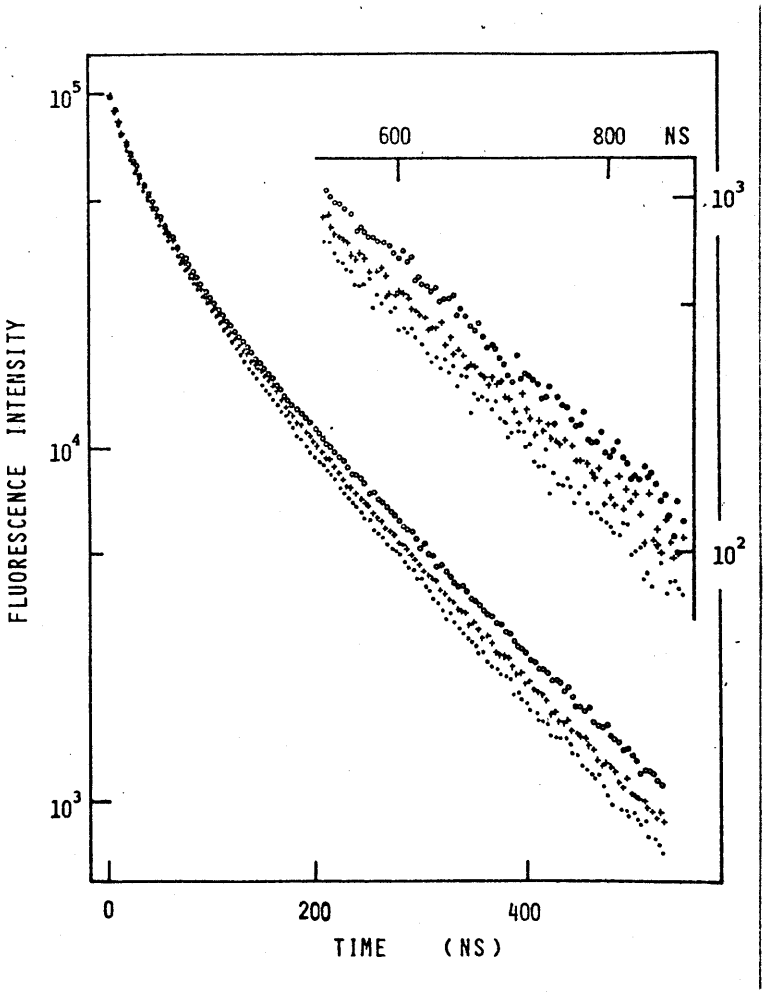

Fig. VII-5. Fluorescence decay curves of PM-labelled F-actin in the absence and in the presence of heavy meromyosin(CT). The molar ratio of heavy meromyosin to actin was 0 (open circle), 1/4 (cross), 1/2 (dot). Excitation was at 337 nm and emission above 370 nm was collected. Solvent condition was identical to that shown in Fig. VII-2.

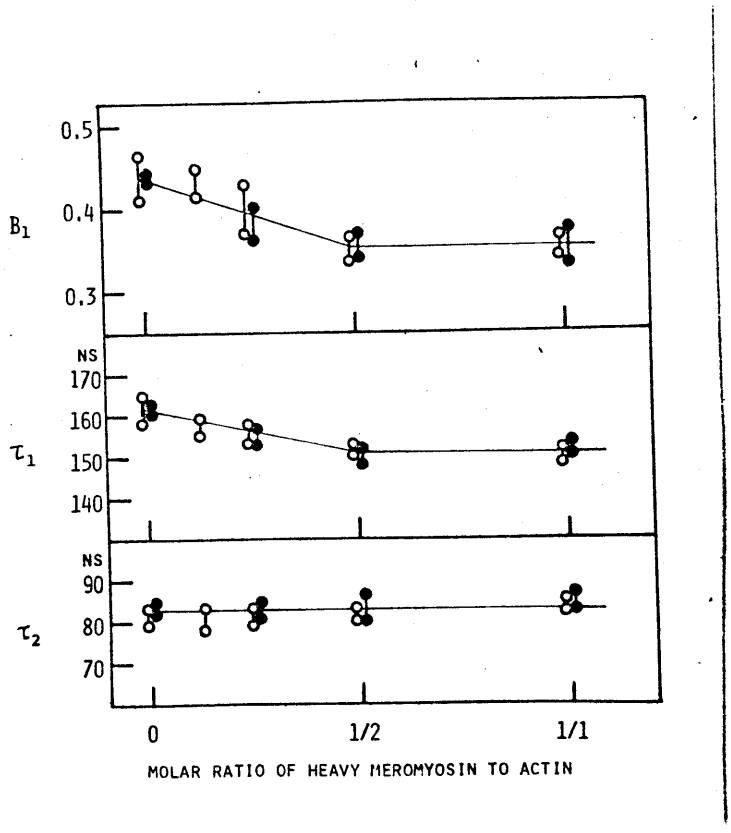

Fig. VII-6. Decay parameters as a function of the saturation of PM-labelled F-actin with heavy meromyosin(CT). Different symbols show the results obtained using different samples. Vertical line shows the range of each decay parameter in which the corresponding value of χ_S^2 was less than 1.005 times of the minimum of χ_S^2

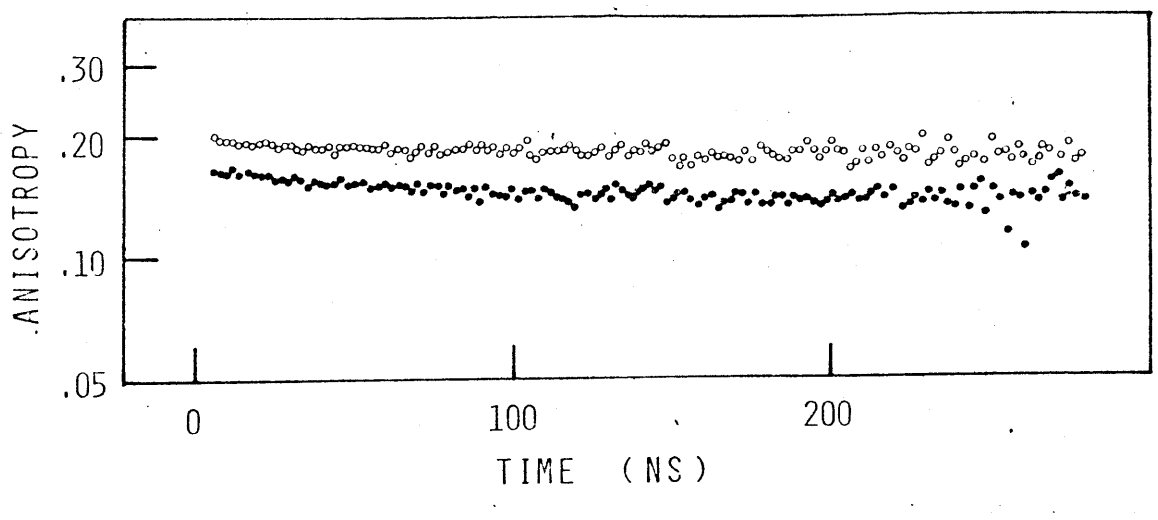

Fig. VII-7. Fluorescence anisotropy decays of PM-labelled F-actin in the absence (open circle) and in the presence (closed circle) of heavy meromyosin(TR); the molar ratio of heavy meromyosin(TR) to actin was 1 : 8. Experimental condition was identical to that in Fig. VII-5.

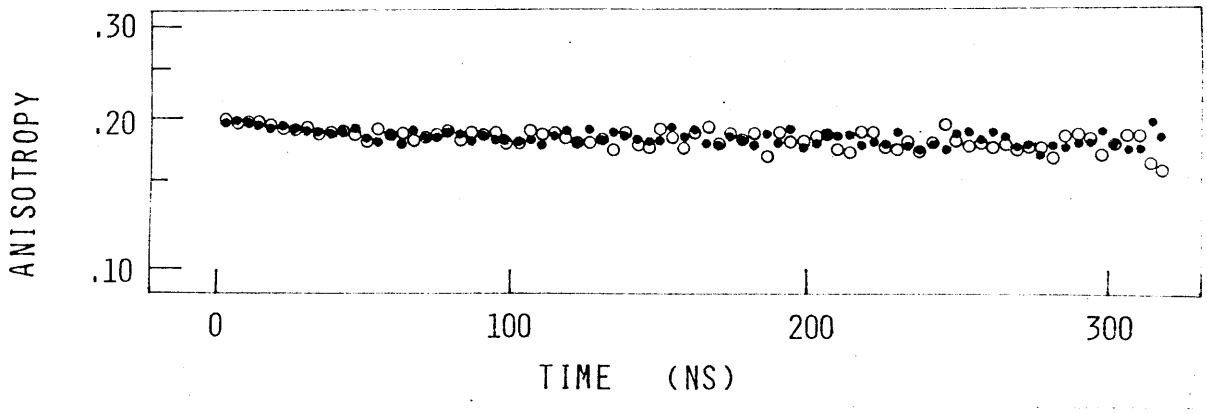

Fig. VII-8. Fluorescence anisotropy decays of PM-labelled F-actin in the absence (closed circle) and in the presence (closed circle) of heavy meromyosin(CT); the molar ratio of heavy meromyosin(CT) to actin was 1 : 8. Experimental condition was identical to that in Fig. VII-5.

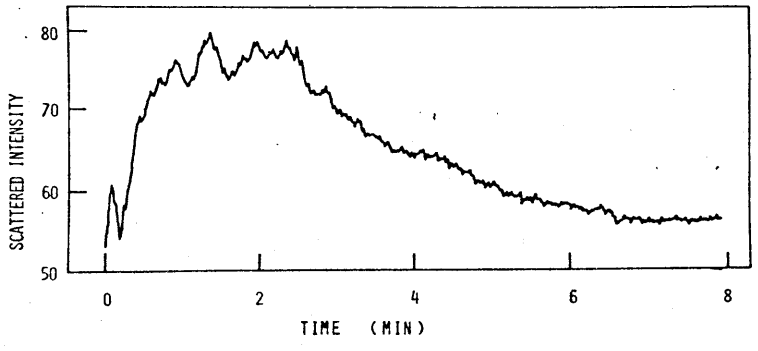

Fig. VII-9. Fluctuation in the scattered intensity of the excitation light by the solution of acto-heavy meromyosin(TR) after being poured into the sample cuvette. The concentration of PM-labelled actin was 0.2 mg/ml and the molar ratio of heavy meromyosin to actin was 1 : 8. Scattered light was viewed at right angle with the excitation beam. Both the excitation and emission wavelengths were set at 355 nm. Solvent condition was identical to that in Fig. VII-1.

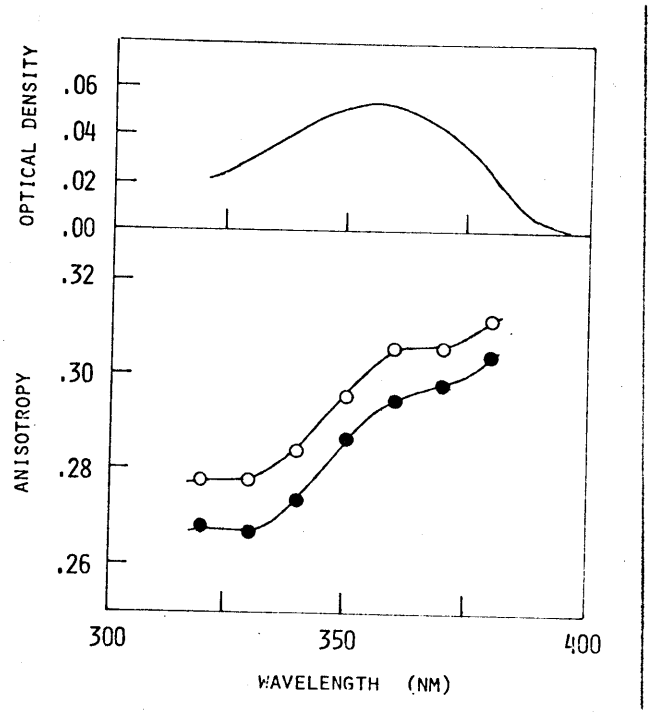

Fig. VII-10. Excitation polarization spectra of ANM-labelled F-actin in the absence (open circle) and in the presence (closed circle) of heavy meromyosin(TR); the molar ratio of heavy meromyosin to actin was 1 : 8. The slit width was 6 nm and emission was observed at 440 nm. Absorption spectrum of ANM-labelled actin is shown in the upper figure. Solvent condition was identical to that in Fig. VII-1.

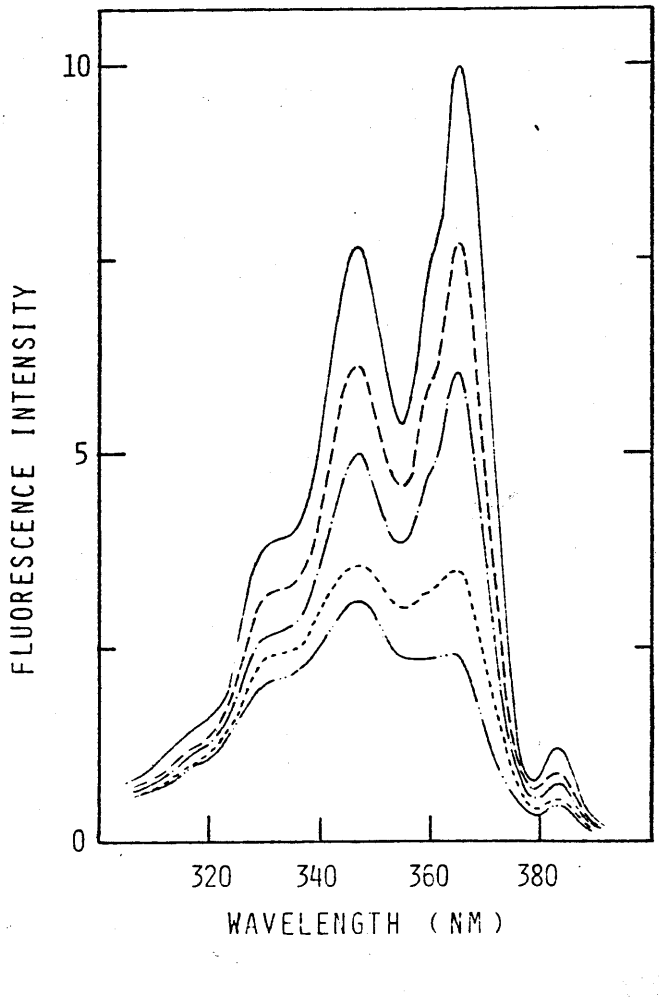

Fig. VII-11. Excitation spectra of PIAA-labelled F-actin in the absence or presence of heavy meromyosin(CT). The molar ratio of heavy meromyosin to actin was 0 (——), 0.125(— — —), 0.25(—·—), 0.5 (-----), 2.2(—··—). The slit width was 3 nm and emission was observed at 407 nm; an optical cut-off filter was set in the emission side in order to eliminate scattered lights. The concentration of PIAA-labelled actin was 0.2 mg/ml and the degree of labelling of actin with PIAA was 95%. Solvent condition: KCl, 50 mM, $MgCl_2$, 2 mM; $CaCl_2$, 0.1 mM; phosphate buffer, 10 mM (pH 7.0); NaN_3, 1 mM; 2-mercapto-ethanol, 1 mM; at 14°C.

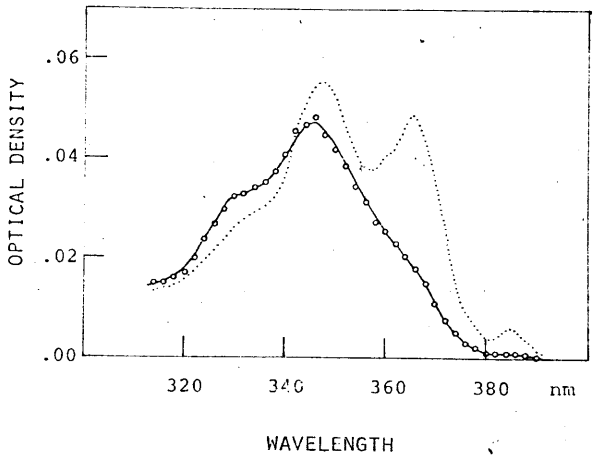

Fig. VII-12. Absorption spectrum (circle) of PIAA-labelled F-actin in the presence of heavy meromyosin(CT). The molar ratio of heavy meromyosin (added) to actin was 2.2:1.0. The concentration of PIAA-labelled actin was 0.2 mg/ml and the degree of labelling was 95 %. A sample cuvette with 0.5 cm length was used. Solvent condition was identical to that in Fig. VII-11. Dotted line shows the absorption spectrum of PIAA-labelled F-actin alone; smooth line shows the one of PIAA-labelled G-actin.

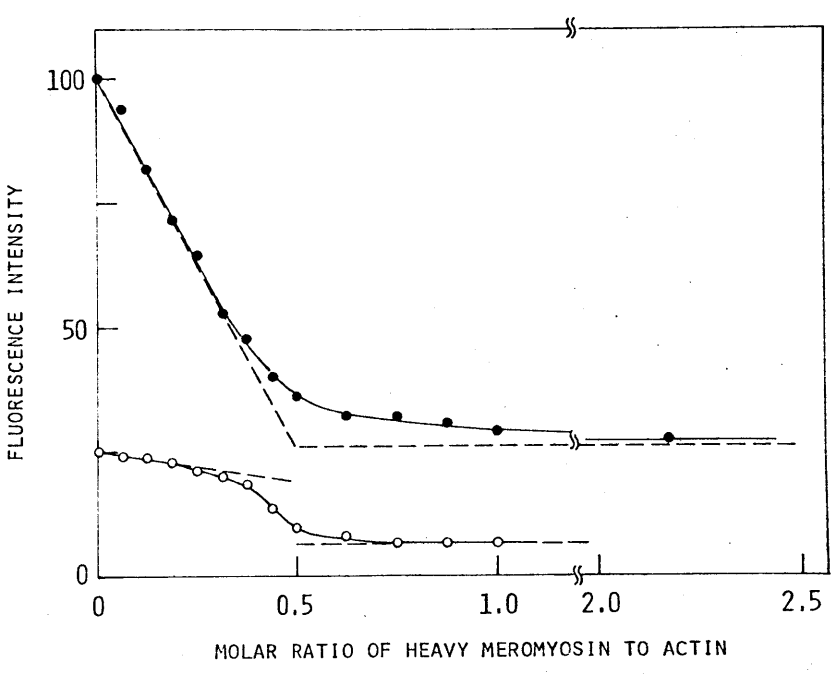

Fig. VII-13. Fluorescence intensity as a function of the saturation of PIAA-labelled F-actin with heavy meromyosin(CT). The data shown by closed circle were obtained when the degree of labelling of actin with PIAA was 95 %. While, the data shown by open circle were obtained when the labelled actin (95 % labelling) was diluted 4-fold by copolymerization with unlabelled actin. The fluorescence intensity was measured at 407 nm after excitation at 365 nm. Solvent condition was identical to that shown in Fig. VII-11.

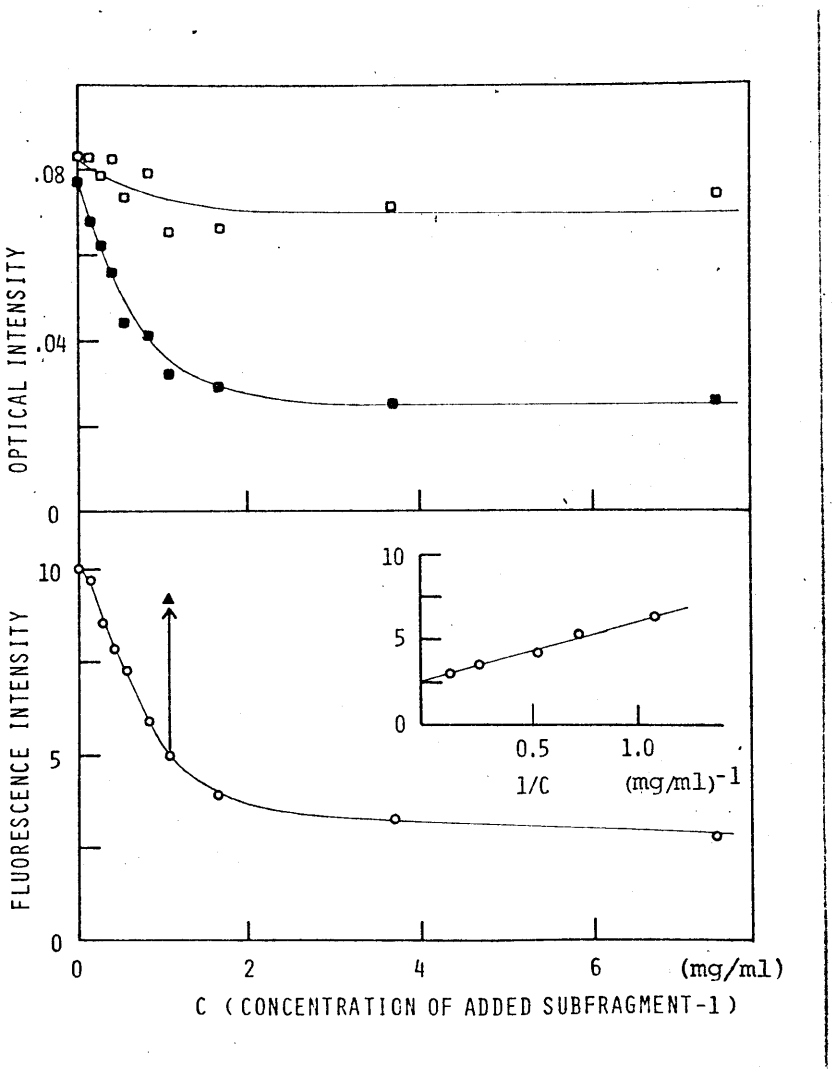

Fig. VII-14. Fluorescence intensity and absorbance as a function of the saturation of PIAA-labelled F-actin with subfragment-1. Fluorescence intensity was observed at 407 nm after excitation at 365 nm (o); absorbance was observed at 345 nm (□) or at 365 nm (■). The concentration of PIAA-labelled actin was 0.2 mg/ml and the degree of labelling was 80%. The turbidity of the solution increased on addition of subfragment-1; optical density at 400 nm increased from 0.02 to 0.07. Its effect on the absorption spectrum was corrected by assuming that the turbidity increases with fourth power of the inverse of wavelength. The fluorescence intensity which would be observed at complete saturation of F-actin with subfragment-1 was estimated by plotting the fluorescence intensity as a function of the inverse of the concentration of subfragment-1 added. The fluorescence intensity observed at 1 - 2 min after ATP (1 mM) being added to the solution of acto- subfragment-1 is shown by closed triangle.

Table VII-1. Dependence of $(d\Delta/d\alpha)^{-1}$ and F_∞/F_0 on the degree of labelling.

γ	$(d\Delta/d\alpha)^{-1}$ (at α=0)	F_∞/F_0
0.95	0.5	0.27
0.75	0.6	0.25
0.46[a]	1.32	0.26
0.46[b]	1.17	0.24
0.24	2.08	0.26

Here γ is the degree of labelling of actin with PIAA; α is the molar ratio of heavy meromyosin(CT) to actin; Δ is the magnitude of decrease in the fluorescence intensity with reference of the maximum decrease, that is, $\Delta = (F_0 - F)/(F_0 - F_\infty)$; F, F_0, F_∞ are the fluorescence intensities observed at a finite value of α, at α=0 and at $\alpha = \infty$, respectively. The fluorescence intensity was observed at 407 nm after excitation at 365 nm. The total concentration of actin was 0.18 - 0.20 mg/ml. Solvent condition: KCl, 0.05 M (or 0.1 M[a], 0.03[b]); $MgCl_2$, 2 mM (or 1 mM[a,b]), phosphate buffer, 10 mM (pH 7.0); NaN_3, 1 mM; 2-mercaptoethanol, 1 mM; at 14°C (or 20°C[a,b]).

References

1. Huxley, H.E. & Hanson, J. (1954) Nature, 173, 973.
2. Huxley, A.F. & Niedergerke, R. (1954) Nature, 173, 971.
3. Ebashi, S. (1972) Nature, 240, 217.
4. Huxley, H.E. (1963) J. Mol. Biol. 7, 281.
5. Huxley, A.F. (1957) in Progress in Biophysics, 7, 255.
6. Straub, F.B. (1942) Studies Inst. Med. Chem. Univ. Szeged, 2, 3.
7. Elzinga, M., Collins, J.H., Kuehl, W.M. & Adelstein, R.S. (1973) Proc. Natl. Acad. Sci. USA. 70, 2687.
8. Elzinga, M. & Collins, J.H. (1975) J. Biol. Chem. 250, 5897.
9. Faust, U., Fasold, H. & Ortanderl, F. (1974) Eur. J. Biochem. 43, 273.
10. Jacobson, G.R. & Rosenbusch, J.P. (1976) Proc. Natl. Acad. Sci. USA. 73, 2742.
11. Hanson, J. & Lowy, J. (1963) J. Mol. Biol. 6, 46.
12. Wakabayashi, T., Huxley, H.E., Amos, L.A. & Klug, A. (1975) J. Mol. Biol. 93, 477.
13. Straub, F.B. (1943) Studies Inst. Med. Chem. Univ. Szeged, 3, 23.
14. Straub, F.B. & Feuer, G. (1950) Biochim. Biophys. Acta, 4, 455.
15. Martonoshi, A. Gouvea, M. & Gergely, J. (1960) J. Biol. Chem. 235, 1700.
16. Hayashi, T. & Rosenbluth, R. (1960) Biol. Bull. 119, 294.
17. Kasai, M., Nakano, E. & Oosawa, F. (1965) Biochim. Biophys. Acta, 94, 494.

18. Cooke, R. & Murdoch, L. (1973) Biochemistry, 12, 3927.

19. Kasai, M., Kawashima, H. & Oosawa, F. (1960) J. Polymer Sci. 44, 51.

20. Oosawa, F., Asakura, S., Hotta, K., Imai, N. & Ooi, T. (1959) J. Polmer Sci. 37, 323.

21. Asakura, S., Kasai, M. & Oosawa, F. (1960) J. Polymer Sci. 44, 35.

22. Kasai, M., Asakura, S. & Oosawa, F. (1962) Biochim. Biophys. Acta, 57, 22.

23. Oosawa, F., Asakura, S. & Ooi, T. (1961) Suppl. Prog. Theor. Phys. Kyoto, 17, 14.

24. Oosawa, F. & Kasai, M. (1962) J. Mol. Biol. 4, 10.

25. Higashi, S. & Oosawa, F. (1965) J. Mol. Biol. 12, 843.

26. Lehrer, S.S. & Kerwar, G. (1972) Biochemistry, 11, 1211.

27. Murphy, A.J. (1971) Biochemistry, 10, 3723.

28. Rich, S.A. & Estes, J.E. (1976) J. Mol. Biol. 104, 777.

29. Szent-Gyorgyi, A. & Banga, I. (1941) Stud. Inst. Med. Chem. Univ. Szeged, 1, 1.

30. Kühne, W. (1864) Untersuchungen über das protoplasma und die Kontraktilität, Engelmann, Leipzig.

31. Guba, F. & Straub, F.B. (1943) Studies Inst. Med. Chem. Univ. Szeged, 3, 46.

32. Lowey, S. & Cohen, C. (1962) J. Mol. Biol. 4, 293.

33. Lowey, S., Slayter, H.S., Weeds, A.G. & Baker, H. (1969) J. Mol. Biol. 42, 1.

34. Moore, P.B., Huxley, H.E. & DeRosier, D.J. (1970) J. Mol. Biol. 50, 279.

35. Perry, S.V. (1951) Biochem. J. 48, 257.

36. Gergely, J. (1953) J. Biol. Chem. 200, 543.

37. Gergely, J., Gouvea, M.A. & Karibian, D. (1955) J. Biol. Chem. 212, 165.

38. Szent-Gyorgyi, A.G., Cohen, C. & Philpott, D.E. (1960) J. Mol. Biol. 2, 133.

39. Szent-Gyorgyi, A.G. (1953) Arch. Biochem. Biophys. 42, 305.

40. Balint, M.A., Schaefer, A., Biro, N.A., Menczel, L. & Fejes, E. (1971) Phisol. Chem. Phys. 3, 455.

41. Weeds, A.G. & Pope, B. (1977) J. Mol. Biol. 111, 129.

42. Weber, A. & Hasselbach, W. (1954) Biochim. Biophys. Acta, 15, 237.

43. Finlayson, B. & Taylor, E W. (1969) Biochemistry, 8, 802.

44. Lymn, R.W. & Taylor, E.W. (1970) Biochemistry, 9, 2975.

45. Bagshow, C.R. & Trentham, D.R. (1973) Biochem. J. 133, 323.

46. Tonomura, Y. (1972) Muscle Protein, Muscle Contraction and Cation Transport, Univ. Tokyo Press, Tokyo.

47. Inoue, A. & Tonomura, Y. (1976) J. Biochem. 80, 1359.

48. Szent-Gyorgyi, A. (1951) Chemistry of Myscular Contraction, Academic Press, New York.

49. Maruyama, K. & Gergely, J. (1962) J. Biol. Chem. 237, 1095.

50. Young, M. (1967) Proc. Natl. Acad. Sci. USA. 58, 2393.

51. Tawada, K. (1969) Biochim. Biophys. Acta, 172, 311.

52. Rizzino, A.A., Barouch, W.W., Eisenberg, E. & Moos, C. (1970) Biochemistry, 9, 2402.

53. Takeuchi, K. & Tonomura, Y. (1971) J. Biochem. 70, 1011.

54. Eisenberg, E., Dobkin, L. & Kielley, W.W. (1972) Biochemistry, 11, 4657.

55. Margossian, S. & Lowey, S. (1973) J. Mol. Biol. 74, 313.

56. Highsmith, S. (1978) Biochemistry, 17, 22.

57. Hill, T.L. (1978) Nature, 274, 825.

58. Eisenberg, E. & Moos, C. (1968) Biochemistry, 7, 1486.

59. Eisenberg, E. & Moos, C. (1970) J. Biol. Chem. 245, 2451.

60. Lymn, R.W. & Taylor, E.W. (1971) Biochemistry, 10, 4617.

61. Stein, L.A., Schwarz, R.P. Jr., Chock, P.B. & Eisenberg, E. (1979) Biochemistry, 18, 3895.

62. Johnson, K.A. & Taylor, E.W. (1978) Biochemistry, 17, 3432.

63. Hozumi, T. & Tawada, K. (1974) Biochim. Biophys. Acta, 347, 469.

64. Elliott, G.F., Lowy, J. & Millman, B.M. (1967) J. Mol. Biol. 25, 31.

65. Huxley, H.E. & Brown, W. (1967) J. Mol. Biol. 30, 383.

66. Offer, G., Baker, H. & Baker, L. (1972) J. Mol. Biol. 66, 435.

67. Szent-Györgyi, A.G. & Prior, G. (1966) J. Mol. Biol. 15, 515.

68. Oosawa, F., Asakura, S., Asai, H., Kasai, M., Kobayashi, S., Mihashi, K., Ooi, T., Taniguchi, M. & Nakano, E. (1964) in Biochemistry of Muscle Constraction (Gergely, J., ed.), pp.158-172, Little Brown and Co., Boston.

69. Asakura, S., Taniguchi, M. & Oosawa, F. (1963) J. Mol. Biol. 7, 55.

70. Moos, C. & Eisenberg, E. (1970) Biochim. Biophys. Acta, 223, 221.

71. Strzelecka-Golaszewska, H., Jakubiak, M. & Drabikowski, W. (1975) Eur. J. Biochem. 55, 221.

72. Fujime, S. & Ishiwata, S. (1971) J. Mol. Biol. 62, 251.

73. Abe, S. & Maruyama, K. (1971) Biochim. Biophys. Acta, 243, 98.

74. Loscalzo, J., Reed, G.H. & Weber, A. (1975) Proc. Natl. Acad. Sci. USA. 72, 3412.

75. Miki, M., Kouyama, T. & Mihashi, K.(1976) FEBS Lett. 66, 98.

76. Carlson, F.D. & Fraser, A.B. (1974) J. Mol. Biol. 89, 273.

77. Harvery, S.C., Cheung, H.C. & Thames, K.E. (1977) Arch. Biochem. Biophys. 179, 391.

78. Ando, T. & Asai, H. (1976) J. Biochem. 79, 1043.

79. Stone, D.B., Prevost, S.C. & Botts, J. (1970) Biochemistry, 9, 3937.

80. Muralt, A. von & Edsall, J.T. (1930) J. Biol. Chem. 89, 315.

81. Weber, H.H. (1935) Arch. Für Physiol., 235, 205.

82. Engelhardt, W.A. & Ljubimowa, M.N. (1939) Nature, 144, 668.

83. Bailey, K. (1948) Biochem. J. 43, 271.

84. Szent-Gyorgyi, A. (1946) Studies on Muscle Inst. Med. Chem. Univ. Szeged.

85. Mihalyi, E. & Szent-Gyorgyi, A.G. (1953) J. Biol. Chem. 201, 189.

86. Tsao, T.C. (1953) Biochim. Biophys. Acta, 11, 368.

87. Koshland, D.E., Budenstein, Z. & Kowalsky, A. (1954) J. Biol. Chem. 211, 279.

88. Hanson, J. & Huxley, H.E. (1955) Sym. Soc. Exp. Biol. 9, 228.

89. Mueller, H. & Perry, S.V. (1962) Biochem. J. 85, 431.

90. Cain, D.F. & Davies, R.E. (1962) Biochem. Biophys. Res. Comm. 8, 361.

91. Ebashi, S. & Kodama, A. (1965) J. Biochem. Tokyo, 58, 107.

92. Hill, A.V. (1965) Edward Arnold, London.

93. Hartshorne, D.J. & Mueller, H. (1968) Biochem. Biophys. Res. Comm. 31, 647.

94. Ebashi, S., Wakabayashi, T. & Ebashi, F. (1971) J. Biochem. Tokyo, 69, 441.

95. Schaub, M.C. & Perry, S.V. (1969) Biochem. J. 115, 993.

96. Sodek, J., Hodges, R.S., Smillie, L.B. & Jurasek, L. (1972) Proc. Natl. Acad. Sci. USA. 69, 3800.

97. Collins, J.H., Potter, J.D., Horn, M.J., Wilshire, G. & Jackman, N. (1973) FEBS Letters, 36, 268.

98. Collins, J.H. (1974) Biochem. Biophys. Res. Comm. 58, 301.

99. Herschel, J.F.W. (1845) Phil. Trans. Roy. Soc. (London) 135, 143.

100. Stokes, G.G. (1852) Phil. Trans. Roy. Soc. (London) 142, 463.

101. Weigert, F. (1920) Verh. d. D. Phys. Ges. 23, 100.

102. Perrin, F. (1926) J. de Phys. 7, 390.

103. Weber, G. (1952) Biochem. J. 51, 145.

104. Tao, T. (1969) Biopolymers, 8, 609.

105. Wahl, Ph., Paoletti, J. & Le Pecq, J.B. (1970) Proc. Natl. Acad. Soc. USA. 65, 417.

106. Yguerabide, J. (1972) Methods in Enzymology, 26, 798.

107. Einstein, A. (1917) Physik Z. 18, 121.

108. Stricker, S.J. & Berg, R.A. (1962) J. Chem. Phys. 37, 814.

109. Weller, A. (1961) Progr. React. Kinetics, 1, 189.

110. Voughan, W.M. & Weber, G. (1970) Biochemistry, 9, 464.

111. Stryer, L. (1966) J. Amer. Chem. Soc. 88, 5708.

112. Kishi, T., Tanaka, J. & Kouyama, T. (1976) Chem. Phys. Lett. 41, 497.

113. Kishi, T., Tanaka, J. & Kouyama, T. (1977) Chem. Phys. Lett. 46, 383.

114. Laws, W.R. & Brand, L. (1979) J. Phys. Chem. 83, 795.

115. Birks, J.B., Dyson, D.J. & Munro, I.H. (1963) Proc. Roy. Soc. A275, 575.

116. Ware, W.R. & Richter, H.P. (1968) J. Chem. Phys. 48, 1595.

117. De Lauder, W.B. & Wahl, Ph. (1971) Biochim. Biophys. Acta, 243, 153.

118. Douzel, B., Gauduchon, P. & Wahl, Ph. (1974) J. Am. Chem. Soc. 96, 801.

119. Brochon, J.C., Wahl, Ph., Jallon, J.-M. & Iwatsubo, M. (1976) Biochemistry, 15, 3259.

120. Jablonski, A. (1960) Bull. Acad. Pol. Sci. Ser. Sci. Math. Astr. Phys. 8, 259.

121. Soleillet, M.P. (1929) Ann. Phys. (Paris) 12, 23.

122. Einstein, A. (1906) Ann. Physik, 19, 371.

123. Tanford, C. (1961) "Physical Chemistry of Macromolecules", John Wiley & Sons, Inc.

124. Perrin, F. (1934) J. Phys. (Paris) 5, 497.

125. Perrin, F. (1936) J. Phys. (Paris) 7, 1.

126. Belford, G.G., Belford, R.L. & Weber, G. (1972) Proc. Natl. Acad. Sci. U.S. 69, 1392.

127. Wahl. Ph., Mayer, G. & Parrod, J. (1970) Europ. Polym. J. 6, 585.

128. Gottlieb, Y.A. & Wahl. Ph. (1963) J. Chim. Phys. 60, 849.

129. Wallach, D. (1967) J. Chem. Phys. 47, 5258.

130. Weber, G. (1952) Biochem. J. 51, 1951.

131. Melhuish, W.H. (1962) J. Opt. Soc. Am. 52, 1256.

132. Lippert, E., Nägele, W., Soibold-Blankenstein, I., Staiger, U. & Voss, W. (1959) Z. Anal. Chem. 170, 1.

133. Chen, R.F. (1967) Anal. Biochem. 19, 374.

134. Azumi, T. & McGlynn, S.P. (1962) J. Chem. Phys. 37, 2413.

135. Tanizaki, Y. (1957) Bull. Chem. Soc. Japan, 30, 935.

136. Ware, W.R., Lee, S.K., Brant, G.J. & Chow, P.P. (1971) J. Chem. Phys. 54, 4729.

137. Martin, L.B. & Doty, D.M. (1949) Anal. Chem. 21, 965.

138. Weber, K. & Osborn, M. (1969) J. Biol. Chem. 244, 4406.

139. Ebashi, S. & Maruyama, K. (1965) J. Biochem. 58, 20.

140. Laki, K., Maruyama, K. & Kominz, D.R. (1962) Arch. Biochem. Biophys. 98, 323.

141. Mihashi, K., Nakabayashi, M., Yoshimura, H. & Ohnuma, H. (1979) J. Biochem. 85, 359.

142. Spudich, J.A. & Watt, S. (1971) J. Biol. Chem. 246, 4866.

143. Perry, S.V. (1955) "Methods in Enzymology", ed. by Colowick, S.P. & Kaplan, N.O. Academic Press, New York, 2, 582.

144. Small, P.A., Harrington, W.F. & Kielley, W.W. (1961) Biochim. Biophys. Acta, 49, 462.

145. Young, D.M., Himmelfarb, S. & Harrington, W.F. (1965) J. Biol. Chem. 240, 2428.

146. Weeds, A.G. & Taylor, R.S. (1975) Nature 257, 54.

147. Weltman, J.K., Szaro, R.P., Frankelton, A.R. Jr., Dowben, R.M., Bunting, J.R. & Cathou, R.E. (1972) J. Biol. Chem. 248, 3173.

148. Scouten, W.H., De Graaf-Hess, A.C., De Kok, A., Grande, H.J., Visser, A.J.W.G. & Veeger, C. (1978) Eur. J. Biochem. 84, 17.

149. Betcher-Lange, S.L. & Lehrer, S.S. (1978) J. Biol. Chem. 253, 3757.

150. Kanaoka, Y., Machida, M., Machida, M. & Sekine, T. (1973) Biochim. Biophys. Acta, 317, 563.

151. Ikkai, T., Wahl, Ph. & Auchet, J.-C. (1979) Eur. J. Biochem. 93, 397.

152. Hundley, L., Coburn, T., Garwin, E. & Stryer, L. (1962) Rev. Sci. Instrum. 38, 488.

153. Sundstrom, V., Rentzepis, P.M. & Lim, E.C. (1977) J. Chem. Phys. 66, 4287.

L54. Kouyama, T. (1978) Japan J. Appl. Phys. 17, 1409.

155. Bédard, G. (1967) Proc. Phys. Soc. 90, 131.

156. Davis, C.C. & King, T.A. (1970) J. Phys. A3, 101.

157. Miehe, J.A., Ambard, G., Zampah, J. & Coche, A. (1970) IEEE Trans. Nucl. Sci. NS-17, 115.

158. Morton, G.A., Smith, H.M. & Krall, H.R. (1968) Appl. Phys. Letters, 13, 356.

159. Simon, R.E., Sommer, A.H., Tietjen, J.J. & Williams, B.F. (1968) Appl. Phys. Letters, 13, 355.

160. Mandel, L., Sudarshan, E.G. & Wolf, E. (1964) Proc. Phys. Soc. 84, 435.

161. Mandel, L. & Wolf, E. (1965) Rev. Mod. Phys. 37, 231.

162. McLean, T.P. & Pike, E.R. (1965) Phys. Letters, 15, 318.

163. Schuyler, R. & Isenberg, I. (1971) Rev. Sci. Instrum. 42, 813.

164. Prescott, J.R. (1966) Nuclear Instrum. and Methods, 39, 173.

165. Breitenberger, E. (1955) Progr. Nucl. Phys. 4, 56.

166. Bennett, R.G. (1960) Rev. Sci. Instrum. 31, 1275.

167. Lewis, C., Ware, W.R., Doemeny, L.J. & Nemzek, Th. (1973) Rev. Sci. Instrum. 44, 107.

168. Wahl, Ph., Auchet, J.-C. & Donzel, B. (1974) Rev. Sci. Instrum. 45, 28.

169. Kawato, S., Kinoshita, K. & Ikegami, A. (1977) Biochemistry, 16, 2319.

170. Conti, C. & Forster, L.S. (1974) Biochem. Biophys. Res. Com. 57, 1287.

171. Grinvald, A. & Steinberg, I.Z. (1974) Anal. Biochem. 59, 583.

172. Marquardt, D.W. (1963) J. Soc. Ind. Appl. Math. 11(2), 431.

173. Easter, J.H., DeToma, R. & Brand, L. (1976) Biophys. J. 16, 571.

174. Bay, Z. (1950) Phys. Rev. 77, 419.

175. Isenberg, I. & Dyson, R.D. (1969) Biophys. J. 9, 1337.

176. Isenberg, I., Dyson, R.D. & Hanson, R. (1973) Biophys. J. 13, 1090.

177. Gafni, A., Modlin, R.L. & Brand, L. (1975) Biophys. J. 15, 263.

178. Valeur, B. (1978) Chem. Phys. 30, 85.

179. Ware, W.R., Doemeny, L.J. & Nemzek, T.L. (1973) J. Phys. Chem. 77, 2038.

180. Wild, U., Holzwarth, A.R. & Good, H.P. (1977) Rev. Sci. Instrum. 48, 1621.

181. Knight, A.E.W. & Selinger, B.K. (1971) Spectrochim. Acta, 27A, 1223.

182. McKinnon, A.E., Szabo, A.G. & Miller, D.R. (1977) J. Phys. Chem. 81, 1564.

183. O'Connor, D.V., Ware, W.R. & Andre, J.C. (1979) J. Phys. Chem. 83, 1333.

184. Bevington, P.R. (1969) "Data Reduction and Error Analysis for the Physical Sciences", McGraw-Hill, New York.

185. Kawasaki, Y., Mihashi, K., Tanaka, H. & Ohnuma, H. (1976) Biochim. Biophys. Acta, 446, 166.

186. Knopp, J.A. & Weber, G. (1969) J. Biol. Chem. 244, 6309.

187. Wu, C.-W., Yarbrough, L.R. & Wu, F.Y.-H. (1976) Biochemistry, 15, 2863.

188. Martonosi, A. (1968) Arch. Biochem. Biophys. 123, 29.

189. Gafni, A. & Brand, L. (1976) Biochemistry, 15, 3165.

190. Brochon, J.C., Wahl, Ph., Doublet, M.-O. & Olomucki, A. (1977) Biochemistry, 16, 4594.

191. Lahmani, F., Tramer, A. & Tric, C. (1974) J. Chem. Phys. 60, 4431.

192. Mihashi, K. & Wahl, Ph. (1975) FEBS Lett. 52, 8.

193. Wahl, Ph., Mihashi, K. & Auchet, J.-C. (1975) FEBS Lett. 60, 164.

194. Tawada, K., Wahl, Ph. & Auchet, J.-C. (1978) Eur. J. Biochem. 88, 411.

195. Porter, M. & Weber, A. (1979) FEBS Lett. 105, 259.

196. Yagi, K., Mase, T., Sakakibara, I. & Asai, H. (1965) J. Biol. Chem. 240, 2448.

197. Gordon, D.J. & Holzwarth, G. (1971) Arch. Biochim. Biophys. 142, 481.

Acknowledgements

I would like to express my sincere thank to Dr. K. Mihashi for his guidance and encouragement through the present work. I would like to thank Dr. Y. Kawasaki who guided me in the field of fluorometry. I am indebted to Prof. F. Oosawa, Prof. S. Hatano, Prof. J. Tanaka and Dr. N. Imai for their thoughtful advices. It is a pleasure to thank Dr. T. Ikkai, Dr. M. Miki and Dr. T. Kishi for their coworking. I would like to thank Dr. S. Iida, Dr. T. Iio, Dr. K. Imakubo, Dr. H. Ohnuma and Dr. M. Taniguchi for their valuable discussions. I wish to thank Mr. Y. Kai, Mr. S. Miyamoto, Dr. H. Ueno, Mr. M. Asai, Mr. Y. Ishii, Mr. S. Sasaki, Mr. S. Yoshino, Mr. M. Nakabayashi, Mr. Y. Hoshihara, Mr. H. Yoshimura for their discussions. I also thank Miss K. Mori for her skilful typing and Mrs. M. Ukai for setting laboratory in order.

The facilities of the Computing Center of Nagoya University were used in this work. Scholarship from April 1979 to March 1980 from Japan Society for the Promotion of Sciences is gratefully acknowledged.

Papers:

1) Miki, M., Kouyama, T. & Mihashi, K. (1976) Fluorescence Study of ε-ADP bound to Rabbit F-actin: Structural Change in the Adenine Subsite of F-actin under the Influence of Heavy meromyosin. FEBS Letters, 66, 98-101

2) Kishi, T., Tanaka, J. & Kouyama, T. (1976) Isotope Effect on the Rate of Dissociation of β-Naphthol in the Excited State. Chem. Phys. Lett., 41, 497-499.

3) Kishi, T., Tanaka, J. & Kouyama, T. (1977) Normal Isotope Effect on the Rate of Dissociation of Carbazole in the Excited State. Chem. Phys. Lett., 46, 383-385.

4) Kouyama, T. (1978) Determination of Fluorescence Anisotropy Decay by Single-Photoelectron Counting at Various Count Rate. Japan. J. Appl. Phys., 17, 1409-1418

5) Ikkai, T., Mihashi, K. & Kouyama, T. (1980) Pulse Fluorimetric Study of Labelled Actin-DNase I complex. FEBS Letters, 109, 216-218.

6) Kouyama, T. & Mihashi, K. Pulse Fluorometry Study on Actin and Heavy Meromyosin Using F-actin Labelled with N-(1-Pyrene)Maleimide. Eur. J. Biochem. (1980) in press.